PONTIFÍCIA UNIVERSIDADE CATÓLICA
DO RIO DE JANEIRO

Matheus Ouverney Ferreira

Surfactants and polymers: from assembly to oil loading

Tese de Doutorado

Thesis presented to the Programa de Pós-Graduação em Química of PUC-Rio in partial fulfillment of the requirements for the degree of Doutor em Química.

Advisor: Prof. Ana Maria Percebom

Co-advisor: Dr. Karina Oliveira Lima

Rio de Janeiro

Setembro de 2024

Pontifícia Universidade Católica do Rio de Janeiro

Matheus Ouverney Ferreira

Surfactants and polymers: from assembly to oil loading

Thesis presented to the Programa de Pós-Graduação em Química of PUC-Rio in partial fulfillment of the requirements for the degree of Doutor em Química.Approved by the Examination Committee.

Prof. Ana Maria Percebom

Advisor

Departamento de Química – PUC-Rio

Dr. Karina Oliveira Lima

Co-Advisor

Departamento de Química – PUC-Rio

Prof. Marcio da Silveira Carvalho

PUC-Rio

Prof. Guilherme Augusto Ferreira

UFBA

Prof. Priscyla Daniely Marcato Gaspari

USP

Prof. Claudia Regina Elias Mansur

UFRJ

Prof. André Silva Pimentel

PUC-Rio

Rio de Janeiro, 27 de setembro de 2024

Matheus Ouverney Ferreira

Holds an Industrial Chemistry degree from the Federal Fluminense University (2018) and M.Sc. Degree in Chemistry from the Pontifícia Universidade Católica do Rio de Janeiro (2020).

Bibliographic data

Ferreira, Matheus Ouverney

Surfactants and polymers: from assembly to oil loading / Matheus Ouverney Ferreira ; advisor: Ana Maria Percebom ; co-advisor: Karina Oliveira Lima. – 2024.

197 f. : il. color. ; 30 cm

Tese (doutorado)–Pontifícia Universidade Católica do Rio de Janeiro, Departamento de Química, 2024.

Inclui bibliografia

1. Química – Teses. 2. Encapsulamento. 3. Triblock copolymer. 4. Nanoparticula. 5. Poloxâmero. 6. Pluronic. I. Percebom, Ana Maria. II. Lima, Karina Oliveira. III. Pontifícia Universidade Católica do Rio de Janeiro. Departamento de Química. IV. Título.

CDD: 540

Acknowledgement

I have much to be thankful for to all those I've met along the way who have always supported me in pursuing my dreams. I dedicate this work, as well as all my achievements, to my parents, Elmo Ferreira and Geraldina Ouverney Ferreira, and to my brothers, Higor Ouverney Ferreira and Antônio Luiz Ferreira Neto, who have always been there to provide unconditional support and motivate me in my studies. This achievement would not exist without you, and my victories are also yours.

To my grandmothers, Maria Durvalina Knupp Ferreira and Janete Ouverney Ferreira, my grandfather, Antônio Luiz Ferreira, and my aunts, for their constant love and care.

To Rodrigo Moura Chichierchio Monteiro, my life partner, my best friend, for all your encouragement, companionship, and support, which were essential for the completion of this work. Thank you for always believing in me. I am grateful and proud every day of everything we have built together. Thank you for embarking on this journey with me, for accompanying me to Sweden, and for always supporting my decisions. This thesis only came to life because you were there. I also want to than Doguinho and Jorginho, who made my days easier during this entire process.

To Carine Class, Carol Class, Anna Carolina Pinho, Marina Schaus, Júlia Rosa, Isabela Oliveira, Cecília Gonçalves and Mariana Nicolau for the shared friendship. Thank you for the laughter, the lighthearted moments, and all the support along this path.

A special thank you to my friends at the M&NLab, who were with me daily during this project: Franccesca Fornasier, Gabriela Fonseca, Lais Helena, Lina Morantes, Oscar Martinez, Thamiris Vilar, Victória Régia, Lorena Pereira, Luan Chagas, and all the new members of the group.

To Professor Karen Edler for the opportunity and experience of conducting part of this work at Lund University, which will certainly accompany me throughout my career. I also want to thank Niamh Leeman, Elly Bathke, Ronak, and Maggy. A special thanks to Bradley Green who welcomed me so well and have become a really good friend in my life.

To my colleagues at Grupo Boticário, who supported me during the final months of writing and welcomed me with open arms into this new chapter of my career, especially Vanessa Carvalho, Júlia Fajardo, Bárbara Alves, Caroline Ferreira, André Matos, and Tássia Araujo. A special thank you to my manager, Isabely Zaqueo.

I am grateful to CNPq, FAPERJ, PUC-Rio, the Department of Chemistry, CNPEM, and Oxiteno and all their collaborators for the investment and infrastructure necessary for this research.

Finally, I would like to thank Professor Ana Percebom and Karina Lima for their guidance and encouragement, which were essential in completing this journey. Thank you, Ana, for always supporting and fostering the growth of your students. You are an inspiration to all of us. Thank you, Karina, for all the partnership, discussions, and conversations. With your help, this work became much lighter.

This work was carried out with the support of the Coordination for the Improvement of Higher Education Personnel - Brazil (CAPES) - Funding Code 001.

Agradecimentos

Tenho muito a agradecer àqueles com quem convivi até hoje e que sempre me apoiaram na busca dos meus sonhos. Dedico este trabalho, assim como todas as minhas conquistas, aos meus pais, Elmo Ferreira e Geraldina Ouverney Ferreira, e aos meus irmãos, Higor Ouverney Ferreira e Antônio Luiz Ferreira Neto, que sempre estiveram presentes para me dar apoio incondicional e me motivar nos estudos. Essa conquista não existiria sem vocês e minhas vitórias também são suas.

Às minhas avós, Maria Durvalina Knupp Ferreira e Janete Ouverney Ferreira, ao meu avô, Antônio Luiz Ferreira, e às minhas tias, pelo carinho constante.

Ao Rodrigo Moura Chichierchio Monteiro, meu companheiro de vida, meu melhor amigo, por todo incentivo, companheirismo e suporte, essenciais para a conclusão deste trabalho. Obrigado por sempre acreditar em mim; todas essas conquistas foram possíveis porque tive seu apoio. Agradeço e me orgulho todos os dias de tudo que construímos juntos. Obrigado por embarcar nessa comigo, por me acompanhar até a Suécia e por sempre apoiar minhas decisões, essa tese só nasceu porque você esteve lá. Obrigado também aos meus filhos pet Doguinho e Jorginho que estiveram fazendo meu dia mais fácil durante toda essa etapa.

À Carine Class, Carol Class, Anna Carolina Pinho, Marina Schaus, Júlia Rosa, Isabela Oliveira, Cecília Gonçalves e Mariana Nicolau pela amizade e companheirismo compartilhados. Obrigado pelos momentos de riso, descontração e por todo apoio nessa caminhada.

Obrigado aos meus amigos do Laboratório M&NLab, que me acompanharam diariamente durante a realização deste projeto: Franccesca Fornasier, Gabriela Fonseca, Lais Helena, Lina Morantes, Oscar Martinez, Thamiris Vilar, Victória Régia, Lorena Pereira, Luan Chagas e todos os novos integrantes do grupo.

À professora Karen Edler pela oportunidade e experiência de realizar parte desse trabalho na Universidade de Lund, que com certeza estará junto a mim durante toda a minha carreira. Também agradeço a Niamh Leeman, Elly Bathke, Ronak e Maggy. Um agradecimento especial a Bradley Green que não só me acolheu tão bem mas se tornou um amigo para vida.

Aos meus colegas de time do Grupo Boticário que me auxiliaram nos últimos meses de escrita e que me receberam de coração aberto nessa nova etapa de carreira, em especial: Vanessa Carvalho, Júlia Fajardo, Bárbara Alves, Caroline Ferreira, André Matos e Tássia Araujo. Um especial agradecimento a minha gestora Isabely Zaqueo.

Agradeço ao CNPq, FAPERJ, à PUC-Rio, ao Departamento de Química e ao CNPEM e a Oxiteno e todos os seus colaboradores pelo investimento e infraestrutura necessários para a realização da pesquisa.

Por último, agradeço à Professora Ana Percebom e Karina Lima por toda orientação e incentivo, essenciais para concluir essa jornada. Obrigado Ana por sempre apoiar e incentivar o crescimento dos seus alunos. Você é uma inspiração para todos nós. Obrigado Karina por toda parceria, discussões e conversas, com sua ajuda esse trabalho ficou muito mais leve.

O presente trabalho foi realizado com o apoio da Coordenação de Aperfeiçoamento de Pessoal de Nível Superior - Brasil (CAPES) - Código de Financiamento 001.

Abstract

Ferreira, Matheus Ouverney; Percebom, Ana Maria (Advisor) Lima, Karina Oliveira (Co-Advisor);. **Surfactants and polymers: from assembly to oil loading.** Rio de Janeiro, 2024. 197p. Tese De Doutorado – Departamento de Química, Pontifícia Universidade Católica do Rio de Janeiro.

Oil loading in aqueous formulations is a constant challenge when developing cosmetics with new claims, and different parameters may affect their preparation and properties. For instance, several methods require high energy input or are not adaptable to large-scale production in an industrial context. If nanoparticles with a high amount of oil loading are desired, this becomes even more challenging. Formulating with chemicals already used in cosmetics or using biocompatible ones is also essential. A possible strategy to avoid these issues involves using poly(ethylene oxide)-poly(propylene oxide)-poly(ethylene oxide) ($EO_xPO_yEO_x$), which are already approved for cosmetics and pharmaceutical formulations, their availability in different chain lengths and proportions of EO/PO groups can allow the control of different properties, such as enhancing stability in an aqueous medium by increasing the EO chain length. This thesis aims to design, obtain, and characterize different colloids, in four different papers, using triblock copolymers to uptake hydrophobic ingredients in aqueous formulations. By employing simple preparation methods, we explore a range of colloidal structures, from nanoparticles to microcapsules, aiming to understand how the copolymer's structure influences the final properties. These methods included spontaneous capsule formation through charge-driven complexation to the use of copolymers to stabilize liquid crystals dispersions. In the first study, core-shell particles were obtained through complexation between oxidized cellulose nanofibrils (OCNF) and poly(diallyldimethylammonium chloride) (PDADMAC), with triblock copolymers enhancing stability and oil loading. This method resulted in stable particles with high oil incorporation capacity, suitable for controlled release of active ingredients. In the second study, dispersing lamellar phases formed by sodium lauryl sulfate (SDS) and fatty alcohols using triblock copolymers enabled the formation of nanoparticles with water like viscosity and high stability, suitable for products with light textures. The third study utilized complexation between oppositely charged surfactants and polymers to form nanoparticles with high oil loading capacity, where the triblock copolymer improved stability and loading efficiency. Finally,

the fourth study explored the use of cocamidopropyl betaine as a surfactant, forming micelles that can be used in personal care formulations. The results highlight the potential of these systems for applications in cosmetic products, where stability and active ingredient incorporation are essential.

Keywords

Surfactants; polymers; encapsulation, colloids

Resumo

Ferreira, Matheus Ouverney; Percebom, Ana Maria (Orientadora); Lima, Karina Oliveira (Coorientadora);. **Surfactantes e Polímeros: da autoassociação até o encapsulamento de óleos.** Rio de Janeiro, 2024. 197p. Tese De Doutorado – Departamento de Química, Pontifícia Universidade Católica do Rio de Janeiro.

A incorporação de óleo em formulações cosméticas apresenta vários desafios, pois diferentes parâmetros podem afetar sua preparação e propriedades. Por exemplo, diversos métodos exigem alto fornecimento de energia ou não são adaptáveis para escalas grandes, principalmente em um contexto de aplicações industriais. Se nanopartículas com uma alta incorporação de óleo forem desejadas, os desafios são ainda maiores. Além disso, é essencial formular com produtos químicos já utilizados em cosméticos ou utilizar aqueles que são biocompatíveis. Uma possível estratégia para contornar esses problemas envolve o uso de poli (óxido de etileno) -poli(óxido de propileno)-poli(óxido de etileno) (EOxPOyEOx), que já são aprovados para formulações cosméticas e farmacêuticas. Sua disponibilidade em diferentes comprimentos de cadeia e proporções de grupos EO/PO permite controlar diversas propriedades, como aumentar a estabilidade em meio aquoso ao aumentar o tamanho da cadeia EO. A presente tese tem como objetivo projetar, obter e caracterizar diferentes coloides usando copolímeros tribloco para absorção de ingredientes hidrofóbicos em formulações aquosas, em quatro estudos diferentes. Empregando métodos de preparo simples, exploramos uma variedade de estruturas coloidais, desde nanopartículas até microcápsulas, com o objetivo de entender como a estrutura do copolímero influencia as propriedades desses sistemas. Esses métodos incluíram desde a formação espontânea de cápsulas por complexação eletroestática até o uso de copolímeros para estabilizar dispersões de cristais líquidos. No primeiro estudo, partículas núcleo-casca foram obtidas por complexação entre nanofibrilas de celulose oxidadas (OCNF) e poli(dialildimetilamônio) (PDADMAC), com copolímeros tribloco promovendo a estabilidade e a carga de óleo. Esse método resultou em partículas estáveis e com alta capacidade de incorporação de óleo, adequadas para a liberação controlada de ingredientes ativos. No segundo estudo, a dispersão de fases lamelares formadas por sulfato de laurila de sódio e álcoois graxos em copolímeros tribloco permitiu obter nanopartículas com viscosidade ajustável e boa estabilidade, adequadas para produtos com texturas leves. O terceiro estudo utilizou complexação entre surfactantes e polímeros

de cargas opostas para formar nanopartículas com alta capacidade de carga de óleo, onde o copolímero tribloco aumentou a estabilidade e a eficiência de carga. Finalmente, o quarto estudo explorou o uso de betaína cocamidopropil como surfactante, formando micelas que podem ser utilizadas em formulações de cuidados pessoais. Os resultados destacam o potencial desses sistemas para aplicações em produtos cosméticos, onde a estabilidade e a incorporação de ingredientes ativos são essenciais.

Palavras-chave

Surfactantes, polímeros, encapsulamento, coloides

Table of Contents

List of Figures

Chapter 5:

Chapter 7:

List of Schemes

List of Tables

Chapter 3:

Chapter 4:

Chapter 5:

Chapter 6:

Chapter 7:

CHAPTER 1

INTRODUCTION

1.1. Colloids and oil loading – An outlook of this work

Colloids are mixtures where one substance is dispersed within another, without the dispersed particles settling out or merging into the surrounding medium. These particles are typically within the nanometer to micrometer range, allowing for stability and unique properties that differ significantly from those of bulk materials [1]. Such materials include complex coacervates, colloidal dispersions, liquid crystals, gels, emulsions, and nanocellulose-based materials [1].

Colloids are found in several products in daily life, such as creams, paints, toothpaste, and foods. Despite their apparent diversity, these systems share a common feature: a complex structure often comprising polymers, particles, or surfactants designed to achieve specific structures and properties. In this PhD thesis, we focused on applying colloids for oil loading in aqueous systems. Oil loading refers to the process by which oil or other hydrophobic substances are encapsulated within a material, forming a core and a shell that isolates and protects these substances from environmental factors or when it is dispersed into the matrix.

The use of vehicles for the loading or encapsulation of active ingredients has been widely explored across various sectors [2]. This technology offers numerous possibilities for creating a diverse range of products. In the personal care and hygiene industry, encapsulation is a valuable tool for enhancing the delivery of substances such as antioxidants and vitamins. It also contributes to the stability of these systems, as active ingredients in cosmetics are generally unstable and sensitive to temperature fluctuations, pH changes, light exposure, and oxidation. Encapsulating these substances reduces their exposure, thereby increasing their stability. Another possible property of interest is the gradual release of these substances, which decreases skin contact time, minimizing the

risk of irritation. The increased quantity and depth of active ingredient penetration into the skin is another possibility when using nanometric vehicles. Hence, loading the oil in soft materials can promote greater product efficacy, stability, safe administration, and controlled release.

However, loading high levels of hydrophobic substances in aqueous formulations is a challenge, usually overcome by preparing emulsions in the cosmetic industry. However, emulsions present some limitations, such as the requirement of high energy input, possible instability, and droplets too large to achieve skin permeation. Besides, emulsions are usually very viscous, limiting their use only to products where this characteristic is desired. Different types of soft materials can be explored as alternatives to emulsions. Research in this area suggests that both the industrial and academic sectors have been investigating nanometric systems such as micelles [3,4], solid lipid nanoparticles [5–7], polymeric nanoparticles [8], [9,10], and others to achieve better application and product development, not only in the field of personal care but in various other areas as well [6,11–13]. However, scaling-up the process to obtain some of these vehicles can be complicated due to the use of very specific homogenizers or chemicals, limiting their application on a large scale.

This thesis presents the preparation of three different colloids for loading oil in aqueous systems, including oppositely charged nanoparticles, lamellar dispersions and core-shell cellulose particles. It was initially conceived in partnership with the company Oxiteno. This thesis hypothesized that triblock copolymers of poly (ethylene oxide)-poly(propylene oxide)-poly(ethylene oxide) ($EO_xPO_yEO_x$) could be used to obtain and stabilize nanometric soft materials to load oil in aqueous medium for the cosmetics industry. Their EO blocks are hydrophilic and could promote dispersibility and stability in water, whereas the PO blocks could guarantee the oil loading or the interaction with the material of choice. These triblock copolymers are already approved for cosmetics and pharmaceutical formulations [14] and produced in large scale by Oxiteno and other companies.

1.2. Poloxamers

Block copolymers known as Poloxamers, or by the trade names Pluronic®, Kolliphor® and Synperonics™, are a well-established class of synthetic copolymers with applications in various fields such as pharmaceuticals and cosmetics. They are nonionic, amphiphilic triblock copolymers composed of a hydrophobic central block of poly(propylene oxide) (PO) attached to two hydrophilic chains of poly(ethylene oxide) (EO), generally structured as $EO_xPO_yEO_x$ (**Figure 1.1**), where x and y represent the average number of monomeric units in the copolymer. This arrangement results in a polymer where the number of hydrophilic and hydrophobic units can be easily altered [15–17]. These polymers have been extensively studied by various groups, which have shown that they exhibit relatively low toxicity in cultured cells or even cytoprotective effects, making them well-suited for applications in both cosmetics and pharmaceuticals. [15-20]

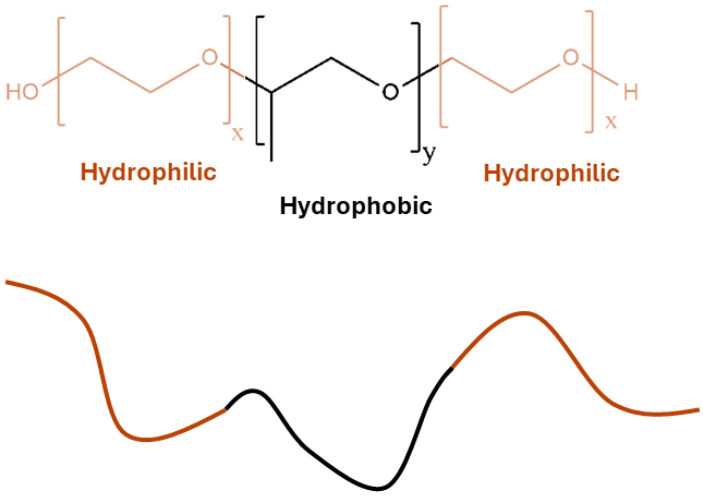

Figure 1.1: Molecular structure and schematic representation of a generic $EO_xPO_yEO_x$ poloxamer.

These copolymers are commercially available in various molecular weights, block lengths, and EO/PO ratios, which determine their different physicochemical properties. **Table 1.1** describes some types of poloxamers available on the market, their properties, and primary uses [18–20].

Table 1.1: Physicochemical characteristics and applications of some popular copolymers. [15-20]

INCI Name	Molecular Structure	Mw ($g.mol^{-1}$)	HLB	CMC ($mmol.L^{-1}$)	Cloud Point (°C) (10 wt%)	Primary use
Poloxamer 182	$EO_{04}PO_{30}EO_{04}$	2110	1 a 7	-	40	Controlled Release, Nonionic Surfactant
Poloxamer 184	$EO_{10}PO_{30}EO_{10}$	2640	10 to 12	0.48	>100	Surfactant, Controlled Release, Pharmaceutical Applications
Poloxamer 334	$EO_{20}PO_{60}EO_{20}$	5260	10 to 12	0.0021	15	Controlled Release
Poloxamer 407	$EO_{90}PO_{60}EO_{90}$	11430	>24	0.0028	>100	Long-Circulating Particles, Slow-Release Gels, Tissue Engineering

One of the main properties of poloxamers is their ability to self-assemble into a variety of structures, as they also act as surfactants. They can self-assemble, forming different aggregates, including micelles, gels, giant micelles, and various mesophases, depending on temperature, concentration, and composition [16,21–24]. Some of their properties can be tuned by controlling these parameters. For example, at room temperature, more hydrophilic poloxamers, with a higher EO/PO ratio value, tend to have higher Critical Micelle Concentration (CMC) values, and vice versa. At a fixed EO/PO ratio, the CMC decreases with increasing molecular weight of the copolymer. If the EO block fraction is less than 10% for a series with the same PO block length, lamellar phases are formed instead of micelles [15,24,25].

Because these polymers also act as surfactants, they can serve as stabilizers in different systems. The versatility of these substances explains the interest in using poloxamers in various industrial applications, as evidenced by numerous patents filed [26–29]. Additionally, the ability to control the size of EO/PO chains allows for understanding how each parameter (degree of polymerization, hydrophobicity/hydrophilicity ratio) affects the loading rate of active ingredients, enabling optimization of the proposed systems.

For instance, Wulff-Pérez et al. [30] demonstrated the formation of stable nanoemulsions using Poloxamer 188 with various natural oils. These nanoemulsions were resistant to coalescence, even when volume fractions above 25% of oil were used. However, the reliance on ultrasonication poses challenges for scaling up the process.

Mészáros et al. [31] proposed the use of a Poloxamer to disperse polymer-surfactant (P-S) complexes in aqueous media by applying a specific method of stop-flow-mixing (**Figure 1.2**). They used the anionic surfactant sodium dodecyl sulfate (SDS), the cationic poly(ethyleneimine) (PEI), and the Poloxamer F108. The presence of EO and PO groups allows Poloxamer to interact with both aqueous media and the hydrophobic sites present in the system. The scheme in **Figure 1.2** shows that the Poloxamer provided steric stabilization, suppressing phase separation in the systems and forming nanoparticles. Despite the specific mixing methodology, which is inadequate for a large scale, the authors did not explore the obtained nanoparticles to verify their capacity for loading hydrophobic substances.

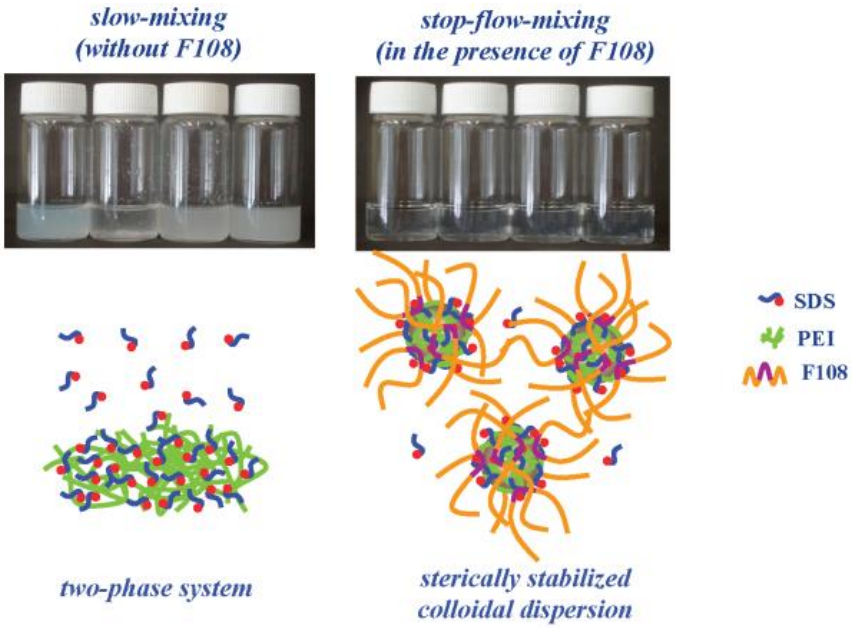

Figure 1.2:Representation of the interaction between SDS-PEI in the absence and presence of Poloxamer. (Mészáros et al. *[31]* – permission of use at the end of this thesis)

Nakano et al. [32] used $EO_{90}PO_{60}EO_{90}$ to prepare cubosomes and hexosomes in aqueous medium with a mixture of monoolein and oleic acid. Cubosomes and hexosomes are particles of the cubic and hexagonal liquid crystalline phases, respectively, dispersed in a liquid medium. They found that increasing the poloxamer concentration led to a decrease in particle size while maintaining the same internal structure, though the particles were highly pH dependent. Despite successfully dispersing liquid crystalline phases, the preparation method is not yet suitable for large-scale production due to its reliance on solvent evaporation (chloroform), followed by drying under vacuum and mixing with a high-pressure emulsifier.

While Poloxamers show promise in both liquid crystal dispersions and oil loading, further research is needed to develop scalable methods for their use in industrial applications. The availability of poloxamers in different chain lengths and proportions of EO/PO groups may be explored to control different properties,

such as enhance dispersibility in an aqueous medium with longer EO blocks or increased oil loading with longer PO blocks.

Given all these properties and considering the advantages and challenges of applying nanometric vehicles in cosmetic formulations, this study employed triblock copolymers in various colloidal systems as a strategy to enhance stability and/or loading of hydrophobic actives and/or promote the dispersion and stabilization of liquid crystals in aqueous media with viscosity close to that of water.

1.3. Liquid crystals for oil loading

Liquid crystals were discovered in 1888 and have attracted extensive interest due to their unique properties [33]. Lyotropic liquid crystals are usually formed in systems with high surfactant concentrations. Essentially, an elevated concentration of micelles can organize themselves to occupy a high volumetric fraction, forming a crystalline structure that can still flow under shear. The weak interactions between the surfactant micelles allow the material to flow under shear stress, like a liquid. However, their ordered structures classify them as crystalline, like solid crystals. The ordered structure produces a distinct interference pattern, identifiable through small-angle X-ray scattering (SAXS) or diffraction [34,35]. This new arrangement significantly increases viscoelasticity [36] and alters other properties, making them highly valuable in various industrial applications, such as the cosmetic industry.

Common examples of lyotropic liquid crystals include cubic, hexagonal, and lamellar phases, as depicted in **Figure 1.3**. The micelles are nearly spherical in the cubic phase, indefinitely long cylindrical in the hexagonal phase, and stacked bilayers form the lamellar phase. The cross-section of the micelles and the thickness of the water layers between the surfactant bilayers can vary depending on the nature of the surfactant [36,37], which SAXS can also determine.

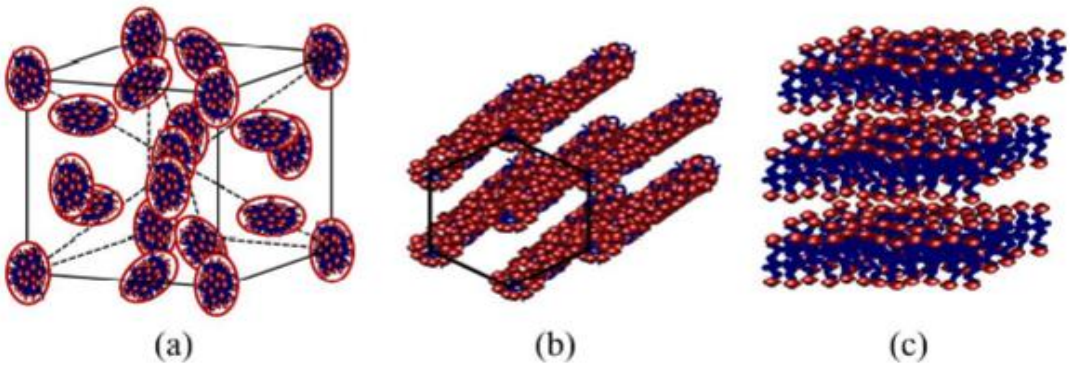

Figure 1.3: Structures of lyotropic liquid crystals (a) Cubic Phase (b) Hexagonal Phase, and (c) Lamellar Phase.[38]

Due to its rheological properties and easy preparation, the lamellar phase is the main liquid crystal used in the cosmetics industry. The alternating bilayers can smoothly slide on the surface of hair or skin. Besides, they are used to stabilize emulsions or prepare liposomes (or vesicles) [34,39]. Liposomes can load both hydrophobic and hydrophilic substances, being very useful to prevent degradation [40]. Liposomes of different types, such as multilamellar vesicles, small unilamellar vesicles, large unilamellar vesicles, multi-vesicular, and sizes from nm to um in diameters can be prepared depending on the compositions and techniques of preparation [41]. However, the preparation method remains challenging in scaling up liposome applications because the techniques involved, such as lipid film formation [42], ethanol injection [43], and ultrasonication [44], either require high energy or are not feasible for industrial-scale production, which increases the cost of it. For instance, Hanley et al. [45] showed the formation of giant multilamellar and large unilamellar vesicles using deoiled lecithin and sunflower lecithin dispersions. These liposomes were formed spontaneously using minimal processing but presented an average diameter of 6-7 μm. Hence, there are still possibilities for improvement in the methods to achieve efficient vehicles in a nanoscale [46].

Most liposome systems are formed by double-chain surfactants, because they assemble in close to zero-curvature aggregates, forming the bilayers, even at small concentrations. A high surfactant concentration is usually required to obtain lyotropic liquid crystals for single-chain surfactants. However, another way to anticipate their formation is the addition of certain chemicals, such as fatty alcohols [47] and oppositely charged polymers [48].

Adding fatty alcohols to surfactants usually induces the formation of a lamellar phase because their molecules can intercalate with the surfactant molecules, acting as cosurfactants and reducing the micellar curvature [49–51,51–53]. Fatty alcohols, used in cosmetics and pharmaceuticals as co-surfactants, are typically manipulated by heating above their melting points, homogenizing under heat, and cooling to room temperature to induce alcohol crystallization and dispersed crystalline structures [49].

Eccleston et al.[47] used SAXS to understand lamellar gel phase properties in pharmaceutical creams with cetrimide and fatty alcohols, measuring interlamellar water layer thickness under high water concentrations

(up to 93%) and correlating the structures with rheological properties and stability. Swelling due to higher interlamellar water content decreased with added salts, reducing electrostatic repulsion. Changing surfactant counter-ions affected interlamellar water content, with bromine increasing swelling and chloride reducing it. SAXS data showed lamellar phases with higher water content having more ordered structures, while those with lower water content were less organized [47].

Liquid crystals in cosmetics are usually limited to emulsions and liposomes due to their high viscosity. However, dispersing them in an aqueous phase can expand their potential to be used as vehicles. For example, dispersions of liquid crystal, such as cubosomes, hexosomes and micellesomes have been being investigated for application in drug delivery [54].

A previous study of our research group explored ionic surfactants with long-chain alcohols to obtain lamellar phases and ethoxylated surfactants to promote their dispersion in aqueous media [55]. However, the formed particles were micrometric, so the ethoxylated surfactants were not sufficient to achieve the nanoscale and keep the dispersion stable in the conditions used in this study.

1.4. Oppositely charged polymer-surfactant nanoparticles for oil incorporation

Another approach to promote the formation of liquid crystals is by mixing ionic surfactants with oppositely charged polymers. These substances are usually combined in various applications, including personal care and pharmaceutical products, making the study of interactions between these systems a key topic in many research, which is particularly important because the properties of the mixture can differ significantly from those of the individual components [56].

In aqueous mixtures of oppositely charged surfactants and polymers, associative phase separation usually occurs, resulting in a concentrated phase of the polymer-surfactant complex (P-S) formed by the P-S interaction and a dilute phase containing the original counterions of these molecules[57]. The concentrated micelles can potentially form liquid crystalline structures, effectively incorporating hydrophobic ingredients due to their hydrophobic interiors. Therefore, the formation of nanoparticles from this concentrated phase represents a potential strategy for developing new methods to load and deliver hydrophobic ingredients.

Recent studies present various strategies to prevent macroscopic phase separation in these systems by modifying the polymer architecture, using specific surfactants, adding a third component, or using specific preparation methods [2,58][59]. Examples of phase separation prevention included controlling ionic strength, pH, and temperature, which influenced the hydrophobic interactions and electrostatic forces governing complex formation. Another effective approach was adjusting the surfactant-to-polymer molar ratio, where an excess of surfactant could led to redispersion of the complexes [59].

Adding nonionic surfactants or polymers can also affect the kinetic stability of oppositely charged P-S mixtures, preventing their separation. For example, the use of n-dodecyl-β-maltoside can significantly suppress precipitation in mixtures of sodium dodecyl sulfate (SDS) with cationic polymers, mainly due to the adsorption of this substance on the surface of the P-S complexes, promoting the dispersion of these systems in water [60].

Another possibility of modifying the polymer architecture to ensure the dispersion and stabilization of the P-S complex in an aqueous medium in nanoparticles is using diblock polymers, with a neutral hydrophilic block covalently bound to the ionic block [61,62]. The ionic block of the polymer strongly interacts with the oppositely charged surfactant, forming a concentrated phase, which is dispersed in nanoparticles and stabilized in the aqueous medium by the hydrophilic neutral blocks, which forms an external hydrophilic shell that keeps the particles stable in an aqueous medium.

Annaka et al. [58] investigated the phase behavior and colloidal structures of complexes formed by a neutral/anionic diblock polymer and a cationic surfactant, dodecyltrimethylammonium bromide (DTAB), whose charge is opposite to one of the polymer blocks. The polymer in question had a neutral block composed of poly(N-isopropylacrylamide), PNIPAM, and an anionic block of poly(acrylic acid), PAA. In this study, techniques such as dynamic light scattering (DLS) and small-angle neutron scattering (SANS) were used to understand the morphology and size of the particles. The results of both techniques indicated that these substances associate into colloidal complexes, with the structure of the complex being directly influenced by parameters such as reactant concentration, ionic strength, and temperature.

Although there are methodologies to prevent phase separation and obtain nanoparticles from oppositely charged P-S mixtures, the mentioned studies did not explore their potential as vehicles. Our research group used nanoparticles formed by the cationic surfactant hexadecyltrimethylammonium chloride (CTAC) and the oppositely charged diblock copolymer poly(ethylene oxide)-b-poly(methacrylic acid) (PEO-b-PMAA), with varying block lengths, to load oily ingredients [2]. The study focused on using hydrophilic diblock polymers containing one negatively charged block and one neutral block associated with a positively charged surfactant. The neutral block would prevent associative phase separation through the dispersion and stabilization of the complexes formed, as shown in **Figure 1.4.** The obtained nanoparticles at a concentration of 2 wt% could upload up to 4 wt% of oily actives with mild stirring, depending on the copolymer block lengths. The results highlight the potential application of these systems. However, a challenge for implementing these systems in real applications is the lack of approval as a cosmetic ingredient and the unavailability

of diblock copolymers with an ionic block and a hydrophilic neutral block in large scale.

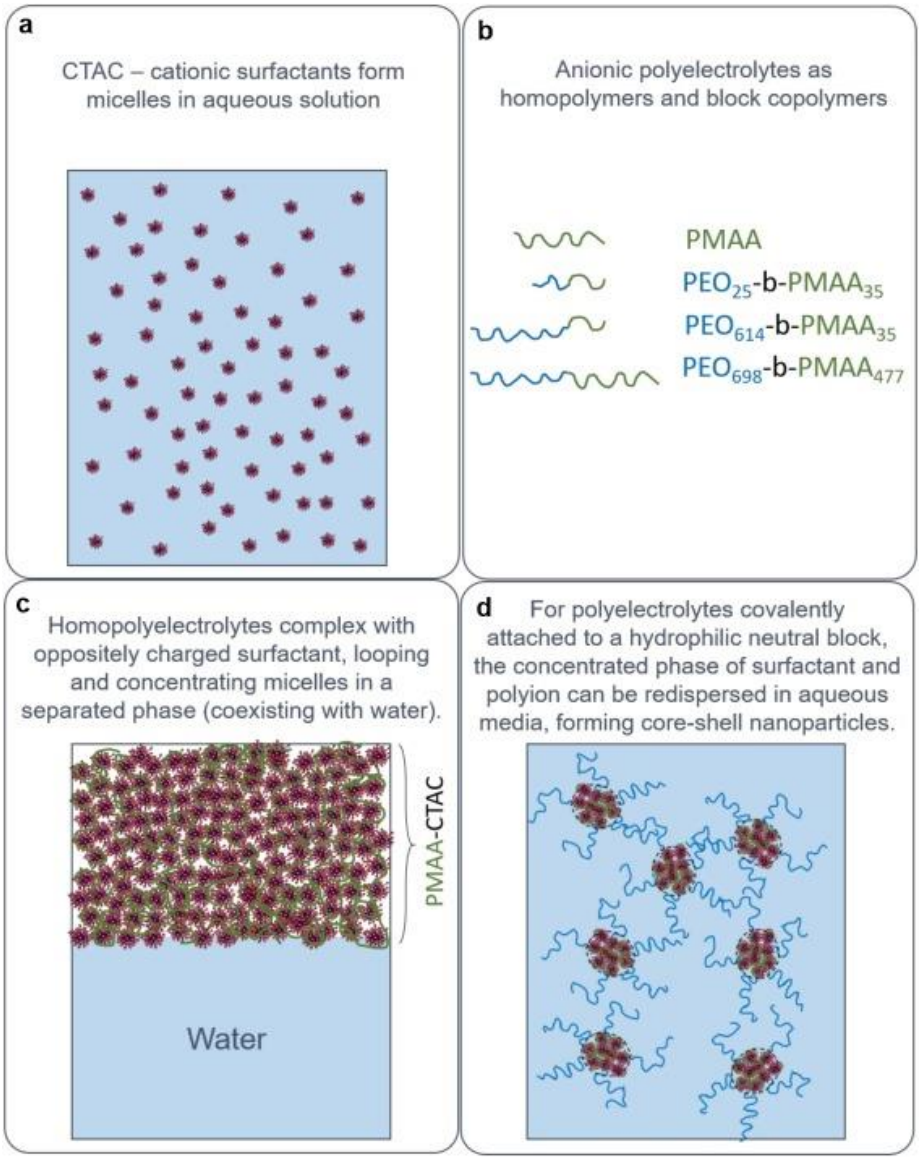

Figure 1. 4: Representation of the phenomena involved in the complexation of polyelectrolytes with oppositely charged surfactants and in the formation of core-shell nanoparticles using diblock copolymers. (Azevedo Stavale A et al.*[2]* permission of use in the end of the thesis)

Obtaining nanoparticles by electrostatic complexation between oppositely charged materials is not limited to polymers and surfactants. The use of biobased materials with a charged surface can also be explored to obtain new materials by complexation, which can be used for oil loading.

1.5. Cellulose nanomaterials

Cellulose is among the most abundant polysaccharides found in nature, sourced from various plants such as wood, flax, cotton, and banana. The linear homopolymer exists in a crystalline, hydrophilic form and can undergo chemical modification due to its hydroxyl groups, with two attached to secondary carbons and one to a primary carbon. It is a low-cost, globally available, biodegradable material with high rigidity in fiber form and low density [40,63–65].

Chemically, cellulose is an unbranched polymer of β-1,4 linked D-glucose units, characterized by a high degree of polymerization [66,67]. The polymer chains are held together by associative van der Waals forces, as well as intra- and intermolecular hydrogen bonds. In woody plants, these cellulose chains form supramolecular structures known as microfibrils, which have a cross-section of approximately 350 nm and can reach lengths of several micrometers [66]. When dispersed in aqueous media, microfibrils flocculate at low concentrations due to net interfibrillar attractive forces [68]. Cellulose nanoparticles can be created through chemical modification, introducing charged chemical functional groups that form electrostatically stabilized colloidal nanoparticles. One example of chemical modification is the 2,2,6,6-tetramethylpiperidine-1-oxyl radical (TEMPO)-mediated oxidation of the primary hydroxyl groups [67,69,70]. This process uses catalytic amounts of TEMPO/NaBr/NaClO to selectively introduce charged carboxylate groups at the C6 position of the glucose rings in cellulose, resulting in negatively charged oxidized cellulose nanofibrils (OCNF). These OCNF belong to the colloidal domain, typically measuring a few hundred nanometers in length and approximately 4 nm in cross-section [71].

OCNF are often used as solid particles to stabilize oil droplets in water, forming oil-in-water (O/W) Pickering emulsions [9]. These emulsions enhance the rheological properties and create stable colloidal dispersions in water without the need for additional thickeners or stabilizers. For example, Yue et al. [72] used a 1.0 wt% OCNF dispersion to stabilize d-limonene, forming an O/W Pickering emulsion that preserved the essential oil. The solid content of OCNF played a crucial role in determining the stability of these emulsions by forming a protective layer around d-limonene droplets, preventing coalescence. Kadam et al. [73] also

reported the formation of Pickering emulsions but using charge driven polycondensation. They utilized stearic acid-functionalized cellulose nanofibers to form stable Pickering emulsions (both oil-in-oil and water-in-oil) and encapsulated N,N-diethyl-3-methylbenzamide (DEET) with an encapsulation efficiency of 98%.

Shi et al. [74] used Pickering emulsions linked with electrostatic attractions to create microcapsules. Stable microcapsules were produced from cationized cellulose nanofibril (CCNF) that were used to stabilize Pickering emulsions following the addition of OCNF dispersions. The complex was formed between CCNF and OCNF networks at the oil-water interface via charge inversion of the primary Pickering emulsions, resulting in high stability for these capsules. A dye was used to study the release of these capsules, revealing that it was released from the oil phase through the CCNF/OCNF complex shell via diffusion.

Pickering emulsions are one of the trending topics on using OCNF for oil loading, but they require high energy input for production. Scaling up is crucial in developing industry-applicable procedures for cellulose materials, particularly regarding their use as delivery vehicles.

Electrostatic complexation of nanocellulose with oppositely charged polymers can be an option for vehicles, as proposed by Calabrese et al. [75]. They used CCNF to produce core-shell particles as vehicles for enzymes through charge-driven complexation. CCNF was extruded dropwise into an aqueous bath containing the negatively charged polymer, polyacrylic acid (PAA). The resulting capsules featured a liquid-like core composed of uncomplexed CCNF in water and a solid-like shell formed by CCNF-PAA complexation. Although the particles have a few millimeters in diameter, they exhibited a semipermeable nature, making them suitable as matrices for physical enzyme entrapment and allowing their use and reuse as microreactors. A significant advantage of this approach was that the capsules were fabricated spontaneously by simply dropping CCNF into the aqueous solution. However, the particles could not load oil due to the aqueous nature of the core.

1.6. Research justification

Polyelectrolytes can form new materials by electrostatic complexation with oppositely charged surfactants or cellulose nanoparticles. The microcapsules formed by cationic cellulose nanofibers and the anionic polymer PAA have already shown potential for encapsulating hydrophilic actives as enzymes [75]. Combining anionic cellulose nanoparticles with a cationic polymer would prove the possibility of expanding the proposed method with different ingredients. However, it would still not solve the challenge of oil loading. Hence, considering the hypothesis that poloxamers can enhance the capability of soft colloids for oil loading, the present study adapted the previous method, combining anionic OCNF with a cationic polymer and poloxamer and using microfluidics to obtain smaller particles and encapsulate a hydrophobic dye.

Poloxamers were also combined with lamellar liquid crystals formed by the anionic surfactant, sodium dodecyl sulfate (SDS), and various fatty alcohols or acids as cosurfactants. The effect of different parameters on the size and stability of the obtained particles was evaluated, such as the proportion of ingredients, and the length of the poloxamers blocks and fatty chains. The results indicated the characteristics to select systems to be tested for oil loading. This part of the study was conducted in partnership with Oxiteno.

Since diblock copolymers with a hydrophilic neutral block attached to an ionic block are not approved as a cosmetic ingredient and are not commercially available on a large scale, the present study used the triblock copolymers of $EO_xPO_yEO_x$ to obtain nanoparticles when combined with oppositely charged surfactants and polymers.

Through these efforts, the study aims to enhance the stability, dispersibility and/or oil loading of the formulated systems, contributing to the efficacy of the formulations in potential future applications by employing triblock copolymers in each system. These polymers are expected to improve the dispersibility of liquid crystal dispersions and enhance oil loading, depending on the EO/PO ratio.

Considering the three mentioned soft materials combined with poloxamers, this research involved the strategic combination of ingredients

through several methods and their structural characterization by different techniques (SAXS, Cryo-TEM, Zeta Potential and DLS, for instance) to propose new systems for oil loading. Despite expanding the potential of applications for those materials, the results can provide important insights for tuning their properties by controlled preparation parameters and for the physical chemistry of colloids.

CHAPTER 2

THESIS GOALS AND OUTLINE

2.1. Goals

The goal of this study is to design, synthesize, and characterize various soft materials using triblock copolymers for loading of hydrophobic ingredients into aqueous formulations. The study aims to evaluate the influence of the copolymer structure on the stability and properties of the resulting materials by employing straightforward preparation methods. Different systems have been produced, in which poloxamers were used in different ways. Therefore, the specific goals include:

- Formation core-shell hydrogel particles using a cationic polymer, poly(diallyldimethylammonium chloride) (PDADMAC), combined with anionic OCNF, using triblock copolymers as a way to enhance oil loading.
- Production and oil loading of micro- and nanoparticles by using triblock copolymer to disperse a lamellar phase formed by an anionic surfactant, sodium lauryl sulfate (SDS) and various fatty alcohols or acids.
- Production and oil loading of nanoparticles by electrostatic complexation of a cationic surfactant, hexadecyltrimethylammonium bromide (CTAB) with an anionic polyion, polyacrylic acid (PAA), in the presence of triblock copolymers.

2.2. Thesis outline

This doctoral thesis comprises three foundational Chapters (1 to 3), which present the ‘Introduction’, ‘Thesis goals and outline’, and ‘Materials and methods’, three ‘Research chapters’ written as independent articles (4 to 7), a chapter of ‘General conclusions of the thesis’ (7) and a final chapter of ‘Bibliography’ (8), where the references for all chapters were consolidated to avoid redundancy. Hence, each ‘Research chapter’ includes an abstract, introduction, methodology, results and discussion, conclusion, and supplementary materials. The ‘Research chapters’ were interconnected through the overarching aim and objectives of the thesis, with each article addressing and building upon limitations identified in the preceding chapter. The figures, tables, and equations were numbered according to the chapter in which they appear, followed by their sequence number on the text, to facilitate navigation through the thesis.

Chapter 1 – Introduction, fundamentals, and literature background

The chapter describes general points important to the comprehension of the thesis regarding different colloidal systems for oil incorporation, including liquid crystals, lamellar phases induced by fatty alcohols, nanoparticles of oppositely charged polymers and surfactants, and the use of poloxamer.

Chapter 2 – Thesis objectives and structure

The current chapter includes the goals and thesis organization.

Chapter 3 – Methodology

This chapter focused on the general methodology of all the chapters.

Chapter 4 - Triblock copolymer micelles for oil loading in core-shell hydrogel capsules of oppositely charged cellulose nanofibers and polyelectrolytes

This chapter is the first version of the manuscript of the study involving oxidized cellulose nanofibrils (OCNF) and poly(diallyldimethylammonium chloride) (PDADMAC) to create stable core-shell particles (CSHCs) through charge-driven complexation, integrating triblock copolymers to enhance oil incorporation. The text has not been revised by all the other co-authors yet. This research was initiated and mainly carried out during a six-month internship in the laboratory of Prof. Karen Edler at Lund University (Sweden), funded by the Institutional Program for Internationalization (CAPES PrInt).

Chapter 5 – Triblock copolymers nanoparticles obtained by a dispersion of lamellae phase composed by sodium lauryl sulfate and different co-surfactants.

This chapter describes the investigation of liquid crystalline phase dispersions to address viscosity-related limitations and expand their application range. By combining SDS, fatty alcohols or acids, and a triblock copolymer, the study addressed the impact of the fatty chain length and poloxamer on particle size and stability, as well as the effect of mineral oil incorporation on dispersibility and stability. This study was exclusively conducted in Brazil in partnership with Oxiteno through the DAI Program (from the Portuguese: *Doutorado Acadêmico para Inovação*) funded by CNPq. The manuscript related to this chapter has been revised by most of the co-authors and will be submitted after incorporating the suggestions from the evaluators of this thesis.

Chapter 6 – Oppositely Charged Polymers-Surfactants Nanoparticles Stabilized by Triblock Copolymers for Enhanced Oil Loading

The manuscript related to this chapter has been submitted to a scientific journal in the field of colloids, revised by 4 referees, altered according to their suggestions, and is awaiting the final decision of the editor. This study investigates nanoparticle formation with hexadecyltrimethylammonium bromide (CTAB), poly(acrylic acid) (PAA), and various EOxPOyEOx copolymer, and how this combination affected oil loading in these systems. Some experiments

described in this charter were performed at Lund University, but most at PUC-Rio.

Chapter 7 – Cocamidopropyl betaine can behave as a cationic surfactant and electrostatically associate with polyacids of high molecular weight.

This chapter is a scientific paper [76] which was, chronologically, the first part of the PhD, before starting the partnership with Oxiteno. It is described as a zwitterionic surfactant that, by electrostatically complexing with an anionic polymer, behaves like a cationic surfactant. This behavior elucidates structures and phenomena explored in systems like those described in Chapter 6. Hence, this part is not related to the use of poloxamers, not aligning directly with the main goal of this thesis. However, the deviation from the original focus was towards following the opportunity of this collaborative project with Oxiteno. Nevertheless, the study was conducted within the timeframe and scope of the doctoral project and has been included in this thesis.

This study investigates the occurrence of phase separation in mixtures between cocamidopropyl betaine (CAPB) and polyanions and how different chain lengths impacted it. Combining different techniques allowed the understating of how nanoscale structures can impact the macroscopic behavior of this mixture.

Chapter 8 – General Conclusions

This chapter combines the conclusions of the different research chapters and links them to the goal of the thesis.

Chapter 9 – Bibliography

This chapter merges the list of all references cited in the thesis.

CHAPTER 3

MATERIAL AND METHODS

3.1 Materials

The materials used in this study included triblock copolymers, $EO_{90}PO_{60}EO_{90}$, $EO_{20}PO_{60}EO_{20}$, $EO_{10}PO_{30}EO_{10}$, and $EO_{04}PO_{30}EO_{04}$, with detailed information available in **Table 3.1**, sodium lauryl sulfate, SDS, and different co-surfactants, cetyl alcohol ($C_{16}OH$), myristyl alcohol ($C_{14}OH$), lauryl alcohol ($C_{12}OH$), octanol (C_8OH), caprylic/capric acid ($C_8/C_{10}COOH$) and CAPB in the form of Oxitaine CP 30 CM (28 wt % in aqueous solution, with 5 wt % of NaCl), generously provided by Oxiteno. Additionally, hexadecyltrimethyl ammonium bromide, CTAB, of ≥ 98% purity, along with polyacrylic acid with two different molecular weigths and degrees of polymerization, PAA 1.8 KDa and PAA 450 KDa, poly(diallyldimethylammonium chloride), PDADMAC, with a molecular weight of 75 KDa, poly(sodium 4-styrenesulfonate) (NaPSS), Mw = 70 kDa, DP ~ 340, 99.9% purity and NaCl were purchased from Sigma-Aldrich at the highest purity available.

Ultrapure water, obtained from Direct-Pure UP Rephile with a conductivity of 18.2 MΩ·cm, was employed for sample preparation. Eucalypt oil (EOil), Bergamot oil (BOil), Sunflower oil (SFOil), Mineral oil (MOil) and Uvinul were acquired from viaAroma, Giroil and Neon respectively.

Oxidized cellulose nanofibrils (OCNF) were prepared via 2,2,6,6-tetramethylpiperidinyloxy (TEMPO)-mediated oxidation as previously reported [77], resulting in a solid paste of ca. 8 wt % in water with a degree of oxidation of 25%. The OCNF was further purified via dialysis under DI water to remove any salt and preservatives. Briefly, approximately 20 g of OCNF slurry was dispersed in 100 mL of deionized water and stirred at room temperature for 30 min. The OCNF dispersion was dialyzed against ultrapure water for 5 days (medium replaced twice daily), using cellulose dialysis tubing molecular weight cut-off (MWCO) 12,400. Finally, the purified OCNF dispersion was freeze-dried.

Table 3.1: Names, weight fraction of ethylene oxide (EO%), average molecular weight (Mw) and hydrophilic-lipophilic balance (HLB) of the triblock copolymers provided by Oxiteno.

Triblock colymers	Trade Name	Poloxamer Name	EO%	Mw (kD)	HLB
$EO_{90}PO_{60}EO_{90}$	Ultraric PE 127	Poloxamer 127	70%	11.43	21
$EO_{20}PO_{60}EO_{20}$	Ultraric PE 334	Poloxamer 334	35%	5.26	15
$EO_{10}PO_{30}EO_{10}$	Ultraric PE 64	Poloxamer 184	35%	2.64	13
$EO_{04}PO_{30}EO_{04}$	Ultraric PE 62	Poloxamer 182	17%	2.11	7

3.2 Experimental Section

3.2.1.Samples Preparation

For sample preparation, the methodology was specified in each chapter according to its content, as different methods were used for each study.

3.2.2. Samples Characterization

This section briefly describes the characterization techniques used throughout the different parts of this thesis.

Visual inspections were used to determine the occurrence of phase separation and registered by photographs. Particle size was measured using Laser Diffraction (LD) using a Mastersizer 3000E (Malvern Instruments Ltd., Br) or Dynamic Light Scattering (DLS) using an SZ-100 Nanopartica instrument from Horiba which is also equipped to perform Zeta Potential measurements. Specific parameters were described in the studies chapters.

SAXS measurements were performed at the Institute of Physics of the University of São Paulo (IF-USP). The used instrument was Xenocs Xeuss

Version 2.0, equipped with a Dectris Pilatus 300k. The beam wavelength employed was 0.154 nm (CuKα line). Each sample was positioned in a capillary sample holder and measured for 5400s. The distance between the sample holder and the detector was 0.2 m, resulting in a q range between 0.2 and 7.2 nm^{-1}. The software Fit2D [78] and SuperSAXS package [79] allowed the subtraction of background and solvent (pure water) and integration of the obtained images. The resulting curves of intensity, denoted as *I(q)*, as a function of scattering vector *q*, were analyzed using OriginLab, the relative peak position was used to determine the correlation distance, $d = 2\pi/q$, by using the q value of the peak.

Cryo-TEM was used at the Brazilian Nanotechnology National Laboratory (LNNano). The samples were diluted to 2 mg $mL^{-1,}$ and a 3 uL droplet was deposited on a 300-mesh lacey carbon-coated copper grid. Samples were prepared in an automated vitrification system (Vitrobot Mark IV, FEI, Netherlands) with a blot force of 0 and a blot time of 3 s. The images were obtained using a TALOS F200C (ThermoFisher Scientific, Oregon, USA) equipped with a 4k x 4k CMOS camera, operating at 200 kV. Particle size was determined by analysing 100 particles for each sample. Optical microscopy was also employed to analyze samples containing particles in the micrometer range. A Bel Photonics XPL-3220 microscope, equipped with a CCD digital camera, was used to capture images under both normal and polarized light to detect birefringence. The presence of a shiny appearance indicates anisotropy, a characteristic feature of the lamellar phase.

Differential Scanning Calorimetry (DSC) experiments were conducted using the N-DSC III calorimeter (TA Instruments, USA) in the temperature range from 10 to 80 °C with a heating rate of 30 °C/hour at LNBio-CNPEM, proposal 20230820. The calorimetric cells were filled with water equilibrated at 10 °C for 10 minutes and examined repeatedly in the range of 10–80 °C until the baseline was reproducible.

CHAPTER 4

Triblock copolymer micelles for oil loading in core-shell hydrogel capsules of oppositely charged cellulose nanofibers and polyelectrolytes

Matheus Ouverney Ferreira[a], Karina Oliveira Lima[a], Bradley Green[b], Laura Deeming[b], Bruna. C. Leopércio[b], Marcio. S. Carvalho[b], Karen J. Edler[c], Ana Maria Percebom[a]*

[a] Department of Chemistry, Pontifical Catholic University of Rio de Janeiro (PUC-Rio), 22451-900, Rio de Janeiro, RJ, Brazil

[b] Department of Mechanical Engineering, Pontifical Catholic University of Rio de Janeiro (PUC-Rio), 22451-900, Rio de Janeiro, RJ, Brazil

[c] Department of Chemistry, Center of Analysis and Synthesis, Lund University, 2228734, Lund, Sweden

*Corresponding author: apercebom@puc-rio.br

Abstract

This study employed oppositely charged cellulose nanoparticles and polyelectrolytes in the presence of triblock copolymers to create millimetric stable core-shell hydrogel capsules particles (CSHC) containing micelles capable of oil loading. The CSHC were formed through charge-driven complexation by extruding a dispersion of anionic oxidized cellulose nanofibrils (OCNF) into a solution containing the cationic poly(diallyldimethylammonium chloride) (PDADMAC) and triblock copolymers of poly(ethylene oxide)-poly(propylene oxide)-poly(ethylene oxide), $EO_xPO_yEO_x$. The capsules were approximately spherical with diameters around 3 mm with a solid-like OCNF-PDADMAC shell of approximately 1 μm, as revealed by optical microscopy. The liquid core was an aqueous OCNF suspension with $EO_xPO_yEO_x$ micelles capable of loading and releasing hydrophobic substances. SAXS data indicated that the $EO_xPO_yEO_x$ did

not affect the capsule structure and the shell morphology. The CSHC maintained stability over three months in saline environments. Microfluidics was employed to produce smaller (~ 0.5 mm) and more monodisperse CSHC than the ones obtained by dropwise extrusion. This study indicates that the preparation of CSHC through charge-driven complexation can be extended to various combinations of oppositely charged cellulose nanoparticles and polyelectrolytes. Besides, their high stability, effective oil loading, and controlled release make CSHC suitable for various applications related to encapsulation and delivery of active ingredients.

Keywords

Poloxamers, hydrogels, cellulose, complex precipitate, oil loading.

4.1 Introduction

Combining oppositely charged polyelectrolytes usually leads to a seggregative phase separation. They form a phase rich in an electrostatic complex of polyelectrolytes and a diluted phase containing the uncomplexed polyelectrolytes [59]. This behavior is driven by favorable mixing enthalpy and increased entropy due to counterion release [2,57,80,81]. The complex of polyelectrolytes can be liquid (complex coacervate) or solid (complex precipitate) [82].

Complex precipitates can be used to form microcapsules, offering a versatile way to encapsulate, protect, and release active ingredients [83]. For instance, Kim et al. [84] fabricated stimuli-responsive polyelectrolyte microcapsules, in a single-step method based on the interaction between polyacrylic acid and branched poly(ethylenimine), capable of loading both hydrophilic and hydrophobic materials, with release triggered by ionic strength. Zou et al. [85] established a straightforward method to control the formation of w/w droplets in microfluidic systems by charge driven complexation between oppositely charged ingredients, whereas the size and uniformity of the droplets

were controlled by fine-tuning the flow of the device. A model enzyme was incorporated and released for 25 h without losing its enzymatic activity.

Although microcapsules have an extensive range of applications as carriers and release vehicles, the vast majority are manufactured using nonbiodegradable polymers obtained from nonrenewable sources [86,87]. However, with the growing awareness of microplastics and green chemistry, polysaccharide-based microcapsules have attracted considerable attention as biodegradable and renewable materials such as cellulose [88,89]. Furthermore, complex coacervates and precipitates can also form when soluble polyelectrolytes mix with colloidal dispersions [90]. Cellulose is the most abundant organic polymer on Earth, and the large agro-industrial residues in Brazil have been used as a source for nanocellulose [91]. The high density of surface hydroxyl groups on nanocellulose enables various chemical functionalization's such as oxidation and cationization [67,69,71,74]. Incorporating a specific amount of charge density on its surface is crucial to provide the necessary electrostatic repulsion forces for the proper dispersion of fibers and to open avenues for new applications. Calabrese et al. [75] showed the formation of capsules based on the charge-driven complexation by dropping cationic cellulose nanofibril into a solution of an anionic polyelectrolyte. The complex precipitate instantaneously formed a shell surrounding an aqueous suspension of cellulose nanofibrils. These capsules could incorporate enzymes and were used for catalysis nucleation. In the present study, we used different materials to adapt this methodology, allowing the encapsulation of hydrophobic ingredients and demonstrating its versatility.

In this study, we used the interaction between anionic oxidized cellulose nanofibrils, OCNF, and the cationic polymer poly(diallyldimethylammonium chloride), PDADMAC, to fabricate stable millimetric core-shell hydrogel capsules (CSHC). Besides, triblock copolymers of poly(ethylene oxide)-poly(propylene oxide)-poly(ethylene oxide), $EO_xPO_yEO_x$, were also incorporated into these systems to provide hydrophobic compartments to improve oil loading. Additionally, microfluidics improved the size control of the capsules, which were characterized by optical microscopy, small-angle X-ray scattering (SAXS) and measurements of zeta potential.

4.2. Experimental Section

4.2.1. Materials

Oxidized cellulose nanofibrils (OCNF), with a degree of oxidation of 25%, were prepared as an 8 wt % solid paste in water using 2,2,6,6-tetramethylpiperidinyloxy (TEMPO)-mediated oxidation, as previously described [77]. OCNF paste was further purified by dialysis in ultrapure (UP) water to remove salts and preservatives. Specifically, approximately 20 g of OCNF suspension was dispersed in 100 mL of deionized water and stirred at room temperature for 30 minutes. The OCNF dispersion underwent dialysis against deionized (DI) water using cellulose dialysis tubing with a molecular weight cut-off (MWCO) of 12,400 for 5 days, with the medium being replaced twice daily. After the dialysis period, the water was separated, and its conductivity was measured to confirm equivalence to UP water. The purified OCNF dispersion was then freeze-dried.

0.9 g of freeze-dried OCNF was weighed and added to 45 mL of UP water to prepare a 2 wt% OCNF dispersion. The mixture was stirred at room temperature for 10 minutes. An ice bath was prepared, and the mixture was ultrasonicated with 1-second on/off cycles at 0.6% amplitude (500 Hz) for 10 minutes. This ultrasonication process was repeated three times until the cellulose became completely clear. During the process, the ice bath was refreshed between cycles to prevent the material from overheating.

Triblock copolymers, $EO_{90}PO_{60}EO_{90}$ (Ultraric PE127) and $EO_{04}PO_{30}EO_{04}$ (Ultraric PE62) at the highest purity available, were kindly supplied by Oxiteno and used as received. Poly(diallyldimethylammonium chloride) 20 wt% solution, PDADMAC, (75 kDa), Nile red dye and sodium chloride were purchased from Sigma-Aldrich in the highest purity available. Mineral oil (MOil) was bought from Neon (Brazil).

4.2.2. Sample Preparation

An aqueous OCNF dispersion (2.0 wt %, pH 7) was extruded dropwise (17.8 ± 0.2 µL) into 50 mL of a 4.0 wt % aqueous solution of PDADMAC (pH 6.5) using a syringe fitted with a blunt end polypropylene dispensing tip (Fisnar Inc., gauge 21, inner diameter 0.513 mm) to create the core-shell particles (CSHC). The ratio between OCNF and PDADMAC was calculated based on the molar fraction necessary for complexation, as described in the **SM 4.8.1** section. The tip was positioned approximately 5 cm above the PDADMAC solution–air interface. For some samples, the PDADMAC solution also contained 6.5 wt% of $EO_{90}PO_{60}EO_{90}$ or $EO_{04}PO_{30}EO_{04}$, and the OCNF dispersion also contained 0.1 wt% of mineral oil and Nile red. Up to 50 CSHC were produced in a single PDADMAC batch to maintain this polymer in excess. CSHC was thoroughly rinsed with deionized water (18.2 MΩ cm) to remove any residual PDADMAC before each experiment. A schematic of the CSHC fabrication and their structure is shown in **Figure 4.1**. The obtained capsules were labeled according to their respective starting materials: OCNF-PDADMAC, OCNF-PDADMAC-$EO_{90}PO_{60}EO_{90}$ or OCNF-PDADMAC-$EO_{04}PO_{30}EO_{04}$.

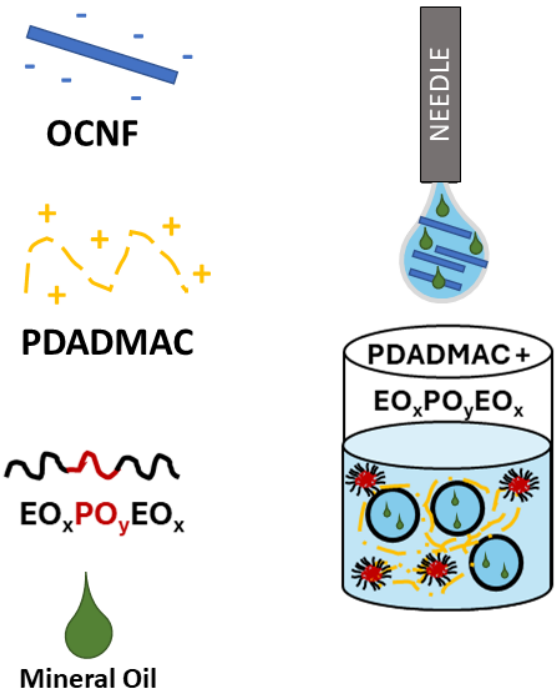

Figure 4.1: Schematic representation of the CSHC fabrication and its structure.

The method of CSHC preparation was also adapted to a microfluidic glass device to reduce and control the size of the capsules. The microfluidic device utilized in this study was designed to facilitate the controlled introduction and mixing of fluids, specifically focusing on the interaction between the OCNF dispersion, triblock copolymer to increase mineral oil incorporation, and PDADMAC to form CSHC. The device's configuration, including round and square capillaries, enabled the precise control of fluid flow and droplet formation. The OCNF 2.0wt% solution flowed through the capillaries and met the continuous mineral oil phase, a crucial step for droplet formation, after that it met the PDADMAC 4.0 wt% - $EO_{90}PO_{60}EO_{90}$ 6.5 wt% mixture. The setup (**Figure 4.2** and **4.3**) includes two types of capillaries: round and square (OD 1.0 mm, ID 0.58 mm, manufactured by World Precision Instruments, Inc.). The round capillaries have an inner diameter of 150 µm, while the square capillaries have an inner dimension of 250 µm. These capillaries are positioned between two microscope slides, with a spacing of 150 µm between them. The overall width of the setup is 1050 µm on one side and 580 µm on the other. Mineral oil and NaCl solution (0.5 mol L^{-1}) were used in the process, where OCNF 2.0wt% droplets are formed and carried through the device. **Figure 4.3** describes where each one of the chemicals were used in microfluids. The resulting particles were collected and further observed under a microscope.

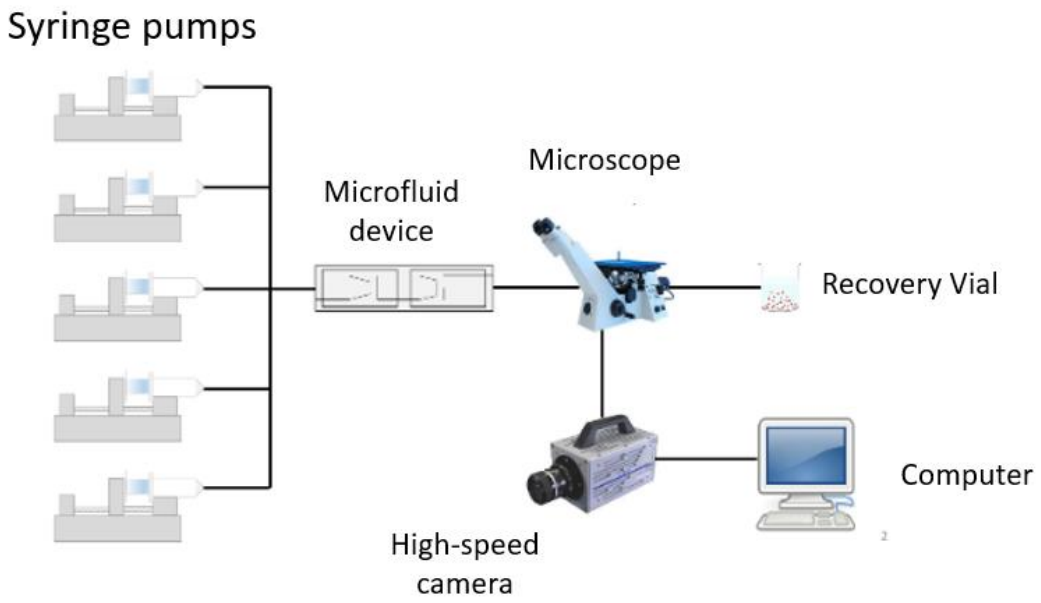

Figure 4. 2: Schematic representation of the experimental microfluidics setup.

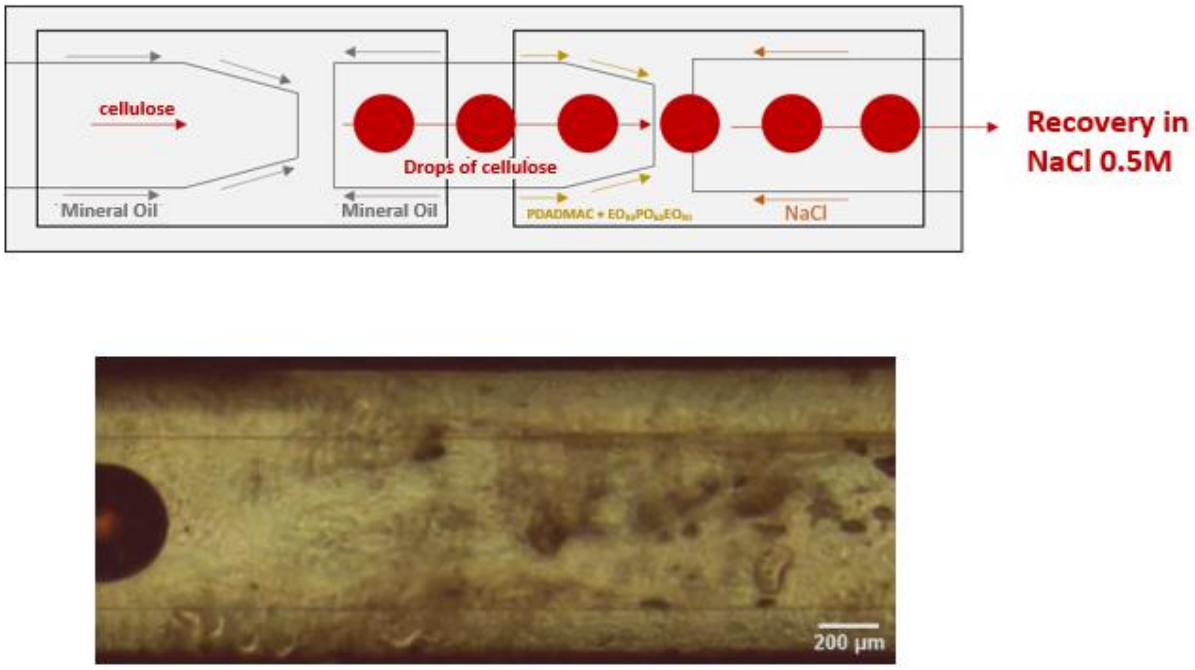

Figure 4. 3: Scheme and image of the microfluidic device used to produce CSHC.

4.2.3. Sample Characterization

The CSHC-shell morphology was visualized by fracturing the CSHC on a glass slide using an optical microscope (Brunel Ltd. SP200 equipped with a Canon EOS 1300D). The intensity profile (in arbitrary units) as a function of distance was measured using the “plot profile” tool in ImageJ, resulting in the size of particles shell.

SAXS measurements were performed using a GANESHA SAXS system (SAXSLAB) at Lund University, using a q-range of (0.1–7 nm^{-1}). Since the entire capsules are too large to fit in the sample holder for in situ analyses and given that they contain both complexed and uncomplexed OCNF, which prevented the individual analysis of both the core and the shell structures, the shell structure was mimicked by pouring, dropwise, 2 mL of OCNF dispersion (2 wt % pH 7) into 50 mL of PDADMAC solution (4.0 wt % pH 6.5) under continuous stirring, allowing complete complexation of the oppositely charged moieties. In some cases, PDADMAC also contained $EO_{90}PO_{60}EO_{90}$ or $EO_{04}PO_{30}EO_{04}$ (6.5 wt%). The complex precipitate was then rinsed with DI water to remove any excess of uncomplexed PDADMAC and centrifuged. These samples were placed in thermostated sandwich holder with disposable mica window, connected to a circulating water bath to maintain the temperature at 25 °C. SAXS pattern of the OCNF dispersion (2.0 wt %) was obtained after loading the suspension into glass capillary tubes (Capillary Tube Supplies Ltd.) of 1.5 mm external diameter. The data were collected with a total acquisition time of 10800 s in a vacuum chamber. All the scattering data were background subtracted and transmission corrected, for the capillary and solvent contribution using the Irena package from IGOR Pro (Wavemetrics, Inc.) [92].

SAXS curves of pure OCNF and OCNF–PDADMAC complexes were fitted to a model of aggregates composed by semi-flexible cylindrical building blocks, that depends on two parameters, Contour length and Kuhn length, corresponding to the overall length of the fibrils and the persistence length, characteristic node-to-node distance between cylinders, respectively, using the NIST SANS Analysis package also within IGOR Pro (Wavemetrics, Inc.) [92]. This model was used with no modification and couples the form factor of randomly oriented homogeneous cylinders, $P_{cyl}(q) = P_{cyl}(q,R,L)$, with a structure factor, S(q)

= S(q,ξ,D), describing an structure as used by Schmitt et al. [93] to compute the scattering intensity I(q) [94,95]. The major radius of the cylindrical building blocks, in this case, OCNF fibrils, was determined by fitting the scattering pattern of a 2.0 wt% OCNF dispersion in the intermediate-q region [96]. For pure $EO_xPO_yEO_x$ micelles, the data were fitted using a spherical micelle core-shell model. This approach followed the methodology employed by Manet et al. [97]. In this model, the micelle core represents the hydrophobic region composed of PO groups, while the shell corresponds to the hydrophilic region formed by EO groups. To simplify the discussion, we focused on two key parameters: the core radius and the shell radius. Electron densities for both regions were calculated using the NIST Scattering Length Density Calculator (National Institute of Standards and Technology). The calculated values were verified by comparison with the literature data reported by Manet et al. [97], ensuring consistency and reliability of the model. Samples containing OCNF-PDADMAC and $EO_xPO_yEO_x$ were treated using both the semi-flexible cylinder model and the spherical micelle core-shell model, as neither of them alone was sufficient to explain the data. This analysis was processed using the NIST SANS Analysis package within IGOR Pro (Wavemetrics, Inc.) with the curve addition mode.

The swelling/shrinking of the CSHC was monitored immediately after fabrication by rinsing and placing them in quartz cuvettes (1 × 1 cm) containing 1 mL of different aqueous media: DI water; PDADMAC (4.0 wt%); PDADMAC (4.0 wt%) with $EO_{90}PO_{60}EO_{90}$ or $EO_{04}PO_{30}EO_{04}$ (6.5 wt%); or NaCl (0.5 mM). The CSHC behavior was imaged over time using a drop-shape analyzer (DSA30R). The area of the CSHC (A, in pixels) was determined from the images using the "analyze particles" tool in ImageJ and normalized as the ration between Final Area (Af) and Initial Area (Af), where Af is the area of the particle at time fs, the moment that the image was taken, and Ai is the initial area of the particle at time = 0s. In cases where the CSHC ruptured, expelled aggregates were excluded from the calculation of the area of the particle; only the remaining shell fragments were measured. This effect led to significant variations in Af after rupture due to irregular osmotic pressure changes between the CSHC core and the surrounding media. Data were obtained from three independent experiments.

Zeta-potential (ζ) of OCNF was measured using a Malvern Zetasizer Nano ZSP (Malvern, UK) and the Smoluchowski approximation. This approximation is independent of the particle shape for the case of $k \cdot a$ >10, where 1/k is the Debye length, and a is the radius of the rod. Hence, the Smoluchowski equation can be used independently from the particle shape for particles with a small double layer and large a. For the present case of OCNF at different NaCl concentrations, the Smoluchowski equation is expected to be in its limits of validity only in the absence of NaCl (where 1/k would be on the order of a few nanometers) while gaining reliability upon NaCl addition where the Debye length thins and the case of $k \cdot a$ >10 is satisfied [98,99]. OCNF dispersions (0.02 wt %) were prepared in NaCl solutions at different concentrations and placed in the folded capillary electrode cell. The ζ average values were obtained from four measurements with 100 scans of three samples.

Transmitted light (%) was measured to detect Nile red release using a spectrophotometer Agilent/HP 8553. For measuring it 5 CSHC were placed in a quartz cuvette (Hellma Analytics, 1 x 1 x 5 cm), and the release was monitored at a wavelength of 532 nm over 6000 s.

4.3 Results and Discussion

4.3.1 Morphology of CSHC

When OCNF was extruded dropwise into the polycation solution, the complexation of OCNF-PDADMAC at the droplet interface instantly occurred, forming a CSHC-shell that hinders further migration of PDADMAC into the CSHC-core. Optical micrographs showed a shell of approximately 1 μm thickness for all samples (**Figure 4.4A, 4.4C, 4.4E**) and capsules with a spherical shape and around 3 mm of diameter (**Figure 4.4B, 4.4D, 4.4F**). To calculate the shell thickness, the plot profile tool in ImageJ was used. This tool allowed us to identify regions of constant pixel intensity at capsules' core and in the medium, enabling the determination of the shell thickness, which corresponds to the region where pixel intensity changes[100]. The appearance of the capsules is very similar to the ones obtained by Calabrese et al.[75], indicating that their method can be

extended to different combinations of oppositely charged nanocellulose and polyelectrolytes. The formation of the capsule was confirmed upon its rupture, revealing an interior composed of hydrogel and a shell with a distinct structure. Hence, CSHC can be depicted by a spherical capsule formed by OCNF-PDADMAC complex shell containing an aqueous dispersion of uncomplexed OCNF in the core. Although the images showed different roughness levels, it could be attributed to water drying on the microscope slide. The subtle differences noted among the samples with or without $EO_xPO_yEO_x$ copolymers were related to the shape of the drop, which determined the shape of the capsule. Hence, the copolymers did not cause relevant differences in the size or structure of CSHC shells and were probably solubilized in the capsule interior.

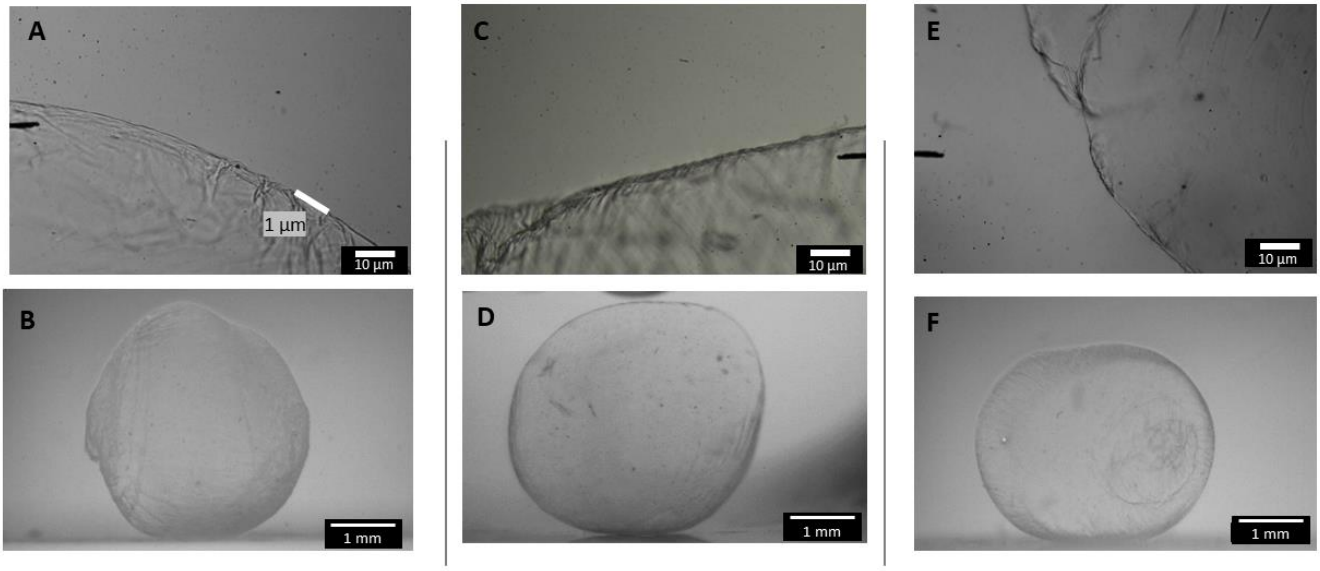

Figure 4.4 Images from optical microscopy of the CSHC-shell (top) and the entire capsule (bottom) of: **A-B)** OCNF-PDADMAC; **C-D)** OCNF-PDADMAC-$EO_{04}PO_{30}EO_{04}$; and **E-F)** OCNF-PDADMAC-$EO_{90}PO_{60}EO_{90}$.

SAXS curves (**Figure 4.5**) of OCNF were fitted using a flexible ellipsoidal cylinder model, commonly applied to describe worm-like micelles [101]. In this model, we assumed that the cellulose nanofibers exhibit some flexibility along their length, with points of contact between the fibrils. This model had already been used to fit curves from complexes of cellulose nanofibrils[93,102,103]. In

this model, the scattering contribution of OCNF was associated with the flexible length of the cylinders, which depended on two parameters: the Kuhn length and the contour length. The Kuhn length was correlated with twice the persistence length, indicating the flexibility of the fibril and, as described by Schmitt et al.[93], associated with the mesh size of the cellulose network. The contour length, on the other hand, was related to the overall length of the fibrils. The contour length was fixed as 160 nm for all samples. This value was chosen based on the length of OCNF obtained by TEM images [96].

For OCNF-PDADMAC, **Figure 4.6**, we observed that shell preserved the scattering contribution related to OCNF cross-section, with some inclination difference at low-q range. Elongated objects, such as OCNF, usually present a scattering intensity decay proportional to q^{-1}, but it was proportional to q^{-2} for CSHC, indicating a strong interaction between the fibrils forming the shell.

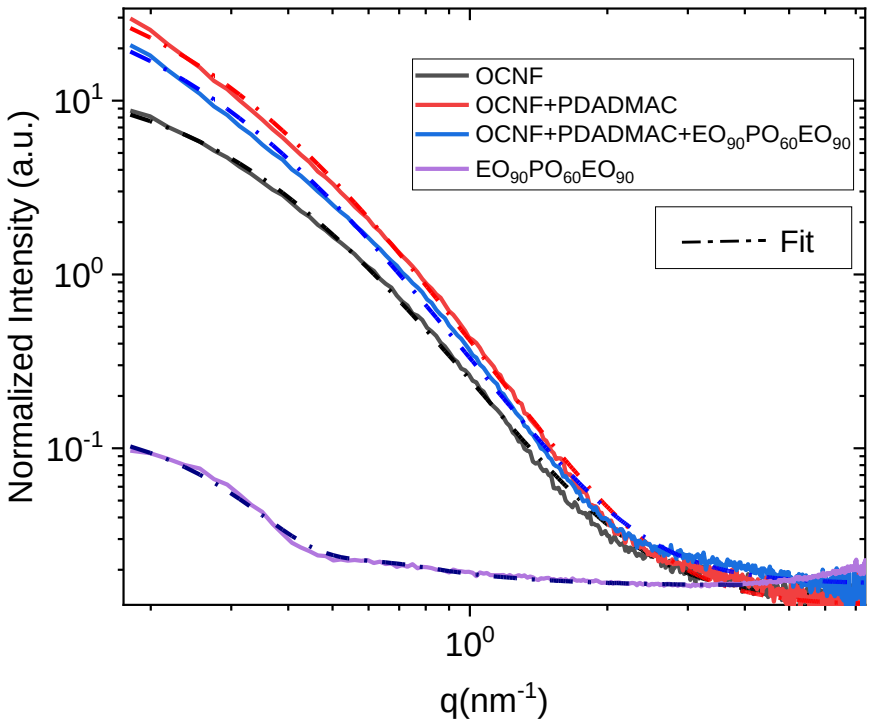

Figure 4.5: SAXS curves of aqueous suspensions of OCNF (2 wt %) and OCNF–PDADMAC (4.0 wt%) with and without $EO_{90}PO_{60}EO_{90}$ (6.5 wt %).

SAXS of CSHC data were also fitted to a model of flexible ellipsoidal cylinder, resembling OCNF, as building blocks (**Figure 4.5**). The contribution of PDADMAC was not included due to its negligible contribution to the scattering intensity. As already mentioned, $EO_{90}PO_{60}EO_{90}$ micelles were fitted as spherical micelles composed by a core-shell structure, with the core consisted of hydrophobic PO groups and the shell formed by hydrophilic EO groups. The fitting revealed a core radius of 4.2 nm and a shell thickness of 5.1 nm, consistent with previously reported values in the literature.[97,104]

For OCNF-PDADMAC-$EO_{90}PO_{60}EO$ we observed that upon poloxamer addition only the flexible ellipsoidal cylinder model was not enough to treat the data, and a micelle core-shell model was added to it by using the sum up mode of IGOR software, showing that poloxamers were presented as micelles in the mixture. The values obtained by fitting SAXS data were described at **Table 4.1**

Table 4.1: Values obtained by fitting SAXS data from dispersions of OCNF, OCNF+PDADMAC and OCNF-PDADMAC-$EO_{90}PO_{60}EO_{90}$ to a flexible ellipsoidal cylinder model.

	OCNF	**OCNF-PDADMAC**	**OCNF-PDADMAC-$EO_{90}PO_{60}EO_{90}$**
Contour Length (nm)	160	160	160
Kuhn Length (nm)	30 ± 2	6.3 ± 0.5	6.5 ± 0.3
Major Radius (nm)	4.1 ± 0.5	4.5 ± 0.4	4.5 ± 0.4
Core Radius (nm)	NA	NA	4.2 ± 0.5
Shell Radius (nm)	NA	NA	5.1 ± 0.6

The Kuhn length obtained from the fittings, representing the characteristic distance between nodes in the OCNF, decreased with complexation to PDADMAC. This suggests that the addition of the polycation brought the OCNF closer together due to electrostatic attraction, indicating that the cellulose network became more compact, reducing their flexibility and mesh size. The major radius

also exhibited a slight increase, which could be attributed to the adsorption of the polymer onto the fibrils.

When comparing the results of fittings combining the spherical micelle core-shell model with the flexible cylinder model for the mixture of OCNF-PDADMAC, we observed that OCNF-PDADMAC retained the same structure, while the copolymer formed micelles of approximately 10 nm in size. This result aligns with previous reports on copolymer micelles [105]. Furthermore, we concluded that upon the addition of copolymers the structure of CSHC was the same, therefore, the triblock copolymers did not affect CSHC structure, but mainly created hydrophobic compartments inside the capsules due to the presence of micelles.

Based on the results, we propose that the CSHC consists of a 1 µm shell composed of OCNF-PDADMAC, formed through charge-driven complexation as indicated by our SAXS data. Inside, the core was an OCNF hydrogel matrix containing $EO_xPO_yEO_x$ micelles, that could be used for oil loading, as described in **Figure 4.6**.

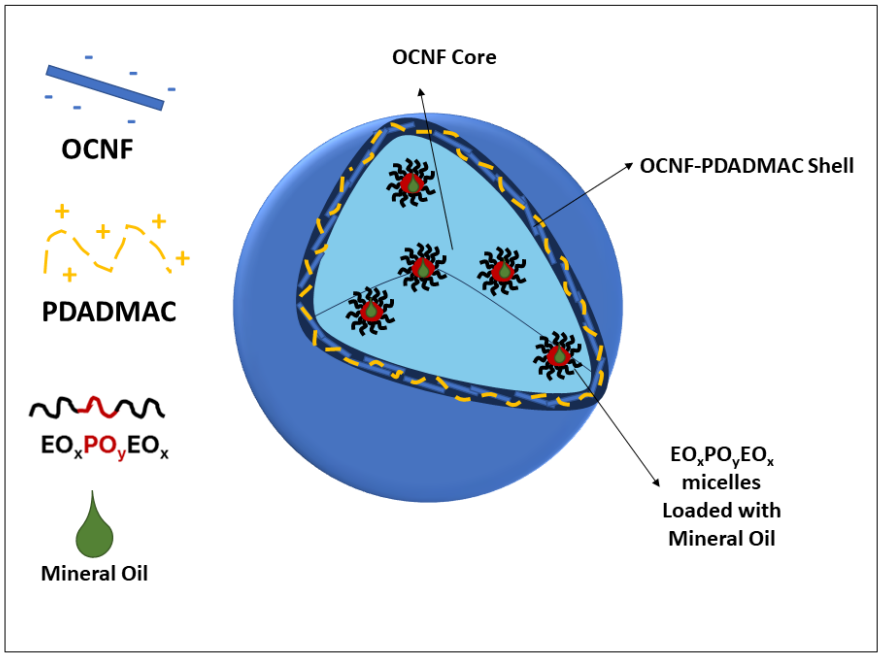

Figure 4. 6: Schematic representation of CHSP particles, featuring a shell composed of complexed OCNF-PDADMAC and a core consisting of uncomplexed OCNF and triblock copolymer micelles, with mineral oil loaded.

4.3.2 Swelling/shrinking behavior and stability

CSHC swelling and shrinking behavior were monitored over time, showing that their stability was highly dependent on the medium. The CSHC shell shrunk in aqueous solution of PDADMAC (4.0 wt%) or PDADMAC (4.0 wt%) with $EO_{90}PO_{60}EO_{90}$/$EO_{04}PO_{30}EO_{04}$ (6.5 wt%) between 0 and 2000s, but in different rates (**Figure 4.7A-B**). Differences in osmotic pressure could cause this effect because the molar concentration of $EO_xPO_yEO_x$ was different in the three systems (0, 5, and 28.5 mmol L^{-1}, respectively). Hence, the shrinking rate increased with the molar concentration. CSHC swelled in DI water, causing shell rupture and leakage after 1600 s (**Figure 4.7C-D**). The same behavior was observed by Calabrese et al.[75], but with a fracture 2x faster, suggesting that the interaction of OCNF-PDADMAC was stronger. Moreover, CSHC was stable for at least three months in aqueous solution of NaCl (>0.5 mmol L^{-1}) even in the presence of $EO_xPO_yEO_x$ copolymers (**Figure 4.7E-F),** with minimal shrinking up to 1000s, which can be related to electrostatic interactions between charged moieties.

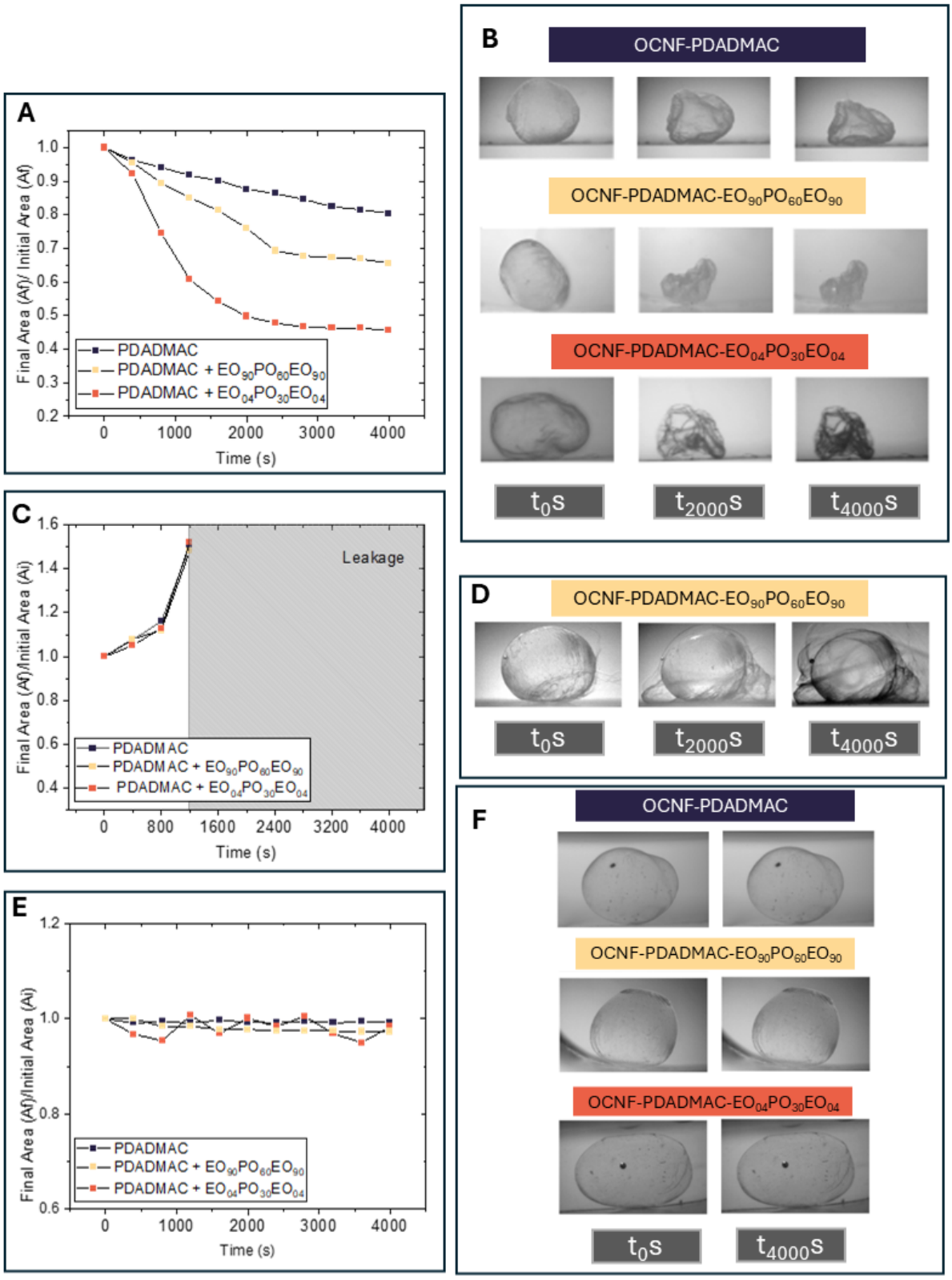

Figure 4.7*:* Relative areas and photographs of CSHC over time to verify their swelling or shrinking behavior in different media: **A-B)** PDADMAC 4 wt% or PDADMAC-$EO_{90}PO_{60}EO_{90}$/ $EO_{04}PO_{30}EO_{04}$ 6.5 wt%, **C-D)** Deionized (DI) Water **E-F)** Solution of NaCl 0.5 mol.L^{-1}.

According to a previous study, NaCl can enhance or hinder the interfibrillar interactions within OCNF in the core [106]. ζ values were measured at different concentrations of NaCl. In DI water, OCNF showed a ζ = -42 mV, and upon NaCl addition, this value approximated to zero (**Figure 4.8A**), indicating shielding of the negatively charged moieties. Hence, adding NaCl can reduce electrostatic repulsion between fibrils, resulting in more attractive interfibrillar interactions, which could strengthen the CSHC shell. This effect could explain the high stability of CSHC in NaCl 0.5 mM at 80 °C for at least a week, as shown in **Figure 4.8B**.

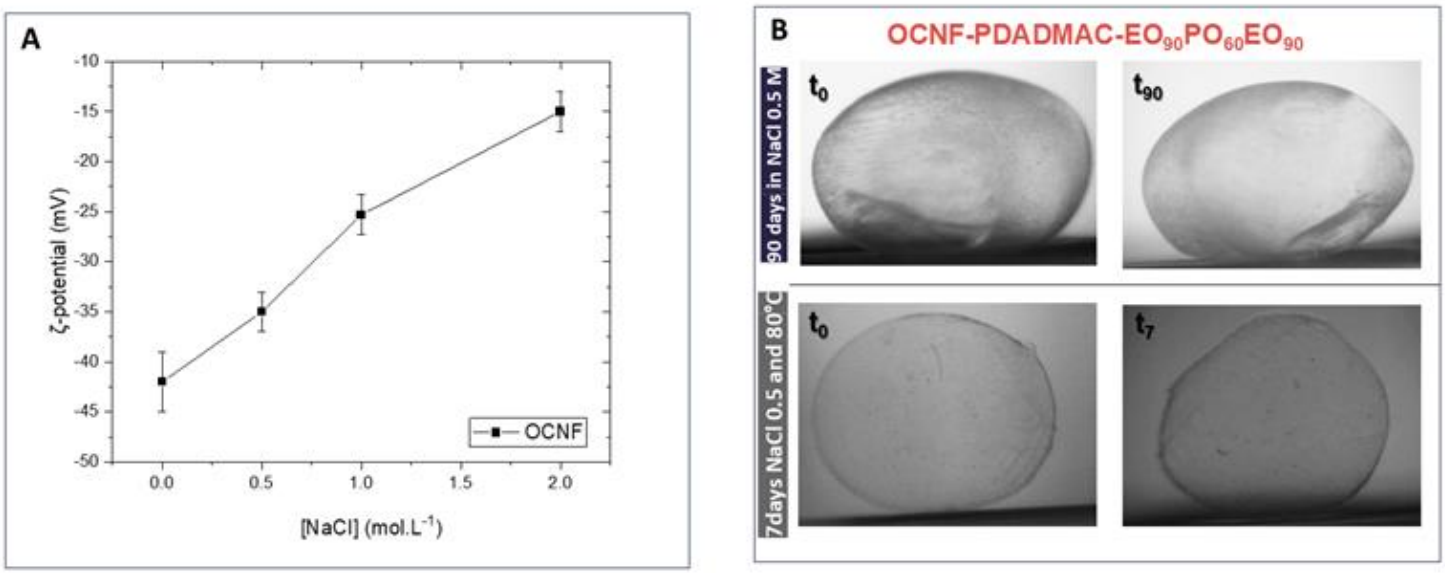

Figure 4.8: A – Zeta potential values of OCNF at different concentrations of NaCl in water. **B** – Photographs of OCNF-PDADMAC-EO90PO60EO90 capsules in NaCl 0.5 mol L^{-1} at room temperature or 80 °C after different periods.

4.3.3 Capsules for oil loading

Nanocellulose hydrogels have been widely used to load and deliver active substances[107]. However, maintaining the encapsulation over extended periods remains a significant challenge, hindering their practical use and recyclability. We investigated the oil loading capacity of CSHC particles with and without $EO_{90}PO_{60}EO_{90}$ or $EO_{04}PO_{30}EO_{04}$. As expected, CSHC with $EO_xPO_yEO_x$ was efficient in loading Mineral oil and a lipophilic dye (Nile red), whereas the ones

without $EO_xPO_yEO_x$ were not (**Figure 4.9**). Without the $EO_xPO_yEO_x$ we didn't observed the formation of CSHC, where the oil and the structure remained dispersed in the interface. Therefore, the triblock copolymers played a crucial role in facilitating the formation of CSHC, likely due to micelle formation in the core, which ensured efficient oil loading within the particles, or the increased viscosity of PDADMAC + $EO_xPO_yEO_x$ mixtures, which may have contributed to improved CSHC formation.

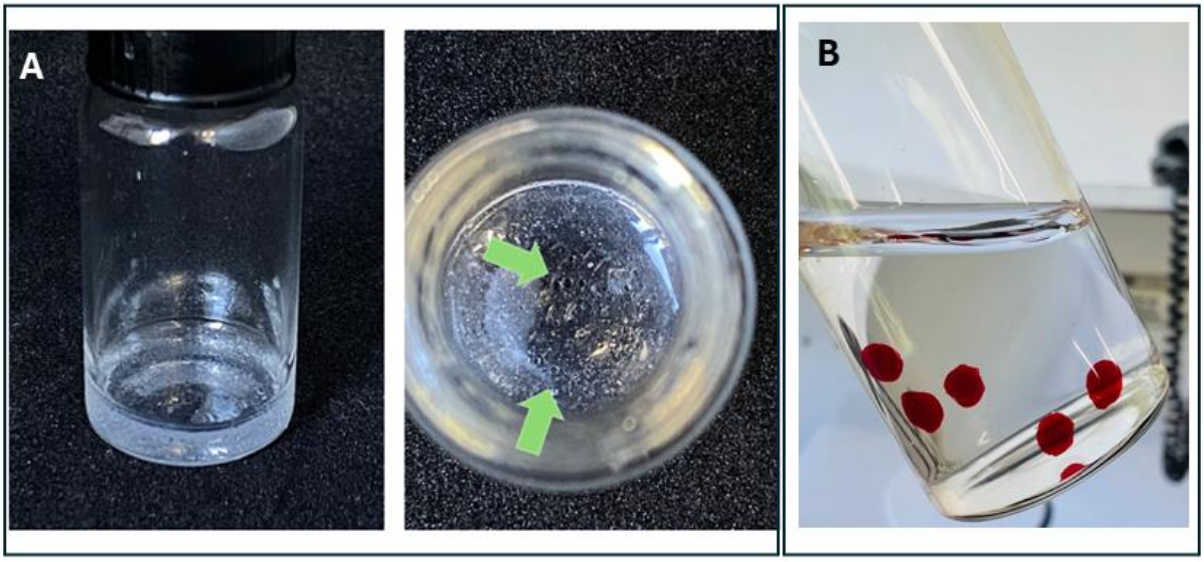

Figure 4.9: Photographs of **A)** Samples where Mineral Oil was added into an OCNF dispersion. **B)** OCNF-PDADMAC-$EO_{90}PO_{60}EO_{90}$ capsules loaded with mineral oil and the lipophilic dye, Nile red.

The release of Nile red into the medium was monitored by the absorbance at 532 nm (**Figure 4.10**) after adding CSHC into UP water. Both CSHC released dye until 2000 s, with a typical diffusion-controlled release behavior, where the release rate decreases over time as the concentration gradient driving the diffusion diminishes. The similarity observed between the absorbance graphs in the presence of the two poloxamers indicated that different types of copolymers could achieve the same release outcome. This suggested that more than one type, regardless of its chemical characteristics, was compatible with the capsule.

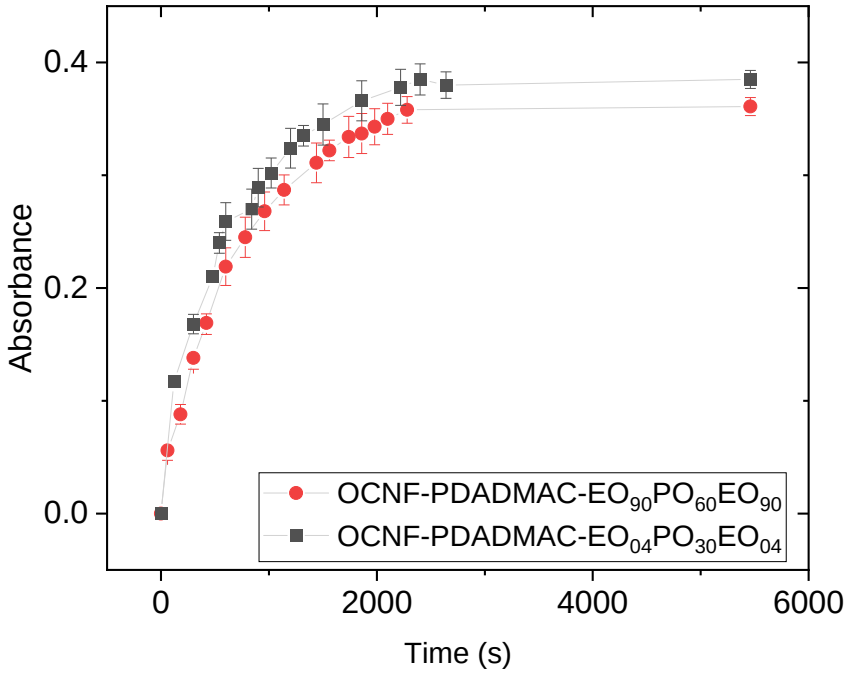

Figure 4.10: Absorbance measurements ate 532 nm over time to verify Nile red release from OCNF-PDADMAC-$EO_xPO_yEO_x$ capsules.

4.3.4 Production of core-shell OCNF particles in microfluidics devices

Adapting the extrusion method for microfluidics allowed for obtaining of CSHC with smaller and monodisperse sizes, keeping their capability to load hydrophobic ingredients (**Figure 4.11**). The CSHC obtained by microfluidics exhibited an average size of 500 µm, 6 x smaller than those obtained by the dropwise extrusion (**Figure 4.11**). The final collection in NaCl solution kept the capsules stable, and they are currently being studied in terms of controlled release. These results revealed more possibilities of adapting the method of obtaining CSHC by combining oppositely charged nanocellulose and polyelectrolytes to control their properties according to the desired application.

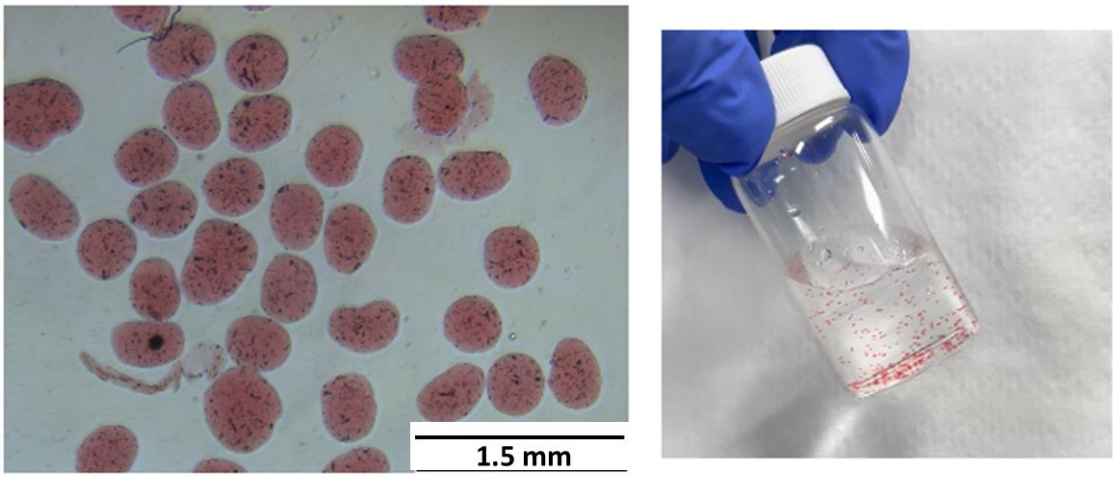

Figure 4.11: A) Image of optical microscopy and **B**) photograph of OCNF-PDADMAC-$EO_{90}PO_{60}EO_{90}$ capsules obtained by microfluidics containing mineral oil and Nile red.

4.4 Conclusion

In this study, we obtained spherical core-shell hydrogel capsules (CSHC) capable of oil loading by using a cationic polymer (PDADMAC) complexed with anionic cellulose nanofibrils (OCNF) and triblock copolymers ($EO_xPO_yEO_x$). The use of microfluidics further enhanced the process, enabling the production of smaller (0.5 mm) and more monodisperse capsules compared to the dropwise extrusion method (3 mm). The results indicated that the triblock copolymers had a crucial role in effective oil loading and did not affect the shell. They probably formed micelles in the capsule core to dissolve or disperse hydrophobic substances, as tested with mineral oil and Nile red. SAXS revealed that the shells kept a strong interaction between nanofibrils, which explains their robustness and stability in NaCl solutions, even at high temperatures and after long periods.

The ability to control the size of CSHC through microfluidics and the possibility of obtaining capsules by different combinations of nanocellulose with

oppositely charged polyelectrolytes present new opportunities for tailoring these capsules for specific applications, including loading and controlled release.

4.5 Funding

This study was financed in part by the Brazilian agencies: Conselho Nacional de Desenvolvimento Científico e Tecnológico (CNPq), Fundação Carlos Chagas Filho de Amparo à Pesquisa do Estado do Rio de Janeiro (FAPERJ, Programa Jovem Pesquisador Fluminense E-26/201.674/2021) and Coodenação de Aperfeiçoamento de Pessoal de Nível Superior - Brasil (CAPES, Finance Code 001). KOL received a scholarship from FAPERJ (E-26/203.210/2022/ SEI- 260003/009029/2022). MOF received scholarship from CNPq (140638/2021-0). AMP received a grant from CNPq (304212/2022-9).

4.6 Acknowledgments

We thank Oxiteno for generously providing the triblock copolymers.

4.7 Declaration of Competing Interest

The authors declare that they have no known competing financial interests or personal relationships that could have appeared to influence the work reported in this paper.

4.8 Supplementary material

4.8.1 Definition of the ratio between OCNF and PDADMAC

It’s well documented that the molar ratio and consequently the charge density are key factors to guarantee that a complex coacervation occurs. Therefore, the mole fraction, f, of the oppositely charged species must be calculated to ensure complete complexation of the OCNF with the PDADMAC

across the CSHC/water interface without any free OCNF remaining. This fraction, f, was calculated as shown in **Eq. 1**.

$$f = \frac{m_{OCNF}\alpha_{OCNF}}{m_{OCNF}\alpha_{OCNF} + \frac{m_{PDADMAC}\alpha_{PDADMAC}}{MM_{PDADMAC}}}$$

$$(Equation\ 4.1)$$

In this equation:

• m_{OCNF} is the mass of OCNF used (g).

• α_{OCNF} is the mol/g of carboxyl group functionalization on the OCNF surface, determined to be 0.00154321 mol/g. – using the conductivity titration described below.

• $m_{PDADMAC}$ is the mass of PDADMAC in the solution (g).

• $MM_{PDADMAC}$ is the molecular weight of the PDADMAC repeating unit (161.67 g/mol).

• $\alpha_{PDADMAC}$ =1 since each repeating unit of PDADMAC bears a positive charge.

With m_{OCNF}= 0.032 g, considering 2 wt% of OCNF and m_{OCNF} as the mass required to form 80 capsules, in the medium and to achieve a mole fraction f=0.5, indicating a perfect charge balance between OCNF and PDADMAC, the required mass of PDADMAC was determined as approximately 0.8 wt%, however considering that PDADMAC was sold in a 20 wt% solution, we need approximately 4.0 wt% of it. This ensures that the entire amount of OCNF interacts with the PDADMAC to produce at least 80 capsules.

4.8.2 Conductometric Titration

The degree of oxidation (DO) of OCNF was determined using conductometric titration, as previously described by Habibi et al. Briefly, cellulose samples (50 mg) were suspended in 15 mL of 0.01 mol·L^{-1} HCl solution. After stirring, the suspensions were titrated with 0.01 mol·L^{-1} NaOH. The titration curve are presented in **Figure 4.12**, representing the average of a triplicate. The DO was calculated using the following equation:

$$Equation\ 4.1 \quad DO = \frac{162\ x\ C\ x\ (V_2 - V_1)}{w - 36\ x\ C\ x\ (V_2\ -\ V_1)}$$

Where:

- **C**: NaOH concentration
- **V_1 and V_2**: Volumes of NaOH
- **W**: Weight of the freeze-dried cellulose used
- The value of 36 corresponds to the difference between the molecular weight of the anhydroglucose unit and the sodium salt of the glucuronic acid moiety.

After calculation, we obtained a DO of 25%, which aligns with the expected value as previously reported by Calabrese et al [96].

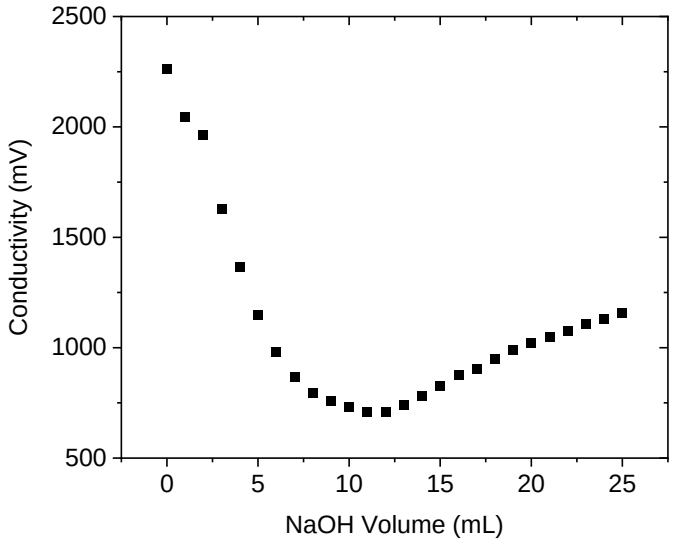

Figure 4.12: Conductimetric Titration curves of OCNF.

CHAPTER 5

In **Chapter 4**, we successfully incorporated small amounts of oil into a system composed of OCNF, PDADMAC, and $EO_xPO_yEO_x$. However, the oil content remained low, and the resulting particles were not at the nanoscale, which would limit their application in targeted delivery systems, for example. Despite the potential of this technology, we chose to explore an alternative approach known for its ability to achieve high oil incorporation and produce nanoscale particles: the lamellar phase.

This chapter focuses on the second study of this thesis, where we investigated lamellar phase dispersions using triblock copolymers in combination with various fatty acids and alcohols. We aimed to develop a system capable of achieving high oil incorporation.

Triblock copolymers nanoparticles obtained by a dispersion of lamellae phase composed by sodium lauryl sulfate and different co-surfactants

Matheus Ouverney Ferreira[a], Lorena Oliveira Pereira[a], Karina Oliveira Lima[a], Ana Maria Percebom[a]*

[a] Department of Chemistry, Pontifical Catholic University of Rio de Janeiro (PUC-Rio), 22451-900, Rio de Janeiro, RJ, Brazil

*Corresponding author: apercebom@puc-rio.br

Highlights:

- Incorporating fatty alcohols into ionic surfactants aids in forming lamellar liquid crystals.
- The introduction of triblock copolymers enhances the dispersion and stability of particles.
- Shorter chain co-surfactant (C_8/C_{10}OOH) produce smaller particle diameters and better dispersion.

- Longer chain co-surfactants (C_{12}-C_{16}OH) result in larger particles with more hydrophobicity.
- Stability tests showed that C_8/C_{10}COOH systems maintained integrity for over 120 days.

Keywords: fatty alcohols/acid, lamellar phase, triblock copolymers, particle dispersions.

Abstract

Liquid crystalline phases formed at high surfactant concentrations exhibit unique properties, such as spontaneous self-organization and a high capacity for incorporating hydrophobic actives. However, their high viscosity can limit their application in products like sprays. This study explores the potential of liquid crystalline phase dispersions to overcome viscosity-related limitations and expand their applications. A lamellar phase was achieved using a combination of sodium lauryl sulfate (SDS), various fatty alcohols or acids, and a triblock copolymer. SDS was mixed with fatty chains to facilitate lamellar phase formation. Different fatty chains were employed to optimize these structures, and their properties were described using various techniques, including microscopy, size distribution, DSC, and X-ray scattering analysis.

Our results indicated that the size of the fatty chain significantly affects particle size and stability. Systems with shorter chain lengths, such as C_8/C_{10}COOH, formed smaller particles, while longer chains like C_{12}OH, C_{14}OH, and C_{16}OH resulted in larger particles and reduced stability. Incorporating mineral oil into the particles via sonication improved dispersibility and reduced particle size, particularly for C_{12}OH and C_8/C_{10}COOH, demonstrating notable stability for over 120 days. Cryo-TEM analysis confirmed the formation of spherical, homogeneous nanoparticles, while DSC and SAXS analyses provided insights into their crystalline structures and phase transitions. Systems containing C_{12}OH and C_8/C_{10}COOH were identified as the most promising for practical applications, demonstrating high stability and effective incorporation of hydrophobic actives.

This study highlights the importance of understanding phase behavior and structural preferences induced by triblock copolymers for optimizing nanoparticle-based delivery systems.

5.1 Introduction

Liquid crystalline phases, formed at high surfactant concentrations, offer numerous advantages such as spontaneous self-organization, high capacity for incorporating hydrophobic actives, and retention of surfactant's versatile and valuable properties [59,108–110]. Dispersions of liquid crystal can expand the possibilities of application to systems like spray or nanoparticles for controlled delivery [111]. Hence, strategies for dispersing liquid crystals in the nanoscale can broaden its range of applications. For instance, diblock copolymers of poly(ethylene oxide)-*b*-poly(methacrylic acid) were combined to a cationic surfactant to concentrate the micelles, forming a liquid crystalline structure by electrostatic complexation but dispersed in nanoparticles due to the hydrophilic EO blocks [56]. These systems presented high oil loading and stability. However, these copolymers are not commercially available on a large scale, which makes it challenging to use these systems in industry.

Another well-known method for forming liquid crystalline structures involves mixtures of surfactants with fatty alcohols or acids [112–115]. These fatty alcohols and acids are commonly used in cosmetics and pharmaceuticals as co-surfactants. Typically, formulations are prepared by heating these alcohols above their melting points, followed by homogenization under heating and cooling to room temperature, which induces crystallization of the alcohols and forms dispersed crystalline structures [116]. Depending on the temperature, chain length, and agitation process, various crystalline structures can form, each providing distinct sensory experiences based on their rheological properties [117]. The varying chain lengths of these fatty components result in the formation of distinct structures. For instance, longer fatty chains increase the surfactant’s critical packing parameter (CPP), favoring the formation of a lamellar phase, and increasing hydrophobicity in the medium. It could influence the dispersibility of

the liquid crystal in aqueous media and its capacity to incorporate oily ingredients [51].

For instance, Fontell et al. [53] studied the lamellar phase in a ternary system containing cationic surfactants, fatty alcohols, and water, which was highly influenced by the chain length of the fatty alcohol. These played a crucial role in determining the phase behavior and structural organization of the system. Short-chain alcohols, such as methanol or ethanol, resulted in a limited presence or even absence of the lamellar phase, confining it to small regions of the phase diagram. As the alcohol chain length increased, as seen with octanol, decanol, and notably n-dodecanol, the lamellar phase became more prominent, occupying a broader central region, and allowing for significant water incorporation. Dodecanol, with its longer carbon chain, further stabilized the lamellar structure and promoted the formation of inverse cubic and hexagonal phases. These phases reflected changes in the system's spontaneous curvature due to the increase in the CPP. The inclusion of dodecanol not only enhanced the structural integrity of the lamellar phase but also supported the formation of more complex phases, expanding the system's potential for applications in solubilization processes and controlled release systems.

Percebom et al. [50] described that the inclusion of long-chain fatty alcohols promoted the stability of the lamellar phase by matching the hydrophobic tail length of the surfactant, thereby enhancing the alignment and packing within the bilayers in systems formed by the surfactant hexadecyltrimethylammonium bromide, C_{16}TAB, or its complex salts formed with polyacrylate, $C_{16}TAPA_{30}$. Using long-chain alcohols rather than short-chain alcohols would reduce the disordering into these systems since alcohols appear to disrupt the CCP, increasing the average distance between surfactant molecules, showing that n-alcohols act as cosurfactants, inducing crystalline structures.

Dispersing the lamellar phase could broaden its application, especially in scenarios where the high viscosity, typical of this structure, is undesirable. In this context. In line with this approach, a previous study by Macedo et al. [37] investigated the use of various ionic surfactants, including sodium lauryl sulfate (SDS), in combination with long-chain alcohols to generate a lamellar phase. The study aimed to enhance the dispersion of this liquid crystal in water by

incorporating nonionic surfactants, thereby creating nanoparticles that could be able to load oil. However, the conditions employed in the study were insufficient to achieve the lamellar phase's dispersion into nanoparticles or load oil into microparticles.

Using different molecules to obtain lamellar dispersion is a topic where different groups are acting, and one class of substance that have been used extensively in cosmetics and pharmaceuticals industries are the poloxamers, also known as pluronics, to favor it. Poloxamers are a class of nonionic surfactants that consist of polyethylene glycol (EO) and polypropylene glycol (PO) copolymers [16,24,118,119]. Their structure allows them to be used to improve the stability of nanoparticles in water medium, since it also contains EO blocks [120]. For instance, Tilley et al. [121] explored the role of the triblock copolymer in stabilizing dispersions of liquid crystalline nanoparticles, specifically cubosomes and hexosomes. The research focused on how Pluronic F127 associates with these particles, both on their external surfaces and within their internal structures, and how this association influences the stability and behavior of the dispersions. The study found that the interaction between Pluronic F127 and the nanoparticles is strongly influenced by the lipid composition and internal architecture of the particles. These findings underscore the critical role of copolymers in stabilizing such dispersions, suggesting that careful control of copolymer concentration is essential for optimizing the formation and stability of liquid crystal dispersions for potential applications. Although, its well-known to use copolymers to enhance liquid crystal dispersions, much it still needed to improve its application, since until nowadays high-energy methods are still needed to obtain it, mostly if high oil incorporation is desired [54].

This study aimed to disperse the lamellar phase formed by sodium lauryl sulfate (SDS) and various co-surfactants (fatty alcohols with chain lengths ranging from C8 to C16 and caprylic/capric acid) using a triblock copolymer ($EO_{10}PO_{30}EO_{10}$). While the hydrophobic blocks of PO are expected to form mixed micelles with the ionic surfactants, the hydrophilic blocks of EO are expected to extend toward the aqueous medium to ensure dispersibility and stability in water. Furthermore, the impact of the fatty chain length was evaluated on the oil loading capacity and stability of the system. The study systematically characterized the

structures formed by sodium lauryl sulfate (SDS), $EO_{10}PO_{30}EO_{10}$ and various co-surfactants by different techniques: optical microscopy, cryogenic transmission electron microscopy (cryo-TEM), laser diffraction, dynamic light scattering (DLS), high-sensitivity differential scanning calorimetry (DSC) and small-angle X-ray scattering (SAXS).

5.2. Experimental Section

5.2.1. Materials

Most of the chemicals used in this work were kindly supplied by Oxiteno and used as received, being them: anionic surfactant sodium dodecyl sulfate (SDS-Alkopon NS ECO 92F), triblock copolymer ($EO_{10}PO_{30}EO_{10}$- Ultraric PE64), cetyl alcohol (C_{16}OH-Alkonat 1698), lauryl alcohol (C_{12}OH-Alkonat 1214CH), and caprylic/capric acid (C_8/C_{10}COOH-Ultracid 810). Myristyl alcohol (C_{14}OH-) and octanol (C_8OH) were purchased from BASF in the highest available purity, 95%. Ultra-pure water (18.2 MΩ·cm) obtained from Direct-Pure UP Rephile was used to prepare the samples. Isoamyl cocoate (IsoCo) and isoamyl palmitate (IsoPa) from Oxiteno, mineral oil (MOil) from Neon, Uvinul MC 80 (Uvinul) from BASF and bergamot oil (BOil) from viaAroma were used to test oil loading in the selected systems.

5.2.2. Sample Preparation

The samples were prepared by weighing fixed amounts of 0.12 g of SDS in 30 mL of water, 0.36 g co-surfactant, and 0.12 g of $EO_{10}PO_{30}EO_{10}$, (which is a proportion of 1:3:1). The SDS solution was mixed with the co-surfactant, followed by the immediate addition of the $EO_{10}PO_{30}EO_{10}$ solution. The mixture was homogenized by a mechanical stirrer at 900 rpm for 15 min at a temperature above the melting point of the fatty component (35 °C for C_8/C_{10}COOH, 35 °C for C_{12}OH, 50 °C for C_{14}OH, and 60 °C for C_{16}OH). In some cases, 0.06 g of mineral

oil was added to a 20 mL portion of the obtained suspension, followed by sonication for 3 min at a continuous cycle of 0.5 A on a Hielscher UP50H ultrassonicator.

5.2.3. Sample Characterization

Visual inspection to determine the occurrence of phase separation was registered by photographs.

Particle size distributions were measured using laser diffraction (LD) or dynamic light scattering (DLS). LD measurements were conducted using a Mastersizer 3000E (Malvern Instruments Ltd., Br) particle size analyzer based on laser light diffraction. Mie theory was employed to determine the size distribution, using distilled water as the dispersing medium (refractive index of 1.33), and fatty alcohol/ fatty acid as the dispersed medium (refractive index of 1.44, adsorption index of 0.01, and density of 1 $g.cm^{-3}$). All measurements were conducted for 20 s, maintaining obscuration between 10 and 15%, at room temperature (25°C), with a stirring speed of 1600 rpm. The results were reported as averages of 5 replicates with the respective standard deviation. DLS measurements were conducted using an SZ-100 Nanopartica instrument from Horiba, equipped with a 10 mW laser with a wavelength of 532 nm. Each sample (0.4 mL) was added to a polystyrene cuvette with four optically clear sides and a path length of 10 mm, and completed with Ultra-Pure water to 2 mL. The cuvettes were previously rinsed with fresh ultra-pure water and immediately covered after sample addition to avoid contamination with dust. All experiments were performed in triplicate at 25 °C, with a time exposure of 120 s and a scattering angle of 90°. The acquired data were processed using the HORIBA NextGen Project SZ-100 software, employing Inverse Laplace Transform (ILT) to obtain intensity distributions and mean hydrodynamic radii.

SAXS measurements were performed at the Institute of Physics of the University of São Paulo (IF-USP). The used instrument was Xenocs Xeuss Version 2.0, equipped with a Dectris Pilatus 300k. The beam wavelength employed was 0.154 nm (CuKα line). Each sample was positioned in a capillary

sample holder, and a thermal bath was used to maintain a constant temperature of 30 °C during the whole measurement time (3 h). The distance between the sample holder and the detector was 0.2 m, resulting in a q range between 0.2 and 7.2 nm^{-1}. The software Fit2D [78] and SuperSAXS package [79] allowed the subtraction of background and solvent (pure water) and integration of the obtained images. The resulting curves of intensity, denoted as *I(q)*, as a function of scattering vector *q*, were analyzed using OriginLab, the relative peaks position, measured using OriginLab, was used to determine the correlation distance, d = 2π/q, by using the q value of the peak.

Cryo-TEM was used at the Brazilian Nanotechnology National Laboratory (LNNano). The samples were diluted to 2 mg $mL^{-1,}$ and a 3 uL droplet was deposited on a 300-mesh lacey carbon-coated copper grid. Samples were prepared in an automated vitrification system (Vitrobot Mark IV, FEI, Netherlands) with a blot force of 0 and a blot time of 3 s. The images were obtained using a TALOS F200C (ThermoFisher Scientific, Oregon, USA) equipped with a 4k x 4k CMOS camera, operating at 200 kV. Particle size was determined using ImageJ software and analysing 100 particles for each sample. Optical microscopy was also employed to analyze samples with particles in the micrometer range. A Bel Photonics XPL-3220 microscope, equipped with a CCD digital camera, was used to capture images in brightfield and polarized light to detect birefringence and correlate with the possible presence of the lamellar phase.

DSC experiments were conducted at LNBio-CNPEM, proposal 20230820. using the N-DSC III calorimeter (TA Instruments, USA) in the temperature range from 10 to 80 °C with a heating rate of 30 °C/hour. The calorimetric cells were filled with water equilibrated at 10 °C for 10 minutes and examined repeatedly in the range of 10–80 °C until the baseline was reproducible. After calibrating the baseline with water, the sample cell of the calorimeter had its replaced by another containing the lamellar phase dispersions. The temperature scanning process with the equipment containing the lamellar phase dispersion involved a single heating run from 10 to 80 °C. This procedure was conducted in duplicate: after the first scan, another aliquot of the same sample was injected, and a second scan was performed. The contribution of heat capacity at constant pressure (Cp, $kJ \cdot mol^{-1} \cdot K^{-1}$) of the buffer solution was subtracted from the Cp values of the

lamellar phase dispersion in the investigated temperature range. The calorimetric enthalpy variation (ΔHcal) for the phase transition process was determined by calculating the area of the thermogram after baseline correction, and the temperature of melting (Tm) was determined as the center position of each peak.

5.3. Result and Discussion

5.3.1 Influence of fatty chain length on particle formation

All the samples formed by 1.0 wt % of SDS, cosurfactants and $EO_{10}PO_{30}EO_{10}$ in water were turbid. The viscosity and turbidity of these samples were highly dependent on the co-surfactant chain size, with C_8/C_{10}COOH and C_8OH resulting in turbid-opalescent samples with water-like viscosity, while C_{16}OH produced opaque and viscous samples. (**Figure 5.1**).

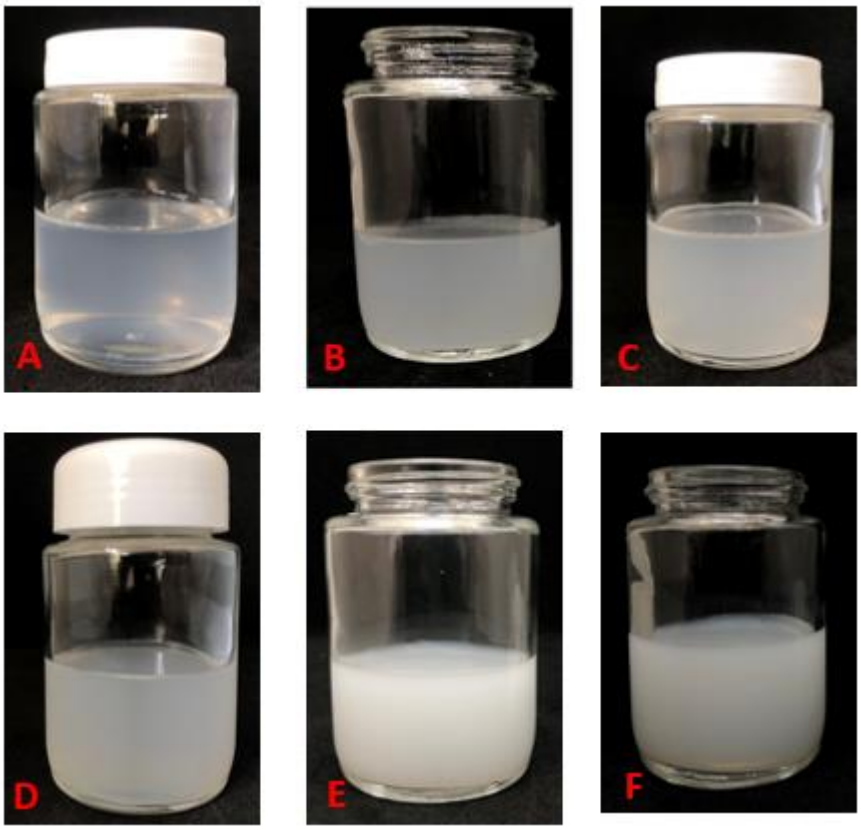

Figure 5. 1: Pictures of SDS: cosurfactant: $EO_{10}PO_{30}EO_{10}$ at 1.0 wt% containing A) C_8/C_{10}COOH; B) C_8OH; C) C_{10}OH; D) C_{12}OH; E) C_{14}OH; F) C_{16}OH

Laser diffraction and dynamic light scattering showed that the diameters ranged from 149 nm to 91 µm for the samples with different cosurfactants (**Figure 5.2 and Table 5.1**). These results indicated a smaller particle diameter when using shorter chain lengths. Increasing the chain length also enhanced the hydrophobicity of the fatty alcohol, resulting in a lower HLB and higher CPP (critical packing parameter), which could lead to an increase in particle size as already observed for Vankalaya et al. [122]. They observed that the fatty chain length dictated the size of their particles, which ranged from 77 nm (C_{12}OH) to 503 nm (C_{16}OH). Shi et al. [123] also demonstrated that the length of the alkyl chain in lipid particles primarily affected their size, and our findings were consistent with this observation. C_8 and C_{10}OH showed phase separation after 7 days, and therefore these co-surfactants were used only to understand the effect of chain length in the particles' preparation.

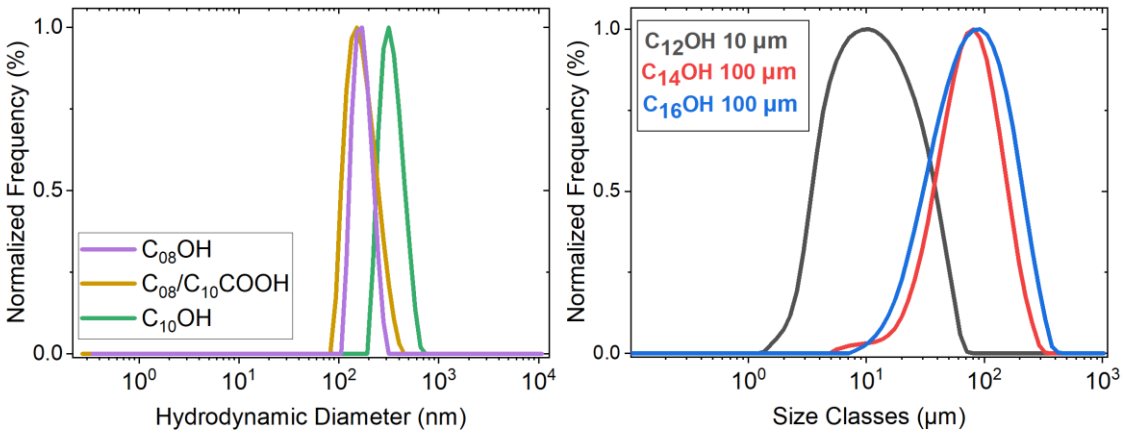

Figure 5.2: A) Laser diffraction results for SDS:co-surfactant: $EO_{10}PO_{30}EO_{10}$, using $C_{12}OH$, $C_{14}OH$ and $C_{16}OH$. **B)** DLS results for $C_{10}OH$, C_8OH and $C_8/C_{10}COOH$.

Table 5.1 Hydrodynamic diameters and D50 values for different SDS:co-surfactant: $EO_{10}PO_{30}EO_{10}$

Cosurfactant	Hydrodynamic Diameter* (nm)	Dv50** (µm)
$C_8/C_{10}COOH$	149 + 10	NA
C_8OH	162 ± 15	NA
$C_{10}OH$	348 ± 25	NA
$C_{12}OH$	NA	12 ± 2
$C_{14}OH$	NA	75 ± 8
$C_{16}OH$	NA	91 ± 9

*Average and standard deviation of mean hydrodynamic diameter values from at least three measurements ** Median particle size distribution values from at least three measurements. NA not applied:

The obtained systems were observed by microscopy analysis, with optical microscopy used for $C_{12}OH$, $C_{14}OH$, and $C_{16}OH$, and cryo-transmission electron microscopy (Cryo-TEM) for $C_8/C_{10}COOH$ (**Figure 5.3**). The results revealed that using $C_8/C_{10}COOH$ led to the formation of spherical nanoparticles with a homogeneous interior (**Figure 5.3A**). In contrast, $C_{12}OH$ resulted in the formation of polygonal microparticles with a heterogeneous interior (**Figure 5.3B**). The black dots observed in the interior could be attributed to lauryl alcohol that was

not incorporated into the particles but acted as nucleation points for their creation. With an increase in the co-surfactant chain length to $C_{14}OH$ and $C_{16}OH$, heterogeneous aggregate formation was observed, indicating that more hydrophobic systems exhibited lower stabilization and inferior dispersion, with the same behaviour of black spots being noted.

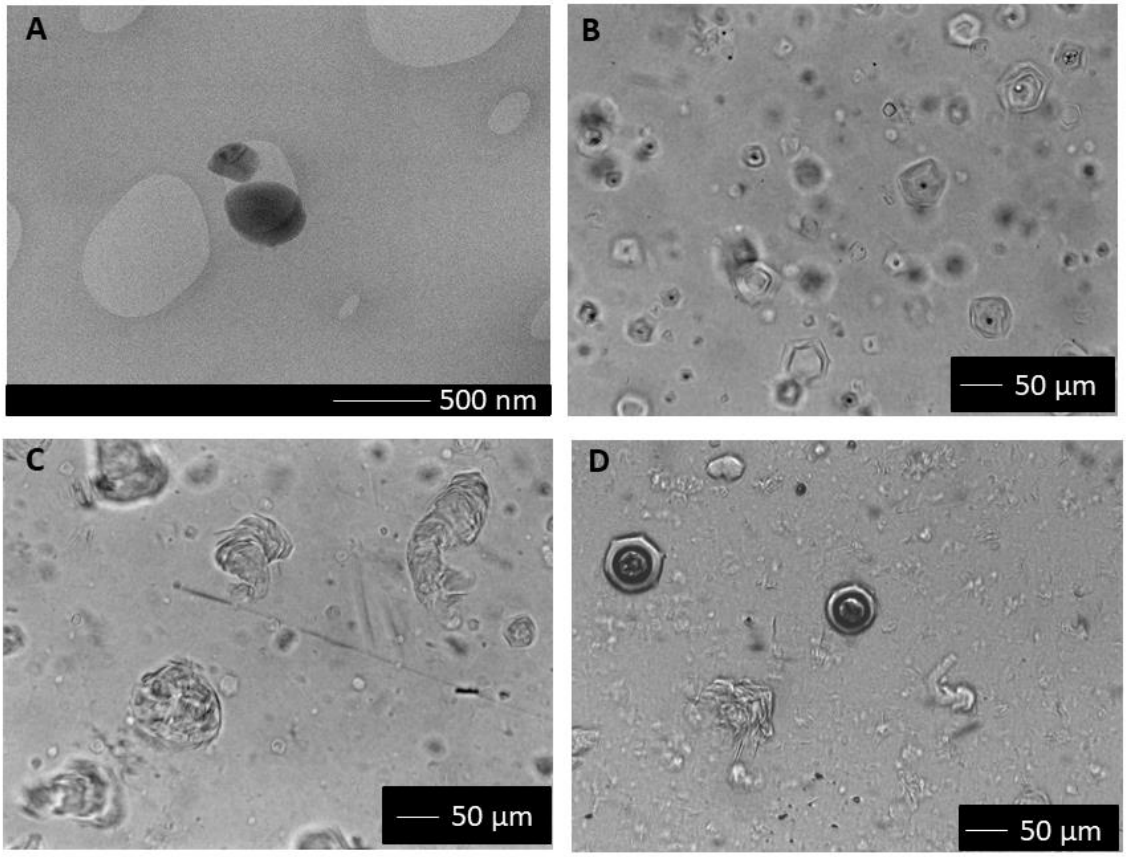

Figure 5. 3: Images of microscopy for SDS:co-surfactant:$EO_{10}PO_{30}EO_{10}$ samples. **A:** $C_8/C_{10}COOH$;**B:**$C_{12}OH$;**C:**$C_{14}OH$;**D:**$C_{16}OH$

Differential Scanning Calorimetry (DSC) analysis was conducted to determine the presence of crystalline structures. The DSC curves (**Figure 5.4**) indicated that carbon chains with fewer than 12 carbons did not exhibit any transitions, suggesting the absence of crystalline structures. This lack of crystalline transitions could indicate the formation of nanoparticles without the anticipated lamellar structure. In contrast, samples containing carbon chains longer than C_{12} exhibited several transition peaks. For the $C_{12}OH$ sample, three endothermic peaks were observed, as detailed in **Table 5.2**. These peaks overlapped,

necessitating deconvolution for a more precise analysis. The enthalpy associated with each transition was calculated based on the deconvoluted peak values [27].

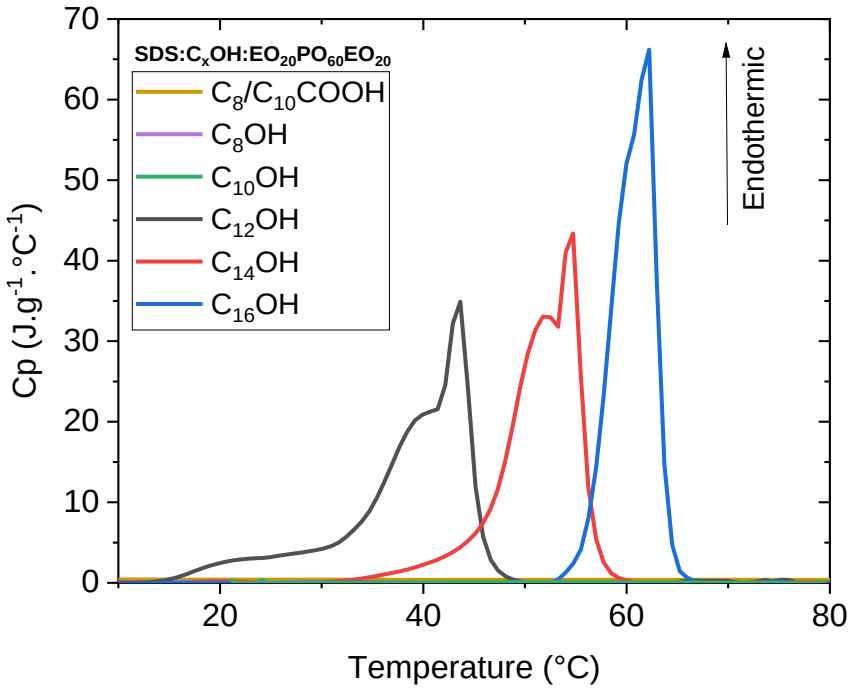

Figure 5. 4: DSC analysis for SDS:co-surfactant: $EO_{10}PO_{30}EO_{10}$ systems.

Table 5. 2 Phase transition data (temperature, heat capacity (Cp), and enthalpy values) obtained by DSC analysis.

Samples of SDS:X: $EO_{10}PO_{30}EO_{10}$	**Tm (°C)**			**Cp ($J.g^{-1}°C^{-1}$)**			**dH ($J.g^{-1}$)**		
$C_8/C_{10}COOH$	0			NA			NA		
C_8OH	0			NA			NA		
$C_{10}OH$	0			NA			NA		
$C_{12}OH$	21.5	40	43.5	4.01	21	35	79.4	160.27	53.04
$C_{14}OH$	NA	51	54.9	NA	33	42.96	NA	180	138.5
$C_{16}OH$	NA	60	62	NA	54	65	NA	180	148

NA: not applied

The first peak was attributed to the polymorphs commonly found in fatty acids, such as lauryl alcohol. Similar observations were reported by Philip et al. [124], who identified multiple peaks within the same temperature range (14.5 °C

and 25 °C), attributing them to solid-solid or solid-liquid phase transitions prior to complete liquefaction. The presence of excess $C_{12}OH$ was inferred from microscopy images, which showed $C_{12}OH$ within some particles. The other two peaks was postulated to be associated with a structural transition within the formed lamellae [125–127].

For $C_{14}OH$ and $C_{16}OH$, two peaks were observed in each system. The first peak was related to solid-liquid transitions, while the second was attributed to structural transitions within the lamellae. It is evident that different fatty alcohols lead to an increase in the transition temperature, which was associated with the increase in carbon chain length, which was also observed by Percebom, et al. [50]. Additionally, the enthalpy values of the transitions indicated that the process is more endothermic for longer carbon chains, Usma et al.[128] reported similar results where an increase in the alcohol content promoted a clear decrease in dH, and a broadening in the gel-to-fluid phase, due to n-decanol shorter chain, which hinders the crystalline organization of the bilayer. A similar resulted was also observed by Karl et al. [129] , where the thermal behavior and molecular organization of long-chain alcohols in ternary systems with surfactant solutions was evaluated. DSC revealed distinct endothermic peaks corresponding to the melting of fatty chains, with peak temperatures increasing with carbon chain length, similar with the results found in this work.

Since crystalline transitions potentially related to liquid crystal structures were observed using DSC analysis, SAXS analysis was employed to confirm the formation of it. Lamellar phase was confirmed by the peak positions (**Figure 5.5**), for samples containing $C_{12}OH$, $C_{14}OH$ and $C_{16}OH$. To better understand the organization of the lamellar phase, a model incorporating a random lamellar head/tail sheet with a Caille structure factor was applied to fit the data. However, due to the low sample concentration (1% wt), resulting in noisy data, fitting the data into the model proved challenging. Hence, we used only the position of the peaks to obtain the distance interplanar, d, for the lamellae. We observed an interplanar distance of 34.9, 40.5 and 48.3 nm for $C_{12}OH$, $C_{14}OH$ and $C_{16}OH$, respectively.

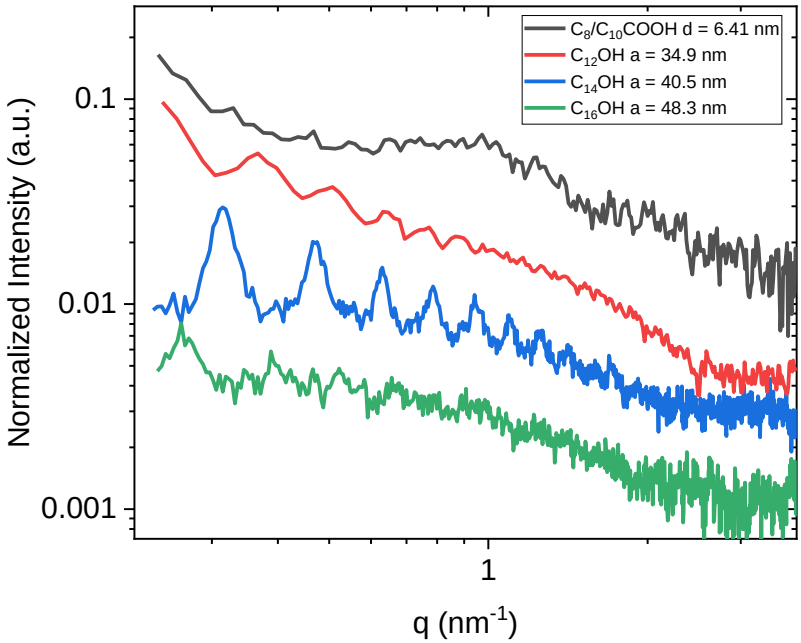

Figure 5. 5: SAXS curves for samples containing SDS:cosurfactant:$EO_{10}PO_{30}EO_{10}$

Notably, in systems containing $C_8/C_{10}COOH$, a liquid crystal phase was not observed, which aligns with the DSC results where no transitions were detected. Instead, we identified the formation of a broad peak (0.97 nm^{-1}), which was associated with the onset of some organization.

Tests for mineral oil incorporation using magnetic stirring were initially conducted in all systems produced; however, effective incorporation was not achieved, **Fig 5.12 SM**, in any of the cases. Tests involving the addition of oil during the process were also conducted; however, this resulted in emulsions, which was not the goal of this work. In search of alternatives, the application of energy through a probe sonicator was chosen. This approach proved to be effective for incorporating mineral oil, but this energy input could result in modifications in the systems structure [130], therefore all systems in the absence of mineral oil were subjected to sonication and characterized (see **section 5.8.1 of SM**), which resulted in a significant reduction in particle size in systems containing $C_{12}OH$, $C_{14}OH$, and $C_{16}OH$.

5.3.2 Influence of oil mineral loading on particles size and Structure

Mineral oil (0.06 g) was introduced into 20 mL of the system (0.2 g of particle) using a sonicator probe as previously described. DLS measurements revealed a size of 149; 151; 122 and 450; 213 and 1200 nm for $C_8/C_{10}COOH$, $C_{12}OH$, $C_{14}OH$ and $C_{16}OH$, respectively (**Figure 5.6**). $C_{12}OH$ and $C_8/C_{10}COOH$ presented a smaller particle size and formation of a monodisperse population, while for $C_{16}OH$ and $C_{14}OH$ two nanometric populations were observed.

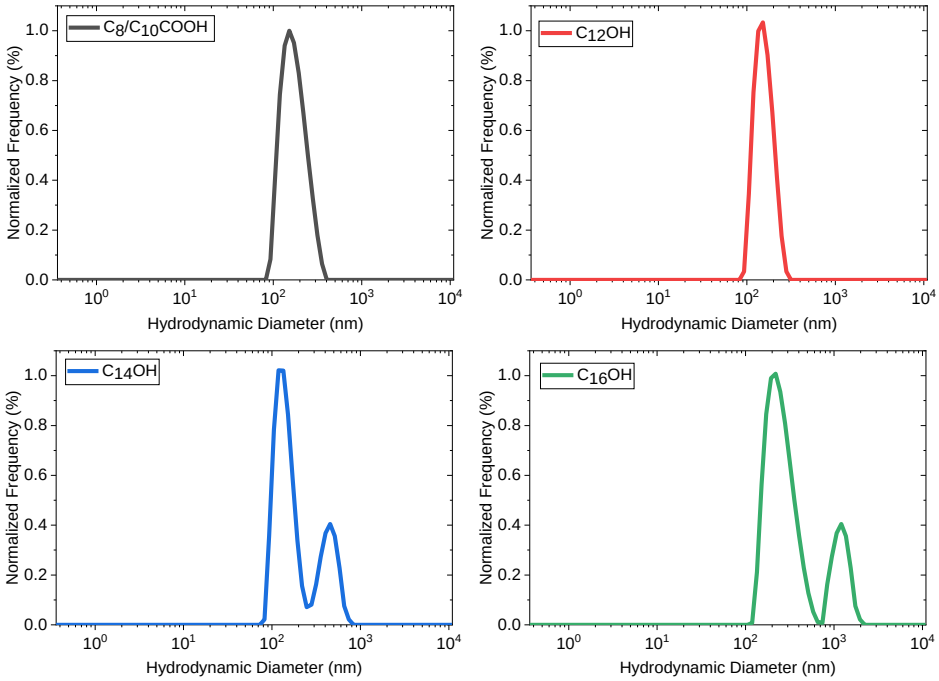

Figure 5.6 Hydrodynamic diameter distributions of samples containing 1.0 wt % of SDS:cosurfactant:$EO_{10}PO_{30}EO_{10}$ nanoparticles and 0.3 wt% of MOil .

In comparison with sonicated samples without oil (**Fig 5.11 SM**), we observed that upon oil addition the size distribution was broader for samples containing $C_8/C_{10}COOH$, indicating that particles are more uniform in the absence of oil, therefore oil may promote some change in the structure of these samples. For $C_{12}OH$, $C1_4OH$ and $C_{16}OH$ the presence of oil resulted in a reduction in the

average hydrodynamic size of the particles. The reduction in particle size in these specific systems is associated with a notable improvement in their dispersibility. This result is crucial for ensuring the uniform distribution of active components, contributing to the efficacy of the system in potential future applications. However, it is important to note that, despite the observed benefits, phase separation was identified in the systems containing $C_{14}OH$ and $C_{16}OH$. This instability can compromise the efficacy of active encapsulation, as phase separation is undesirable in this context. Consequently, these samples were excluded from future testing plans. In contrast, the samples containing $C_{12}OH$ and $C_8/C_{10}COOH$ demonstrated notable stability for over 120 days. This prolonged durability suggests that these systems are promising for practical applications, highlighting their ability to maintain structural integrity over time.

Both systems containing $C_{12}OH$ and $C_8/C_{10}COOH$ were analysed by Cryo-TEM (**Figure 5.7**), revealing the formation of spherical and homogeneous nanoparticles in both cases. Specifically, for $C_8/C_{10}COOH$, the use of sonication and mineral oil incorporation did not appear to affect the morphology of the particles. In contrast, for $C_{12}OH$, nanoparticles with very different morphologies compared to samples non-sonicated and without oil (**Figure 2B**) were obtained, which were more dispersed and with a homogeneous interior.

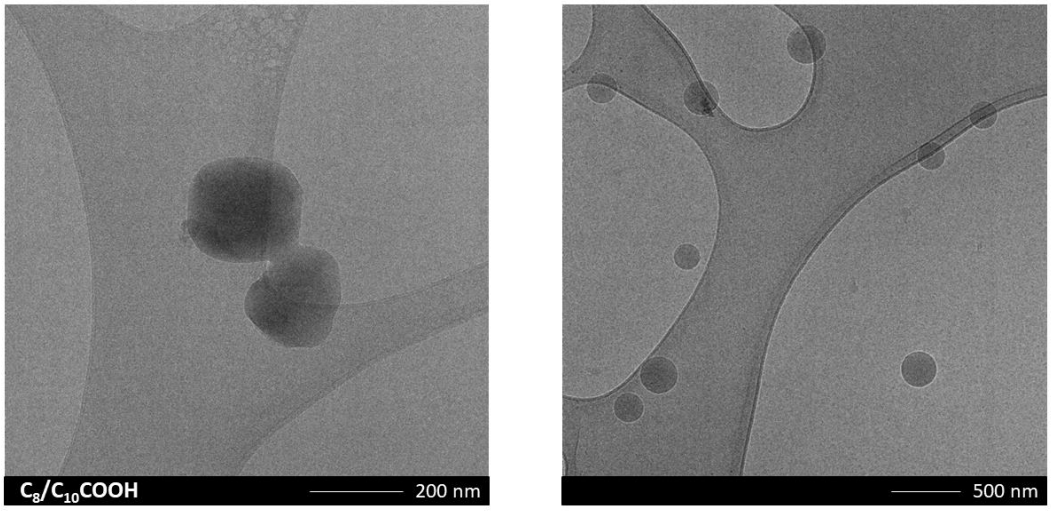

Figure 5.7 Cryo-TEM images of samples containing 1 wt% of SDS:cosurfactant:$EO_{10}PO_{30}EO_{10}$ nanoparticles.

DSC analysis was also conducted not only to determine the presence of crystalline structures but also to observe if there was any effect of incorporating

oil into the structure of the samples. Although the systems containing $C_{14}OH$ and $C_{16}OH$ were excluded from future encapsulation tests, DSC analysis were conducted on all systems to understand the role of the mineral oil in presence of different co-surfactants. According to the results in **Figure 5.8**, the incorporation of oil reduced the phase transition for $C_{12}OH$, $C_{14}OH$, and $C_{16}OH$, while $C_8/C_{10}COOH$ did not show any phase transition, consistent with the observations for samples without oil. For $C_{12}OH$ to $C_{16}OH$, the enthalpy associated with each transition was calculated based on the deconvoluted peak values (**Table 5.3**). For $C_{12}OH$, we observed that only two transitions observed in **Figure 5.8** shifted: the first was kept, indicating that lauryl alcohol was also present in the structure, and the other two shift to lower temperatures. The small enthalpy values can be explained by the relatively minor rearrangements of the lamellae needed for converting the lamellar structure to a different structure, indicating that oil loading caused lamellae repacking. For $C_{14}OH$ and $C_{16}OH$, a similar behavior was observed, with only one peak present, which could be associated with the fact that introducing mineral oil led to system self-rearrangement, as the previously excess fatty alcohol was solubilized into the oil matrix. Moreover, the reduction in the transition temperature could indicate that introducing mineral oil resulted in a less structured system, as observed by De Souza, et al. [131].

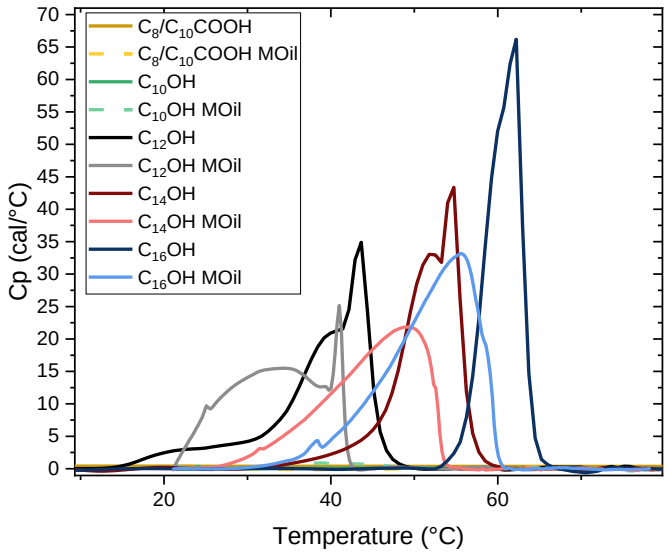

Figure 5. 8: DSC analysis for SDS:co-surfactant: $EO_{10}PO_{30}EO_{10}$ systems after Mineral Oil loading.

Table 5. 3: Phase Transition Data (Temperature, Heat Capacity (Cp), and Enthalpy Values) obtained by DSC analysis of samples containing Mineral Oil.

Samples of SDS:X: $EO_{10}PO_{30}EO_{10}$	**Tm (°C)**			**Cp ($J.g.^{-1}°C^{-1}$)**			**dH ($J.g^{-1}$)**		
$C_8/C_{10}COOH$	0			NA			NA		
C_8OH	0			NA			NA		
$C_{10}OH$	0			NA			NA		
$C_{12}OH$	21.5	37	40.9	14.6	12.8	24.9	178.5	61.2	21.5
$C_{14}OH$	NA	NA	46.1	NA	NA	21.2	NA	NA	286.9
$C_{16}OH$	NA	NA	52.9	NA	NA	31.5	NA	NA	373.9

Since phase transitions were identified, we also used SAXS to confirm these structures. Although the systems containing $C_{14}OH$ and $C_{16}OH$ were excluded from future encapsulation tests, SAXS measurements were conducted on all systems to understand the role of the co-surfactant in particle structure, **Figure 5.9**. For $C_8/C_{10}COOH$, as observed in non-sonicating samples, it was impossible to use a fitting model due to noisy data. However, we observed that sonication did not alter the position of the peak for $C_8/C_{10}COOH$ when comparing both data, suggesting that the energy applied does not affect the system's organization but merely reduces particle size (**see Figure 5.15 at SM**), however upon Moil addition we observed a pronounced increase in intensity at low q values, compared to the other samples. This suggests that the presence of Mineral Oil led to the formation of larger or denser structures, since different of sizes were not observed by DLS or Cryo-TEM we believed that denser structures were formed. For $C_{12}OH$ and $C_{14}OH$, upon incorporating oil, the lamellar phase was disrupted, increasing the interplanar distance, as we obtained noisy data due to low concentration, it was not possible to discern between peaks and loud, so we assumed that the lamellae phase was not present upon oil addition. For $C_{16}OH$, the uptake of Mineral Oil led to a reduction in the lamella interplanar distance to 28.5 nm, indicating that MOil impacted the packing of its structure, becoming more organized, which is in accordance with the results obtained by DSC measurements.

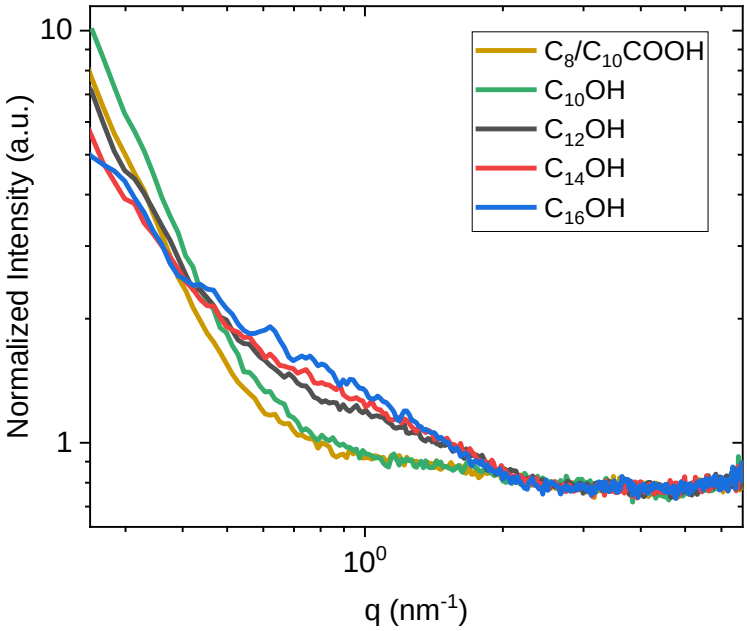

Figure 5. 9: SAXS curves for samples containing SDS:cosurfactant:$EO_{10}PO_{30}EO_{10}$ after Mineral Oil addition.

The SAXS curve analysis for $C_{16}OH$ systems (**Figure 5.9**) revealed that increasing the chain length resulted in greater system organization, indicated by the increased prominence and definition of the peaks. These results suggest more pronounced bilayer stacking as the carbon chain length increases, highlighting a significant influence on the structural organization of these systems. Despite excluding $C_{14}OH$ and $C_{16}OH$ from future tests, the SAXS measurements enrich our understanding of the structure of this system, emphasizing the complexity of the interactions between components and their influence on particle structure. This refined analysis will guide further research to optimize the design of active encapsulation systems.

After optimizing the system, we selected the particles with $C_8/C_{10}COOH$ and $C_{12}OH$ as the optimal ones to obtain particles and to use as loading systems.

5.3.3 Stability

Since both $C_8/C_{10}COOH$ and $C_{12}OH$ resulted in the optimal samples, tests were performed to understand their stability, and which one performed better.

Both samples were kept at 50 °C for 30 days and at room temperature (25°C) for at least 120 days. After this period, the particle sizes were measured (**Figure 5.10 and 5.11**).

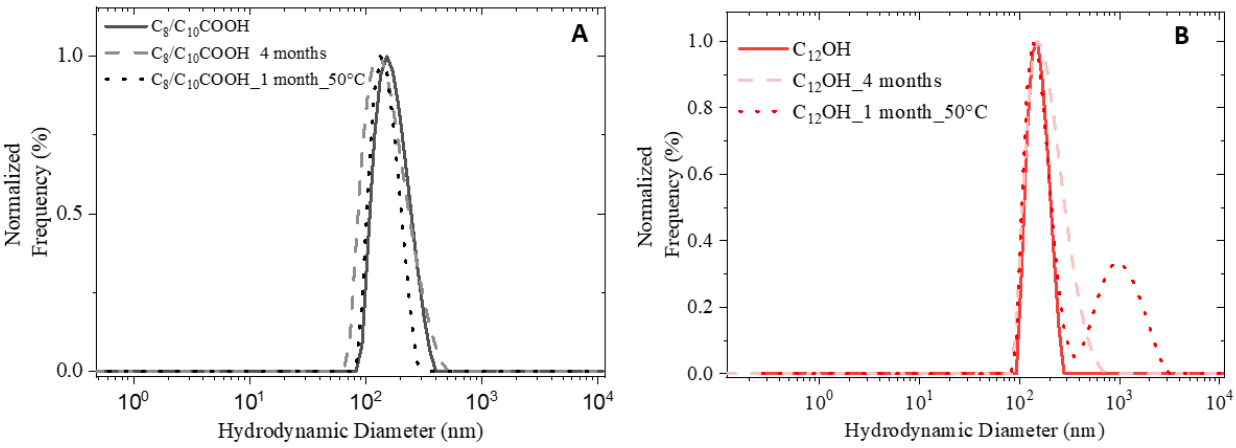

Figure 5. 10: Hydrodynamic Diameter measurements for SDS:cosurfactant: $EO_{10}PO_{30}EO$ with A) $C_8/C_{10}COOH$ after 4 months in room temperature and at 50°C for a month. B) $C_{12}OH$ after 4 months in room temperature and at 50°C for a month.

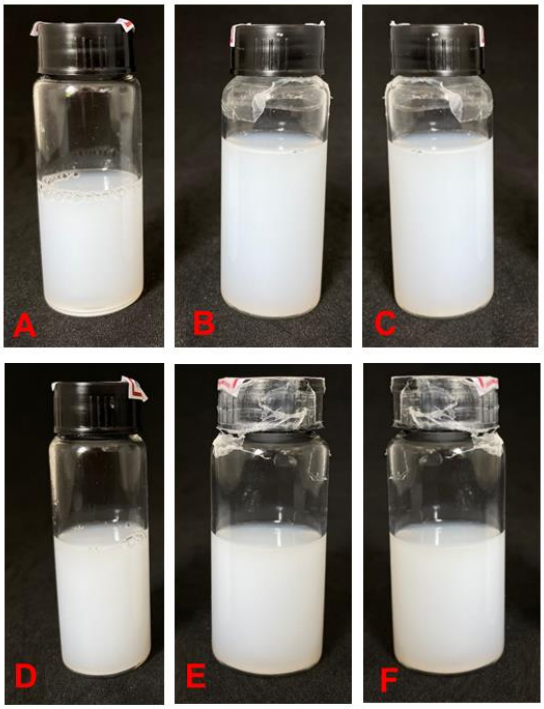

Figure 5. 11: SDS:co-surfactant:$EO_{10}PO_{30}EO_{10}$ for **A**) $C_8/C_{10}COOH$ at first day after preparation; **B)** $C_8/C_{10}COOH$ at 120 days after preparation at room temperature; **C)** $C_8/C_{10}COOH$ at 30 days after preparation at 50 °C. **D)** $C_{12}OH$ on the first day after preparation; **E)** $C_{12}OH$ at 120 days after preparation at room temperature; **F)** $C_{12}OH$ at 30 days after preparation at 50 °C.

No size difference was observed for the samples kept at room temperature after 120 days, indicating that both had high stability. However, after 30 days at 50 °C the samples containing $C_{12}OH$ showed two populations (with no visual phase separation), indicating that this sample is less stable compared to $C_8/C_{10}COOH$, which did not show any size changes in either scenario. Zeta potential measurements were also conducted, yielding a value of –39 mV for $C_8/C_{10}COOH$, which could be related to the higher colloidal stability, due to negative charges COO- groups. Therefore, $C_8/C_{10}COOH$ was selected as the primary sample for the other studies.

5.3.4 Loading of Different Oils

Particles with $C_8/C_{10}COOH$, due to its superior stability, was the system chosen to verify its versatility and capability of incorporating different oils in addition to mineral oil and verify the consequent impact on particle size. Bergamot oil (BgOil) is an essential oil with a cyclic structure and can be used in pharmaceutical and cosmetics formulations [132,133]. Isoamyl cocoate (IsoCo) and palmite (IsoPa) are a constituent of a broader group of cosmetic ingredients, alkyl esters, which consist of the reaction products of fatty acids and alcohols, which functions are mostly related to skin-conditioning. Ethylhexyl Methoxycinnamate (Univul, as its INCI name) is a UVB filter suitable for skin care applications, such as anti-aging face care products and sunscreens. All the systems displayed low viscosity (visually like water), regardless of the oil added (at 0.3 wt %), allowing their use in various formulations, such as spray formulations or scalp care. Adding BgOil, IsoCo, and IsoPa slights decreased the hydrodynamic diameter of the nanoparticle while adding Uvinul increased particle size, **Figure 5.12**. When comparing to Moil all samples resulted in bigger particles, which could indicate that Moil resulted in more compact systems; since all the other oils have smaller molecules, this could indicate that they were affecting the structure of the lamellae, more SAXS analysis could indicate the impact of it in the particle structure. All samples presented phase separation after 1 month, showing that oils choice could affect the stability of the particles. However, since low viscosity was observed the increase of it could led to a higher stability.

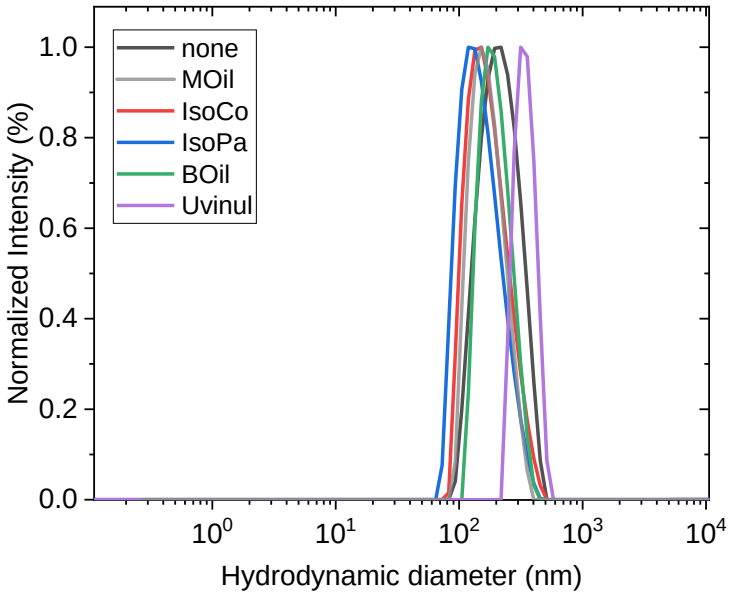

Figure 5. 12 Hydrodynamic diameter distribution of samples containing 0.6 wt % of SDS: cosurfactant: $EO_{10}PO_{30}EO_{10}$ nanoparticles with different oils obtained by DLS.

5.4. Conclusion

This study highlights the potential of liquid crystalline phase dispersions to overcome viscosity-related limitations inherent to high surfactant concentration systems, thereby broadening their application spectrum. By utilizing SDS, fatty alcohols or acids, and a triblock copolymer ($EO_{10}PO_{30}EO_{10}$), we successfully synthesized lamellar phase liquid crystals, resulting in the formation of nanoparticles with varying structural properties. The incorporation of shorter fatty chains led to more stable and smaller particles, while longer chains increased hydrophobicity and particle size, impacting system stability.

Microscopic, DSC, and SAXS analyses confirmed the presence of distinct liquid crystalline structures influenced by the type and length of the fatty chains used. Specifically, C_8/C_{10}COOH and C_{12}OH systems demonstrated high stability and effective dispersion in aqueous media, making them promising candidates for practical applications. Notably, loading mineral oil and other oils into these systems resulted in the formation of monodisperse nanoparticles, further

underscoring their potential for diverse applications in the cosmetic and pharmaceutical industries. Future research will focus on optimizing these systems for specific applications, particularly in active component encapsulation and targeted delivery. Understanding the interplay between surfactant composition, fatty chain length, and co-surfactant ratios will be crucial in refining these dispersions for industrial use, ensuring both efficacy and stability in their intended applications.

5.5. Funding

This study was financed in part by the Brazilian agencies: Conselho Nacional de Desenvolvimento Científico e Tecnológico (CNPq), Fundação Carlos Chagas Filho de Amparo à Pesquisa do Estado do Rio de Janeiro (FAPERJ, Programa Jovem Pesquisador Fluminense E-26/201.674/2021) and Coodenação de Aperfeiçoamento de Pessoal de Nível Superior - Brasil (CAPES, Finance Code 001). KOL received a scholarship from FAPERJ (E-26/203.210/2022). MOF, SCSC, and LOP received scholarships from CNPq (140638/2021-0, 131657/2021-6, and 180745/2022-0, respectively). AMP received a grant from CNPq (304212/2022-9).

5.6. Acknowledgements

We acknowledge the Brazilian Nanotechnology National Laboratory (LNNano) and National Laboratory of Biosciences (LNBio) for the shift allocation and support with Cryo-TEM (Proposal 20230640) and DSC measurements (Proposal 20230820), with a special thank for Gisele Dalmonico, Irís Ribeiro and Leandro Barbosa for their assistance during the shift. We thank Oxiteno for generously providing the triblock copolymers. We are grateful to Cristiano Luis Pinto de Oliveira and his team from the Institute of Physics of the University of São Paulo (USP) for supporting SAXS measurements and for the SUPERSAXS package.

5.7. Declaration of competing interests

The authors declare that they have no known competing financial interests or personal relationships that could have appeared to influence the work reported in this paper.

5.8. Supplementary Materials

5.8.1. Effect of sonication on particle structure:

As mentioned in the paper, we observed a significant oil incorporation upon subjecting systems to sonication, up to 30 %wt in oil. This approach proved to be effective, resulting in a significant reduction in particle size in the systems with $C_{12}OH$, $C_{14}OH$, and $C_{16}OH$ to the nanometric scale compared to the non-sonicated systems, which exhibited micrometric-scale particles.

These systems were evaluated for the incorporation of 30% mineral oil via sonication (**Figure 5.13**), demonstrating that incorporation was possible. In the system containing $C_8/C_{10}COOH$, without significantly impacting the average hydrodynamic diameter of the particles, while for C_{12} to C_{16}, even resulted in a reduction of particle size. This result is crucial for ensuring the uniform distribution of active components, contributing to the efficacy of the system in potential future applications.

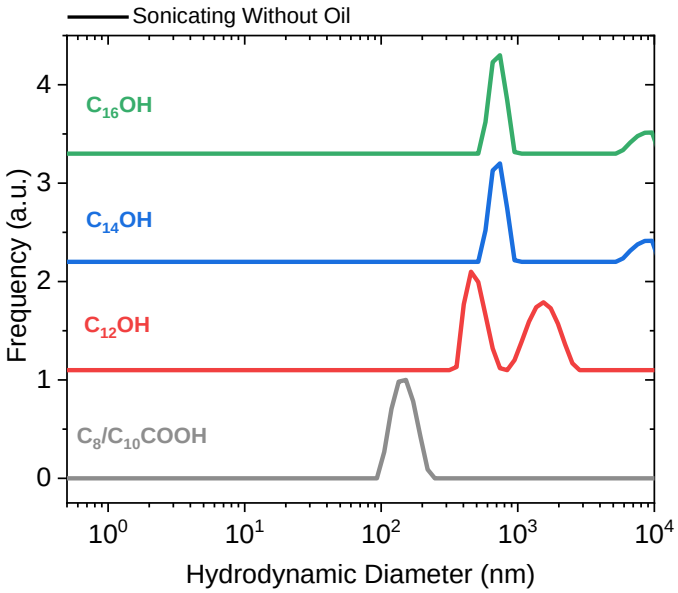

Figure 5. 13: Hydrodynamic diameter measured by DLS from samples containing SDS- co-surfactants-$EO_{10}PO_{30}EO_{10}$- after sonicating without Mineral Oil.

It is important to note that, despite the observed benefits of particle size reduction and notable improvement in the dispersibility of mineral oil, phase separation was identified in the systems with $C_{14}OH$ and $C_{16}OH$ after mineral oil incorporation. This instability can compromise the efficacy of active encapsulation, as phase separation is undesirable in this context. Consequently, the $C_{14}OH$ and $C_{16}OH$ systems were excluded from future testing plans.

Cryo-TEM images of $C_{14}OH$ and $C_{16}OH$, **Figure 5.14**, revealed a correlation between these populations and the presence of particles and lamellae phase sheets, that could be associated with this phase separation.

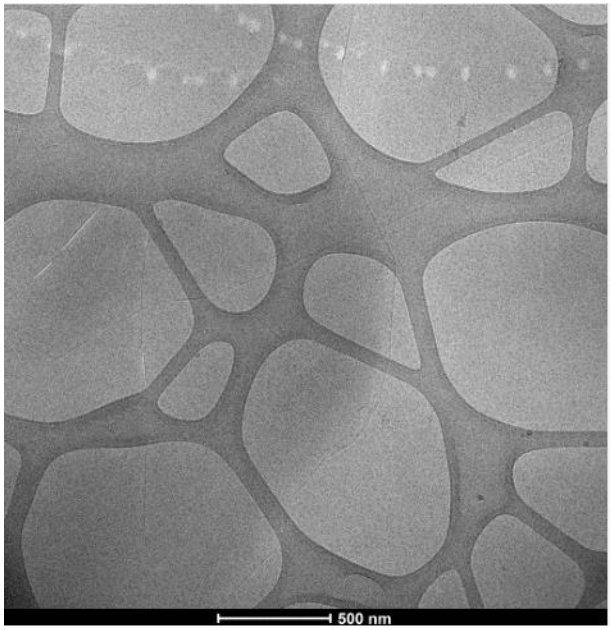

Figure 5. 14: CryoTEM imaging for a sample containing SDS:C_{14}OH-$EO_{10}PO_{30}EO_{10}$.

SAXS measurements showed that for C_8/C_{10}COOH samples sonicating the samples, without mineral oil, didn't affect the particle strucute, as the curve maintained the same. However upon Moil addition an increase of scattering at low q values were observed.

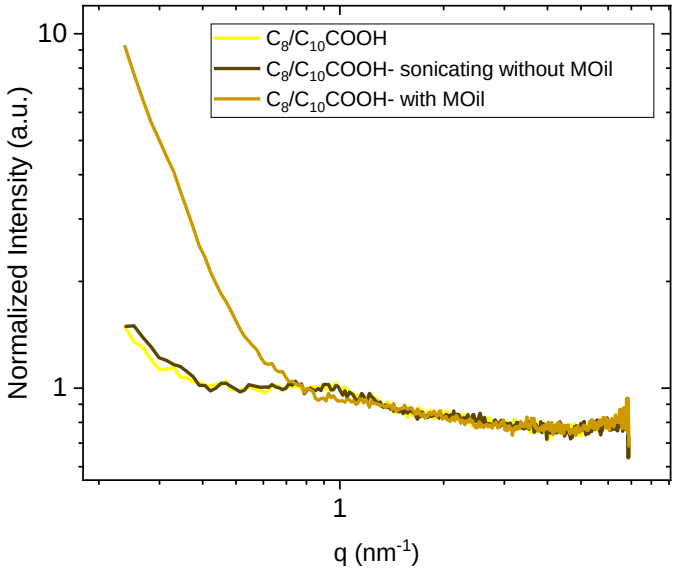

Figure 5. 15: SAXS curves comparing samples containing 1.0wt% of particle for C8/C10COOH system without sonication, sonicating without Mineral Oil and sonicating with Mineral Oil

5.8.2. Test for oil loading with magnetic stirring

For all tested systems, oil incorporation was attempted using only magnetic stirring. As shown in the figure below, although oil incorporation occurred, the particles exhibited instability, leading to phase separation within up to three days. This result suggests that sonication is crucial for both the successful incorporation of mineral oil and the stability of the system.

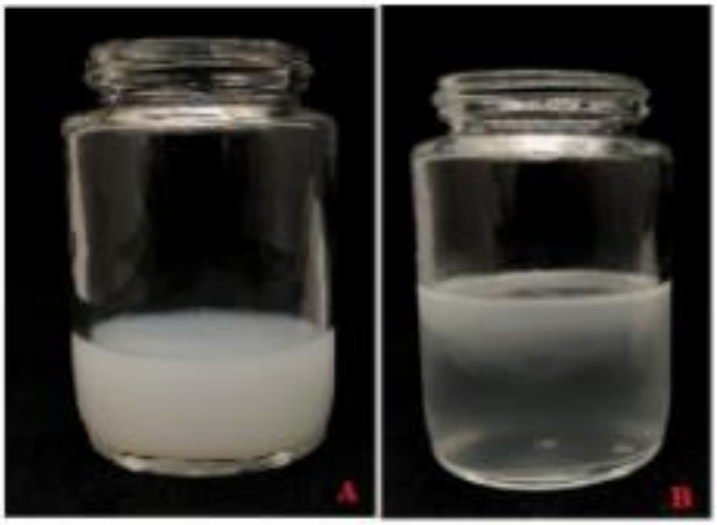

Figure 5. 16: A) SDS-$C_8C_{10}COOH$-$EO_{20}PO_{60}EO_{20}$ after Moil addition with magnetic starring. **B)** SDS-$C_8C_{10}COOH$-$EO_{20}PO_{60}EO_{20}$ after Moil addition with magnetic starring after one day.

CHAPTER 6

As observed throughout this thesis, we successfully obtained cellulose particles capable, which form spontaneously, but capable of incorporating low amounts of oil. In our second study, we managed to incorporate high amounts of oil into lamellar dispersion systems using triblock copolymers. Although particles formed spontaneously, as seen in the case of SDS-C_8/C_{10}COOH-$EO_{10}PO_{30}EO_{10}$, achieving high oil incorporation still required a method involving high energy input.

Therefore, in our next study, we decided to explore an alternative approach to nanoparticles formation: the interaction between surfactant polymers and oppositely charged species. This method was not only aimed at creating systems with low energy input but also at achieving high oil incorporation.

Oppositely Charged Polymers-Surfactants Nanoparticles Stabilized by Triblock Copolymers for enhanced oil loading

Matheus Ouverney Ferreira[a], Lorena Oliveira Pereira[a], Stephany Chaiben[a], Karina Oliveira Lima[a], Karen J. Edler[b], Ana Maria Percebom[a]*

[a] Department of Chemistry, Pontifical Catholic University of Rio de Janeiro (PUC-Rio), 22451-900, Rio de Janeiro, RJ, Brazil

[b] Department of Chemistry, Center of Analysis and Synthesis, Lund University, 2228734, Lund, Sweden,

*Corresponding author: apercebom@puc-rio.br

Graphical Abstract:

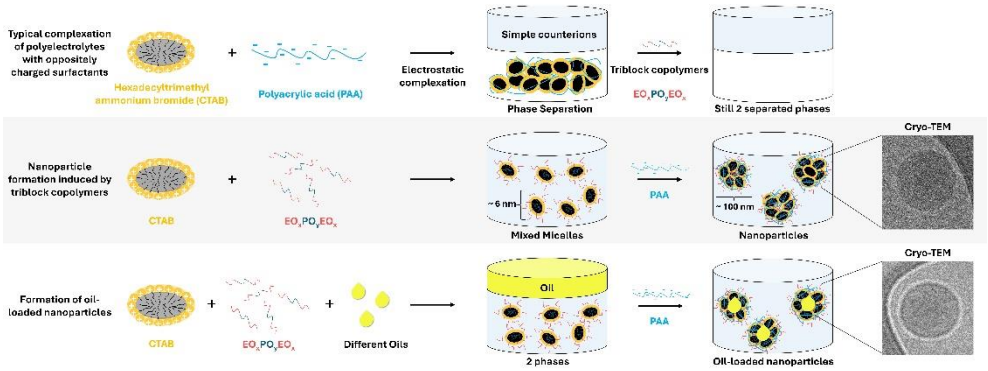

Highlights:

- Triblock copolymers dispersed oppositely charged surfactant-polymer coacervates.
- Spherical nanoparticles for oil loading were formed by applying a low-energy method.
- Materials available on a large scale and easily obtained ensure cost-effective usability.
- Copolymer's ethylene oxide length blocks controlled nanoparticle stability.
- Nanoparticles could be fine-tuned for diverse formulations, including sprays.

Keywords: Core-shell, coacervate, encapsulation, triblock copolymer, colloids.

Abstract

When oppositely charged polymers and surfactants combine, they can form a concentrated phase rich in micelles interconnected by polymer chains. Dispersing this concentrated phase as nanoparticles in an aqueous media can be a way to load and deliver hydrophobic ingredients. This study employed triblock copolymers of poly(ethylene oxide)-poly(propylene oxide)-poly(ethylene oxide), $EO_xPO_yEO_x$, also known as poloxamers or pluronics, to disperse the concentrated phase, forming nanoparticles of aggregated micelles connected by the polyion chains. We showed that nanoparticles formed by hexadecyltrimethylammonium bromide (CTAB), poly(acrylic acid) (PAA), and different $EO_xPO_yEO_x$ copolymers can enhance the loading of oily ingredients compared to pure surfactant micelles. Dispersions with 1.6 wt % of nanoparticles

exhibited water-like viscosity and loaded up to 0.48 wt % of oil. Characterization techniques, including dynamic light scattering (DLS), zeta potential, small-angle X-ray scattering (SAXS), and cryogenic transmission electronic microscopy (cryo-TEM), revealed positively charged spherical 50-180 nm nanoparticles with a core formed by concentrated micelles, that were stable for at least 4 months. Variations in the EO and PO block lengths did not impact morphology, showing that different $EO_xPO_yEO_x$ copolymers were suitable for dispersing the nanoparticles. Increasing EO block length size decreased the diameter of nanoparticles and enhanced stability, providing a means to control their properties. In conclusion, nanoparticles formed by oppositely charged polymer-surfactant mixtures and stabilized by triblock copolymers showed potential for applications, such as sprays, due to their effective oil loading, high stability, and facile preparation.

6.1. Introduction

Oppositely charged polymers and surfactants tend to phase separate at a stochiometric ratio, forming a concentrated phase composed of interconnected micelles and polymer chains. This concentrated phase can potentially be effective for incorporating hydrophobic ingredients due to its hydrophobic interior. Hence, the formation of nanoparticles from this concentrated phase represents a potential strategy to develop new ways of loading and delivering hydrophobic ingredients.

The interactions between oppositely charged polymers and surfactants have garnered significant interest due to their wide-ranging applications across industries such as cosmetics, household products, and enhanced oil recovery [57,134–138]. However, the mixture of these components can have properties completely different from the expected for the individual components, which can be undesirable if not thoroughly understood. In essence, charged polymers can concentrate oppositely charged surfactants, leading to phase separation in a stochiometric ratio [139–144]. This phenomenon results in a concentration of micelles enveloped by polymers that may form liquid crystal phases [2,144–146] capable of incorporating oil [2,147]. Adding hydrophilic blocks to the system can be a way to avoid the macroscopic phase separation but still have particles able to incorporate oil [59,148,149].

Bronich et al. [150] showed for the first time that covalently attaching a hydrophilic block to the polyion chain is an effective strategy to hinder the phase separation of oppositely charged polymer and surfactant. The authors showed the formation of an electroneutral complex (at a stoichiometric ratio of anionic monomer to cationic surfactant) that remained dispersed in water. Other studies using block copolymers [61,62,151–154] observed the formation of core-shell nanoparticles whose interior comprises the surfactant molecules associated with the oppositely charged polymer and the hydrophobic groups of the block copolymer, while the copolymers' hydrophilic groups are in the matrix, increasing the nanoparticle stability. Our group [2] showed that the core-shell nanoparticles formed by electrostatic complexation of charged-neutral block copolymers with cationic surfactants can load hydrophobic ingredients [2]. Longer anionic blocks

resulted in higher oil loading, while longer neutral hydrophilic blocks increased nanoparticle dispersibility and stability [2]. However, these systems require the synthesis of the mentioned diblock polymers, which are not widely available on a large scale for the industry.

Apart from diblock copolymers, grafting EO blocks to a main chain of polyelectrolyte is another strategy to avoid phase separation when mixing the polymer with oppositely charged surfactants. However, instead of dispersing the concentrated phase, this mixture forms water-soluble micelles [155] or liquid crystals at very high concentrations [156], similar to the behavior of regular surfactants. The addition of oils was not tested for these systems, but adding n-alcohols changed their phase behavior [52]. Besides, the grafted polyelectrolytes were synthesized for the study and are not commercially available.

Another approach to obtain dispersions of oppositely charged surfactant-polymer systems involves using nonionic surfactants [157–161]. For instance, octaethylene glycol monododecyl ether ($C_{12}E_8$) led to the total dissolution of ordered complexes, in some oppositely charged polymer-surfactant mixtures whereas in others, a transition to different structures was observed [162]. Janiak et al. [143] also used a nonionic surfactant, penta(ethylene glycol) monododecyl ether ($C_{12}E_5$), to disperse oppositely charged polymer-surfactant systems. Their findings showed the formation of nanoparticles with both hexagonal and bicontinuous cubic internal structures. Specifically, they observed hexagonal structures at lower concentrations of $C_{12}E_5$, while higher concentrations led to a transition to bicontinuous cubic phases, as confirmed by small-angle X-ray scattering (SAXS) analysis. Cryo-transmission electron microscopy (cryo-TEM) images depicted faceted nanoparticles with diameters ranging from 88 to 140 nm, consistent with dynamic light scattering (DLS) measurements. Electrophoretic mobility measurements indicated that the nanoparticles carried a net positive charge, contributing to their long-term stability. Mészáros et al. [163] showed the influence of dodecyl maltoside ($C_{12}G_2$) on the formation of nanoparticles between sodium poly(styrenesulfonate) (PSS) with hexadecyltrimethylammonium bromides (CTAB) by mobility and turbidity measurements. Without $C_{12}G_2$, PSS/CTAB assemblies exhibited negative charges, indicating polymer excess. Upon adding a nonionic surfactant, the charges of PSS molecules are further compensated, the assemblies underwent a charge inversion from negative to

positive, followed by a sharp increase in turbidity, as $C_{12}G_2$ concentration increased precipitation. The presence of nonionic surfactant enhanced the binding of ionic surfactants to polyelectrolyte chains, leading to a decrease in mobility and charge reversal of the assemblies. The formation of water-soluble complexes was also observed by Somasundaran et al. [159], where $C_{12}G_2$ was added to a mixture of oppositely charged guar grafted with hydroxypropyl trimethyl ammonium chloride (HTAC) and sodium dodecyl sulfate (SDS). SDS attaches to HTAC through electrostatic attraction and acts as an anchor for the nonionic surfactant to interact with the complex, which plays a determinant role in its solubility. Although these studies obtained nanoparticles with a hydrophobic core, their internal structure and their ability to encapsulate oils were not studied.

Adding nonionic polymers could also provide stable dispersions of oppositely charged polymers and surfactants. For instance, poly(ethylene oxide), PEO, is adsorbed onto the surface of SDS/ poly(ethyleneimine) (PEI) nanoparticles, depending on its concentration [164,165]. At lower concentrations of PEO (0.1 to 1 $g.L^{-1}$), flocculation occurred. Above 1 $g.L^{-1}$ of PEO, a thick adsorbed layer was formed on the nanoparticle surface, resulting in the steric stabilization of SDS/PEI nanoparticles dispersions. The adsorbed layer also depended on the molecular mass of the nonionic polymer and the preparation method [164,165].

Triblock copolymers, $EO_xPO_yEO_x$, are a class of synthetic copolymers formed by blocks of hydrophilic poly(ethylene oxide) (EO) and hydrophobic poly(propylene oxide) (PO). Due to their amphiphilic nature, they can form different assemblies in water, like micelles or liquid crystals, and have applications in drug delivery, cosmetics, and synthesis of different nanostructures [14,20,21,118,166,167]. For instance, $EO_xPO_yEO_x$ can prevent the aggregation between PEI and SDS when using an apparatus for a stopped-flow mixture, resulting in the complete suppression of PEI/SDS complex precipitation. The authors proposed the formation of sterically stabilized dispersions of nanoparticles with hydrophobic core and hydrophilic corona, although dynamic light scattering was the only technique used for characterizing the structure [31]. Confirming this structure would be important to explore the capacity of the hydrophobic core to dissolve hydrophobic molecules, whereas the hydrophilic shell disperses and stabilizes the system in aqueous medium.

The present study explored the triblock copolymers as agents for dispersing a concentrated phase of oppositely charged surfactant and polymer in the formation of nanoparticles capable of efficiently dissolving hydrophobic molecules within their core while maintaining dispersion in low-viscosity aqueous media by applying a simple mixing protocol. Four different $EO_xPO_yEO_x$ triblock copolymers were employed in an optimized preparation method involving hexadecyltrimethylammonium bromide and polyacrylic acid. The aim was to investigate the capacity of these nanoparticles to load oil and comprehend the impact of different triblock copolymer chain lengths on the nanoparticles' structure, stability, and oil encapsulation capacity. Hence, we proposed a more straightforward way to obtain nanoparticles of oppositely charged surfactants and polyions compared to the ones described in the literature, using chemicals widely available in the industry, which imply a potential application for the delivery of hydrophobic ingredients.

6.2. Experimental Section

6.2.1. Materials

Triblock copolymers, $EO_{90}PO_{60}EO_{90}$, $EO_{20}PO_{60}EO_{20,}$ $EO_{10}PO_{30}EO_{10,}$ and $EO_{04}PO_{30}EO_{04}$ were kindly supplied by Oxiteno and used as received, and their information is available in **Table 6.1**. Hexadecyltrimethyl ammonium bromide (≥ 98%), CTAB, and polyacrylic acid, PAA, (Mv ~ 450 kDa), were purchased from Sigma-Aldrich in the highest purity available. CTAB was selected for this study to precisely control the stoichiometric ratio, as its solid form allows for higher purity and accurate weight measurement. However, some tests were also conducted with Dehyquart A-CA from BASF, which is an aqueous solution of hexadecyltrimethyl ammonium chloride 24-26% used in cosmetic products. Ultra-pure water (18.2 MΩ·cm) obtained from Direct-Pure UP Rephile was used to prepare the samples. Eucalypt oil (EOil) and bergamot oil (BOil) were bought from viaAroma, sunflower oil (SFOil) from Giroil, and mineral oil (MOil) from Neon. The chemical structures of the materials used in this study are presented in **Scheme 6.1-SI**.

Table 6. 1 Names, weight fraction of ethylene oxide (EO%), average molecular weight (Mw) and hydrophilic-lipophilic balance (HLB) of the triblock copolymers provided by Oxiteno.

Polymer	Trade Name	Poloxamer Name	EO%	Mw (kD)	HLB
$EO_{90}PO_{60}EO_{90}$	Ultraric PE 127	Poloxamer 127	70%	11.43	21
$EO_{20}PO_{60}EO_{20}$	Ultraric PE 334	Poloxamer 334	35%	5.26	15
$EO_{10}PO_{30}EO_{10}$	Ultraric PE 64	Poloxamer 184	35%	2.64	13
$EO_{04}PO_{30}EO_{04}$	Ultraric PE 62	Poloxamer 182	17%	2.11	7

6.2.2.Sample Preparation

Samples were prepared by adding a PAA aqueous solution (0.14 wt% or 13.7 $mmol.L^{-1}$ of repeating units, pH of the solution was 4,3 in the range of its pka [168,169]) dropwise (1 drop per second) to an aqueous solution of CTAB (0.5 wt%, 13.7 $mmol.L^{-1}$) and $EO_xPO_yEO_x$ (0.96 wt%) under continuous magnetic stirring. The concentrations in molarity were 0.77 $mmol.L^{-1}$ for $EO_{90}PO_{60}EO_{90}$, 1.77 $mmol.L^{-1}$ for $EO_{20}PO_{60}EO_{20}$, 3.31 $mmol.L^{-1}$ for $EO_{10}PO_{30}EO_{10}$ and 4.38 $mmol.L^{-1}$ for $EO_{04}PO_{30}EO_{04}$. In some cases, a desired amount of oil was also present in the surfactant solution. The supplementary material (**Section 6.8.1**) describes the tests employed to select the mentioned concentrations.

6.2.3. Sample Characterization

Visual inspection was registered by photographs to determine the occurrence of phase separation. Dynamic light scattering (DLS) measurements were conducted using a SZ-100 Nanopartica instrument from Horiba, equipped with a 10 mW laser with a wavelength of 532 nm. Each sample (2.0 mL) was added to a polystyrene cuvette with four optically clear sides and a path length of 10 mm. The cuvettes were previously rinsed with fresh ultra-pure water and immediately covered after sample addition to avoid contamination with dust. All experiments were performed in triplicate at 25 °C, with an exposition time of 120 s and a scattering angle of 90°. The acquired data were processed using the

HORIBA NextGen Project SZ-100 software, employing Inverse Laplace Transform (ILT) to obtain intensity distributions and mean hydrodynamic radii. Zeta Potential was measured using the same equipment at 25 °C. The sample was held in a 1.5 mL U-shaped, disposable, folded capillary cell with two electrodes. The electrophoretic mobility was measured by the same equipment and converted to the zeta potential using its software based on the Smoluchowski Theory.

Small-angle X-ray scattering (SAXS) measurements were performed at the Institute of Physics of the University of São Paulo (IF-USP). The instrument used was a Xenocs Xeuss 2.0, equipped with a Dectris Pilatus 300k. The X-ray wavelength employed was 0.154 nm (CuKα line). Each sample was positioned in a capillary sample holder, and a thermal bath was used to maintain a constant temperature of 30 °C. The measurement duration was 5400 seconds. The distance between the sample holder and the detector was 0.2 m, resulting in a q range between 0.2 and 7.2 nm^{-1}. Fit2D [78] and SuperSAXS package software [79] allowed the subtraction of background and solvent (pure water) and integration of the obtained images. The resulting intensity curves, denoted as *I(q)*, as a function of scattering vector *q*, were fitted to a power law model using OriginLab at low *q* values. The *q* value of the first peak (selected from the peak maximum value) of each curve was used to determine the correlation distance, d = 2π/*q*. A Pm3n cubic structure was identified by the peaks corresponding to crystallographic planes (011),(002),(201),(112),(202), and (301) for some samples. In these cases, the cell parameter, a, was calculated by **Equation 6.1.**

$$q = \frac{2\pi}{a}(h^2 + k^2 + l^2) \qquad \textbf{Equation 6.1}$$

Where h, k, l are the Miller indices of the peak.

The cell volume was calculated using $V = a^3$. The micelle volume was calculated as $V_m = V/(8 \times 0.333)$, considering the presence of 8 quasi-spherical micelles within each unit cell, with a packing parameter of 0.333. Micelle radius was geometrically estimated as $r_m = (3 \cdot V_m/4\ \pi)^{1/3}$.

Cryogenic transmission electron microscopy (cryo-TEM) was used at the Brazilian Nanotechnology National Laboratory (LNNano). The samples were

diluted to 2 mg $mL^{-1,}$ and a 3 uL droplet was deposited on a 300-mesh lacey carbon-coated copper grid (Ted Pella). Samples were prepared in an automated vitrification system (Vitrobot Mark IV, FEI, Netherlands) with a blot force of -3 and a blot time of 3 s. The images were obtained using a TALOS F200C (ThermoFisher Scientific, Oregon, USA) equipped with a 4k x 4k CMOS camera, operating at 200 kV. Particle size was determined by analyzing at least 100 particles for each sample.

The oil loading capacity was accessed by the addition of various amounts of MOil (0.32, 0.48, and 0.64 wt %) into 5.0 mL of the solution containing CTAB and $EO_xPO_yEO_x$, followed by the gradual addition of 5.0 mL of PAA.

6.3. Results and Discussion

6.3.1. Characterization of nanoparticles

All the samples formed by 1.6 wt % of CTAB-PAA-$EO_xPO_yEO_x$ in water are turbid and have water-like viscosity (**Figure 6.1A**). Samples with $EO_{04}PO_{30}EO_{04}$ or $EO_{10}PO_{30}EO_{10}$ presented phase separation after 4 months, $EO_{20}PO_{60}EO_{20}$ after 4 months and 20 days, while samples with $EO_{90}PO_{60}EO_{90}$ remained visually homogenous for at least 6 months. $EO_xPO_yEO_x$ hydrophilic neutral blocks can hinder the macroscopic phase separation, dispersing and stabilizing the complexes in aqueous medium, forming nanoparticles. Based on the studies using hydrophilic blocks attached to the polyion [2,59,144] or by adding $EO_xPO_yEO_x$ [31,170], we hypothesized that the nanoparticles would form a core-shell structure. The core would be formed by polyion chains neutralizing CTAB micelles mixed with $EO_xPO_yEO_x$. The long EO chains would create a "hairy" shell extending towards the aqueous media (**Scheme 6.1**). It is worthmentioning that the samples formed by the posterior addition of $EO_xPO_yEO_x$ to a mixture of CTAB and PAA does not hinder phase separation, indicating that the order of the process is essential to form the nanoparticles.

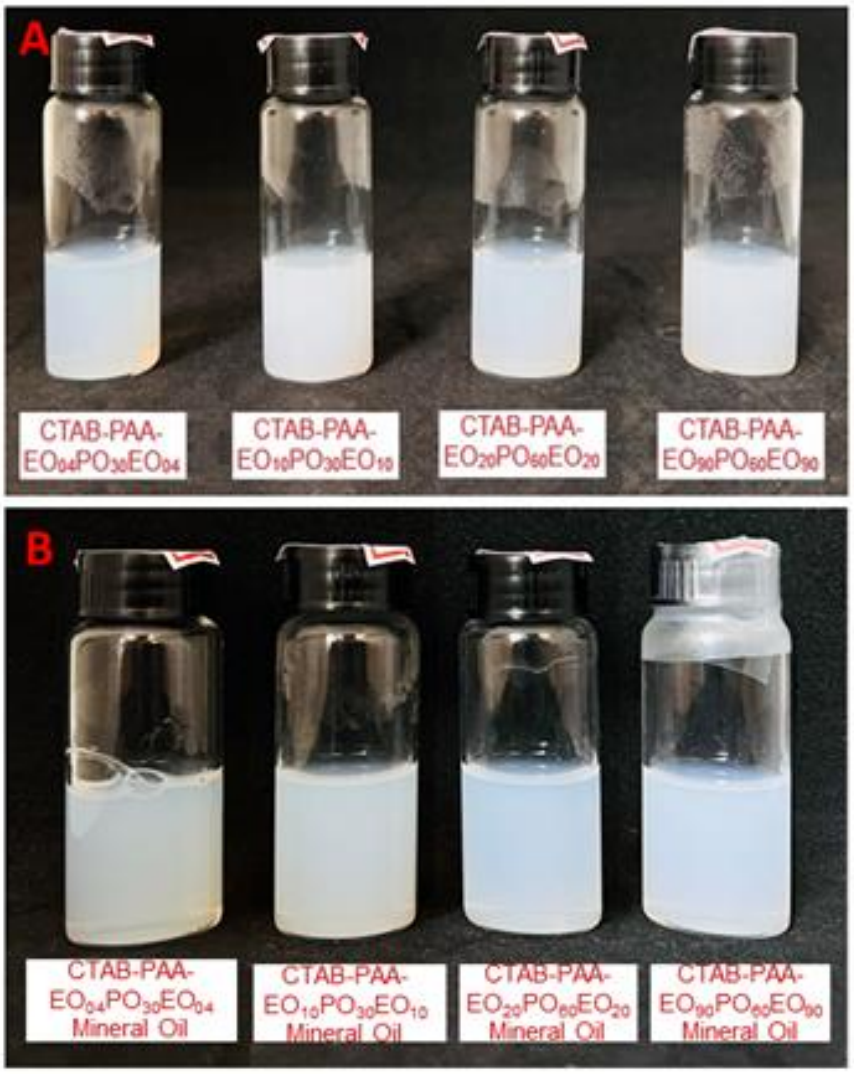

Figure 6. 1 Pictures of CTAB-PAA-$EO_xPO_yEO_x$ nanoparticles at 1.6 wt % **A**) before and **B**) after mineral oil loading (0.48 wt %).

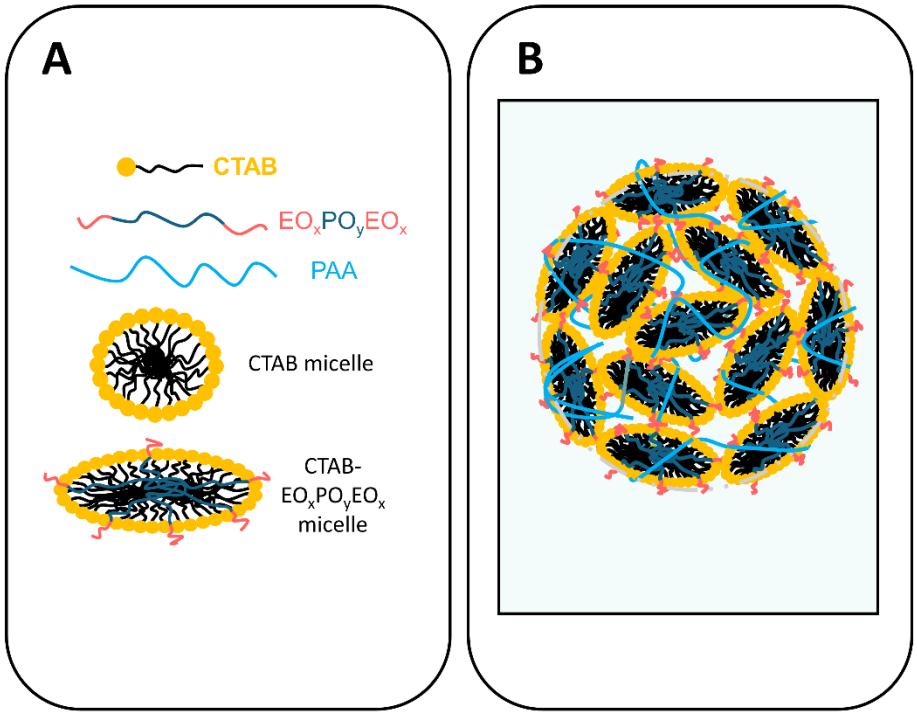

Scheme 6. 1 Representation of (A) components and micelles; and B) hypothetic core-shell structure expected for CTAB-PAA-$EO_xPO_yEO_x$ particles based on the literature *[2,31,144,156]* and confronted with the results of the present study. PAA addition to CTAB-$EO_xPO_yEO_x$ micelles leads to electrostatic interaction, interconnecting the mixed micelles and forming core-shell nanoparticles.

Cryo-TEM images showed the morphology of the nanoparticles (**Figure 6.2A-C and 6.2G-I**), revealing that CTAB-PAA-$EO_xEO_yEO_x$ formed spherical nanoparticles with a diameter varying from 50 to 180 depending on the poloxamer of choice (obtained by measuring 120 particles for each system, diameters measured are described in **Table 6.2**). The interface of the nanoparticles is smooth, and they have a uniform electron density without the expected hairy shell of EO blocks represented in **Scheme 6.1**. Indeed, based on the gyration radius of the hydrophilic block in water [171], the shell would theoretically present a maximum thickness of 1.6 nm. This observation may originate from inadequate contrast or resolution to discern the shell or from the fact that electron microscopy could not resolve them due to solvation effects. Using different $EO_xPO_yEO_x$ did not affect the morphology or diameter of the nanoparticles.

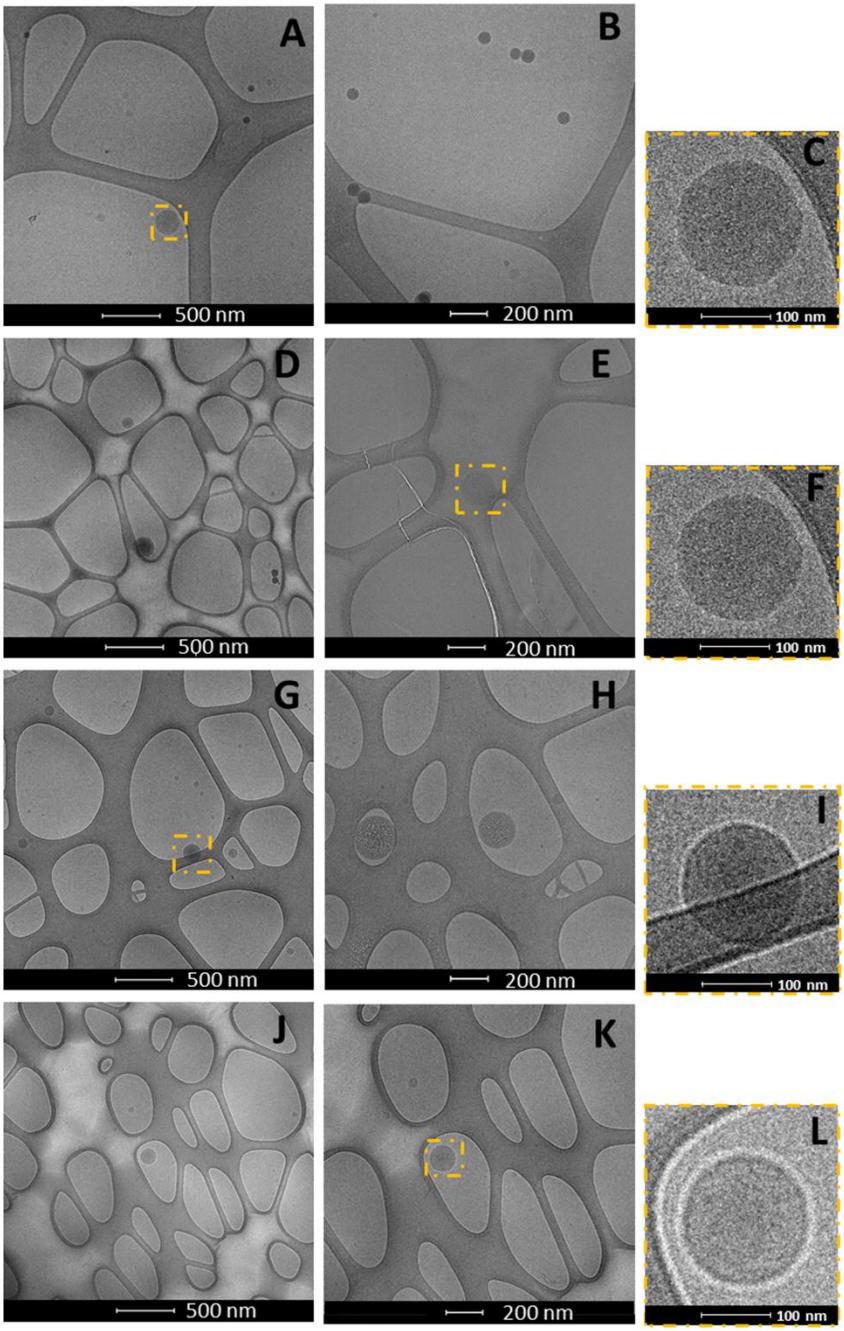

Figure 6. 2 Cryo-TEM images of different CTAB-PAA-$EO_xPO_yEO_x$ nanoparticles: **A-B)** with $EO_{90}PO_{60}EO_{90}$; **C)** Zoom into the region highlighted in yellow in A; **D-E)** with $EO_{90}PO_{60}EO_{90}$ and MOil; **F)** Zoom into the region highlighted in yellow in E; **G-H)** with $EO_{04}PO_{30}EO_{04}$ nanoparticles; **I)** Zoom into the region highlighted in yellow in G; **J-K)** with $EO_{04}PO_{30}EO_{04}$ and Moil. **L)** Zoom into the region highlighted in yellow in K.

Table 6. 2 CTAB-PAA-$EO_xPO_yEO_x$ nanoparticles' diameter measured by Cryo-TEM and DLS.

Samples	Cryo-TEM (diameter) nm	DLS (Hydrodynamic Diameter) nm
$EO_{04}PO_{30}EO_{04}$	70 ± 21	132 ± 5
$EO_{90}PO_{60}EO_{90}$	85 ± 20	161 ± 3

DLS provided size distributions showing that all samples present only one population with mean hydrodynamic diameter varying from 132 to 175 nm depending on the copolymer of choice (**Table 6.2** and **Figure 6.3**), confirming the formation of nanoparticles due to the addition of $EO_xPO_yEO_x$ copolymers. The large difference between the hydrodynamic diameter obtained by DLS and the size measured by TEM could be related to the presence of a hairy shell affecting the diffusion or the difference in weighting between the techniques. When comparing two systems with the same PO block length, the ones with longer EO chains presented slightly larger hydrodynamic diameters, corroborating the hypothesis because larger nonionic blocks would lead to larger corona structures than the others. Measurements after 1 month showed that the diameter of nanoparticles with $EO_{04}PO_{30}EO_{04}$, $EO_{10}PO_{30}EO_{10}$, $EO_{20}PO_{60}EO_{20}$, and $EO_{90}PO_{60}EO_{90}$ increased 14 %, 60 %, 64 %, and 2,5 %, respectively (**Figure 6.3**). Precipitation was observed for $EO_{04}PO_{30}EO_{04}$ and $EO_{10}PO_{30}EO_{10}$ after 120 days and for $EO_{20}PO_{60}EO_{20}$ after 140 days. However, nanoparticles prepared with $EO_{90}PO_{60}EO_{90}$ did not precipitate for at least 6 months and presented the smallest diameter variation, showing that its long EO blocks were important to guarantee stabilization.

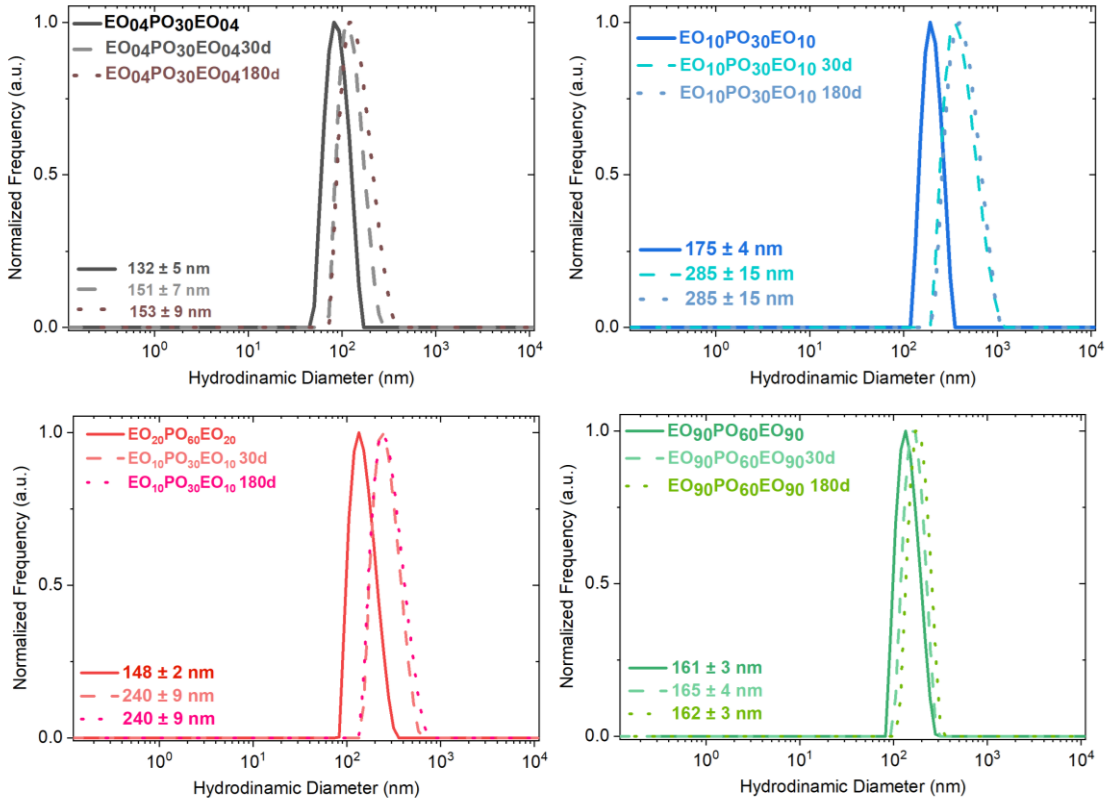

Figure 6. 3: Hydrodynamic diameter distribution of samples containing CTAB-PAA-$EO_xPO_yEO_x$ nanoparticles at 1.6 wt % measured by DLS 1, 120, and 180 days after preparation. The numbers indicate the mean hydrodynamic diameter and the standard deviation of triplicates. *Straight line: samples measured after 1 day, dash line: samples measured 120 days, short-dash line: samples measured after 180 days.

Due to the high stability observed, apparent zeta potential (ζ) was measured for all CTAB-PAA-$EO_xPO_yEO_x$ nanoparticles, presenting a value of 39 ± 5 mV, corresponding to an electrophoretic mobility of 0.00037 ± 0.00004 $cm^2.Vs^{-1}$, which remained the same across all samples. The measurements were performed in water; hence, the potential zeta values are only apparent but indicate positively charged particles. The particles were expected to be electroneutral, but the complexation equilibrium shifted, probably due to the pKa of PAA and the pH of the medium. However, there is no sufficient evidence to

prove this hypothesis. Although a high positive value could be attributed to the high stability, this is not the sole reason. Samples with different $EO_xPO_yEO_x$ presented different times for destabilization and had the same zeta potential value. A possible explanation would be the presence of the expected hairy shell, which would explain why the systems with longer EO blocks exhibited greater stability. All the samples presented a pH of 4.3, indicating that only a fraction of carboxyl groups are ionized in PAA. The degree of ionization affects the overall electrostatic balance within the system, potentially influencing the self-assembly and stability of nanoparticles formed. In the present study, the pH was not varied to study nanoparticle formation by only mixing the raw materials. However, this parameter could be varied to explore other possibilities, such as the controlled release of components loaded in the nanoparticles due to pH sensitivity.

The range of diameter for the obtained nanoparticles is similar to or slightly higher than the ones observed in previous studies, which obtained core-shell structures by using diblock charged-neutral copolymers with oppositely charged surfactants [2,153] or by adding a nonionic surfactant to the complex of oppositely charged surfactant and polymers [41]. The differences between the average sizes observed by TEM and the hydrodynamic diameters obtained by DLS are in the same range as the studies that proposed core-shell structures [153], reinforcing that this structure is also possible in the present system, although the shell was not visible by cryo-TEM, due to the similar electron density of highly hydrated EO and the surrounding water.

USAXS and SAXS curves also provide information for elucidating the structure of the obtained nanoparticles (**Figure 6.4**). The Guinier region is not within the analyzed range of q to calculate the gyration radius, Rg, due to the relatively large sizes of nanoparticles (around hundreds of nanometers, providing $Rg*q > 1.3$). Hence, the decay observed at q values lower than 5×10^{-2} nm^{-1} is probably related to the Porod region, providing information on the surface of the nanoparticles through their fractal dimension. This region was fitted to a power-law model, where $I(q) \sim q^{-\alpha}$, and α is the power-law exponent, which is related to the fractal dimension of the object, Dm (mass fractal for $1 < \alpha < 3$) or Ds (surface fractal for $3 < \alpha < 4$) [172,173]. According to Porod's law, objects with a smooth surface have $\alpha = 4$ [174,175]. For the nanoparticles from the present study, α

varies between 1.9 and 2.4, indicating they are a mass fractal and do not have a smooth surface as seen by cryo-TEM images. The literature presents some values as references for comparison. Interestingly, the range of 2 to 2.5 is mainly related to different conformations of polymer chains [172,173], indicating that the nanoparticle's surface might be formed by a shell of EO blocks extending towards the aqueous medium.

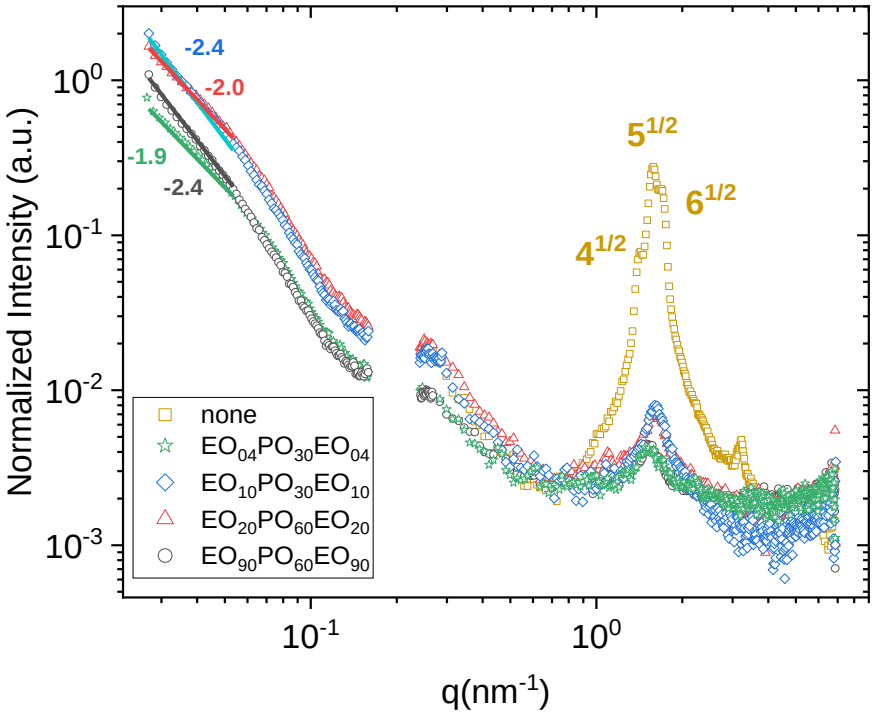

Figure 6. 4 USAXS and SAXS curves of aqueous samples prepared with CTAB 17 mmol.L^{-1}, PAA 17 mmol.L^{-1} and different $EO_xPO_yEO_x$ (0.77 mmol.L^{-1} of $EO_{90}PO_{60}EO_{90}$, 1.77 mmol.L^{-1} of $EO_{20}PO_{60}EO_{20}$, 3.31 mmol.L^{-1} of $EO_{10}PO_{30}EO_{10}$ and 4.38 mmol.L^{-1} of $EO_{04}PO_{30}EO_{04}$). The lines refer to the fitting of $I(q) \sim q^{-\alpha}$, and the values are the power-law exponent (α). Measurements were performed one day after sample preparation.

After characterizing the shell, SAXS data can also be used to gather information about the structure inside the core. Mixing surfactants and oppositely charged polymers at a stoichiometric ratio of charges can form liquid crystals [57]. Previous studies involving the attachment of a hydrophilic block to the

polyelectrolyte [2,176] or the addition of nonionic surfactant [143,176] can keep the presence of a liquid crystalline structure in the dispersed nanoparticles. When aqueous solutions of CTAB and PAA were mixed in stoichiometric proportion of charges (17 mmol.L^{-1} each), a liquid crystalline phase with a cubic Pm3n structure and a unit cell of 9.5 nm was formed, as evidenced by SAXS (**Figure 6.4**). However, by adding $EO_xPO_yEO_x$ copolymers, the SAXS curve exhibited only a broad structure peak. Hence, the copolymers hinder not only phase separation but also the self-organization of micelles in liquid crystals. This disorganization is probably caused by the presence of hydrophobic PO blocks inside the nanoparticle's core. The correlation distance is probably related to the distance between the center of neighboring micelles and can be calculated from the structure peak position ($d = 2\pi/q$). The value of *d* was 4.2 nm for $EO_{04}PO_{30}EO_{04}$ and $EO_{90}PO_{60}EO_{90}$ and 3.8 nm for $EO_{10}PO_{30}EO_{10}$ and $EO_{20}PO_{60}EO_{20}$. A straight hexadecyl chain has 2.15 nm, according to Tanford's equation [177], so CTAB micelles have a diameter of around 4.3 nm. The similarity between the diameter and the correlation distance indicates that the micelles are still in close contact, although not organized. SAXS results from micellar solutions of CTAB with $EO_{90}PO_{60}EO_{90}$ or $EO_{04}PO_{30}EO_{04}$ at the same concentrations used to prepare the nanoparticles corroborate this hypothesis (**section 6.8.2 of Supplementary material**). The micelles formed by CTAB or its mixture with $EO_xPO_yEO_x$ can be considered core-shell ellipsoids with cross-sections in the same size range of the correlation distance obtained by SAXS for the nanoparticles. Therefore, although EO blocks disperse and stabilize the nanoparticles in water, PO blocks likely hinder the organization of the concentrated micelles inside the core.

The obtained results agree with our hypothetical structure. Although they are not an unequivocal proof, we propose that upon PAA addition into CTAB-$EO_xPO_yEO_x$ mixed micelles, the polyanion interconnects several cationic mixed micelles by electrostatic attraction, forming a core rich in the concentrated micelles, while the EO blocks of the nonionic copolymer extend towards the aqueous medium forming a hydrophilic hairy shell, as represented in **Scheme 6.1**. The proposed structure is very similar to core-shell nanoparticles formed by charged-neutral diblock copolymers with oppositely charged surfactants [2,59,176]. Hence, we propose that the nanoparticles obtained in the present

study can also be used to load hydrophobic ingredients in their core formed by concentrated micelles [2].

6.3.2. Oil loading

Mineral oil (MOil) was added during the preparation of the nanoparticles to verify their applicability as vehicles of hydrophobic ingredients. The overall oil-loading capacity was tested with samples containing and increasing concentrations of MOil up to 0.64 wt%. Oil separation was evident at the highest used concentration (**Figure 6.10 of Supplementary material**), indicating that the loading capacity was exceeded. Consequently, suspensions of 1.6 wt% of nanoparticles with 0.48 wt% of MOil were characterized and compared with similar samples without oil. It is worth noticing that the solutions of CTAB, PAA, $EO_xPO_yEO_x$, CTAB-$EO_xPO_yEO_x$, or PAA-$EO_xPO_yEO_x$ are not capable of dissolving or dispersing oil at this concentration by the same method of homogenization used for the nanoparticles.

MOil addition did not alter the visual appearance of the suspensions (**Figure 6.1B**) or the morphology of the nanoparticles (**Fig 6.2D-F and 6.2J-L**) but reduced their hydrodynamic size and increased their polydispersity (**Figure 6.5**), except for the sample with $EO_{90}PO_{60}EO_{90}$. Comparing the different copolymers used in the nanoparticles, the stability was lower for samples made with $EO_{10}PO_{30}EO_{10}$ or $EO_{20}PO_{60}EO_{20}$, presenting oil separation after 2 days, than for samples with $EO_{20}PO_{60}EO_{20}$, which were stable for 60 days, or with $EO_{90}PO_{60}EO_{90}$, which were stable for more than 180 days. However, there is no clear trend of the effects of EO/PO block length on the stability time.

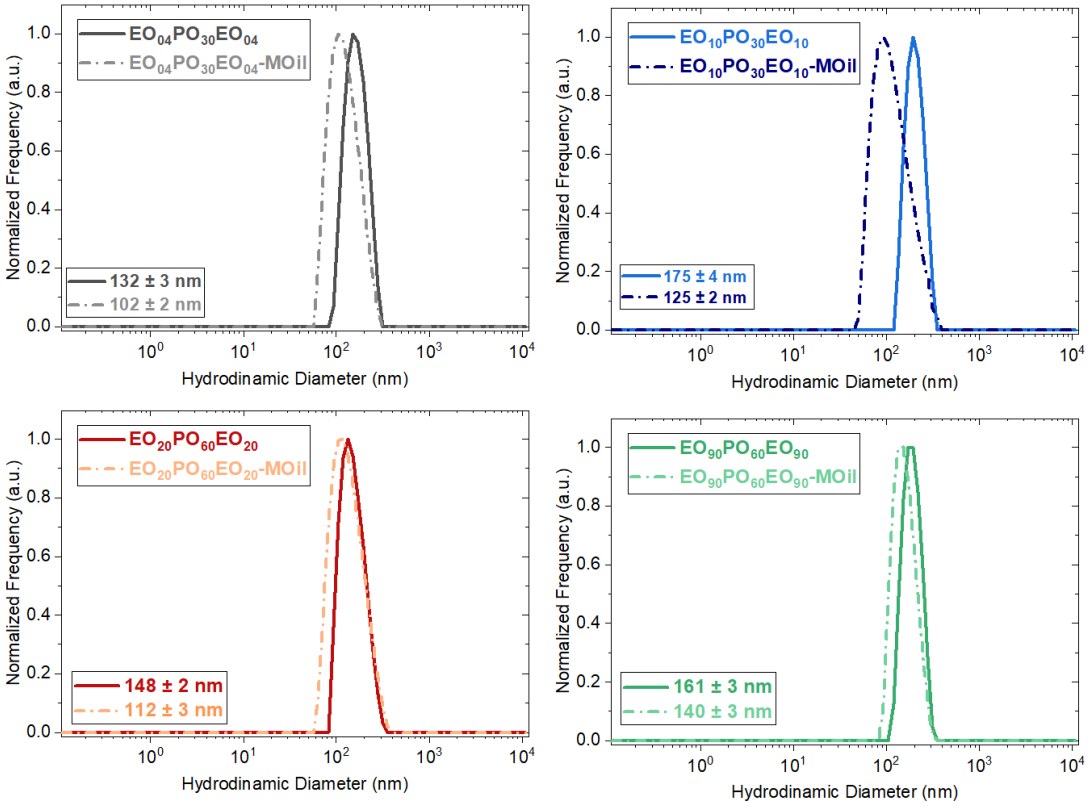

Figure 6.5 Hydrodynamic diameter distribution of CTAB-PAA-$EO_xPO_yEO_x$ nanoparticles at 1.6 wt % obtained by DLS measurements without and with 0.48 wt% of mineral oil, one day after preparation.

A reduction in size after oil addition has already been observed for core-shell nanoparticles [2], which was attributed to the phase transition of the micelles inside the core, observed in SAXS data. However, in the present study, MOil only caused a slight increase in the correlation distance for nanoparticles containing $EO_{04}PO_{30}EO_{04}$ to d = 4.4 nm, comparing with the sample without oil which showed d = 4.2 nm (**Figure 6.6**), suggesting that incorporation of MOil did not alter the structure of the nanoparticles.

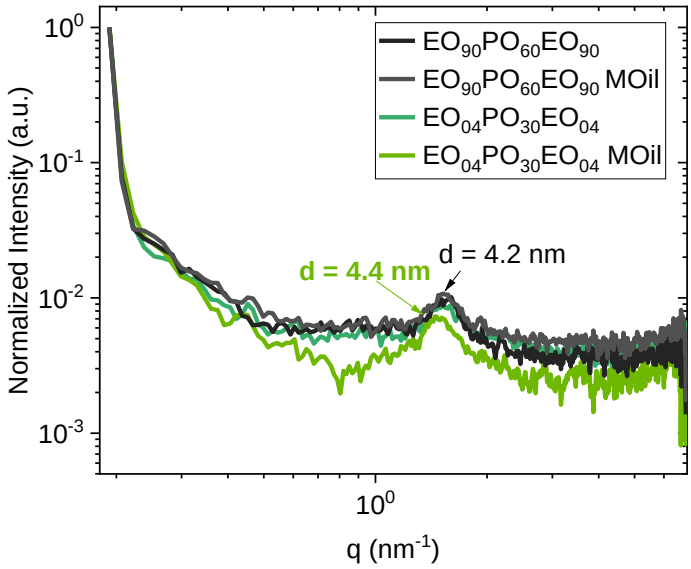

Figure 6.6 SAXS curves of CTAB-PAA-$EO_{04}PO_{30}EO_{04}$ and CTAB-PAA-$EO_{90}PO_{60}EO_{90}$ nanoparticles at 1.6 wt% without and with 0.48 wt% of mineral oil. Measurements were performed one week after sample preparation.

6.3.3. Loading of different oils

CTAB-PAA-$EO_{90}PO_{60}EO_{90}$ system was chosen to compare the effects of different oils due to its superior stability. Various oils were employed to evaluate the system's capability to incorporate oils of diverse polarities and origins, including vegetal and mineral oils. Bergamot oil (BgOil) and Eucalyptus Oil (EuOil) are essential oils with a cyclic structure (**Scheme 6.21-SM**) and can be used in pharmaceutical and cosmetics formulations [133]. Sunflower Oil (SfOil) is a vegetable oil containing predominantly linoleic acid [178]. All the systems displayed low viscosity (visually similar to water), regardless of the oil added (at 0.48 wt %), allowing their use in spray formulations, for example. Adding SfOil and EuOil decreased the hydrodynamic diameter of the nanoparticles to values similar to those observed upon MOil addition. The addition of BgOil did not change the nanoparticles diameters (**Figure 6.7**). As observed for Moil, samples containing BgOil, EuOil did not present phase separation for at least 6 months. However, the sample with SFOil presented oil separation after 3 months.

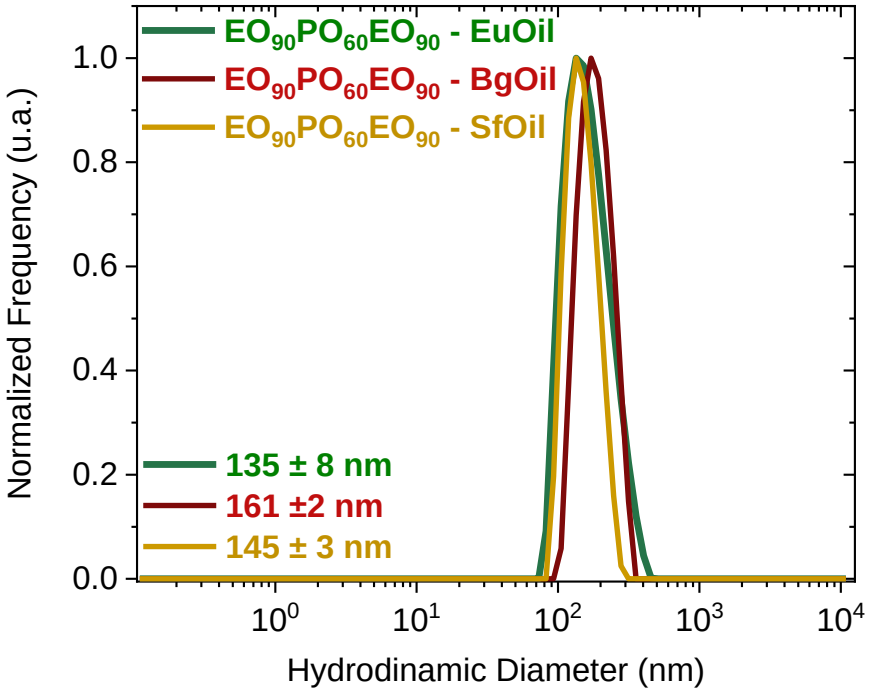

Figure 6. 7: Hydrodynamic diameter distribution of samples containing 1.6 wt % CTAB-PAA-$EO_xPO_yEO_x$ nanoparticles with different oils obtained by DLS, one day after sample preparation.

Although the nanoparticles presented the same diameter range and several months of stability regardless of the oil used, SAXS results show the effect on the core structure (**Figure 6.8**). The correlation peak became narrower and more intense in the following order: MOil, SfOil, EuOil, and BgOil. Moreover, the peaks slightly shifted to lower *q*-values, and a broad signal appeared around 0.08 and 0.06 $Å^{-1}$ for samples containing EuOil and BgOil, respectively. MOil is mainly formed by linear saturated hydrocarbons, and SfOil by unsaturated fatty acids. In contrast, EuOil and BgOil are mainly formed by cyclic compounds, which are very different to the linear CTAB molecules compared to the compounds of MOil and SfOil. Hence, when dissolved in the interior of CTAB micelles, EuOil and BgOil could probably have more impact on the micellar curvature and diameter, affecting their organization. The effect of hydrophobic oil in the core of CTAB was also observed by Akamatsu et al. [179], where SANS measurements was used to study the solubilization of oils in the presence of micelles. This study showed

that limonene (one of the major components of BgOil) was solubilized inside the core of CTAB micelles, which could be related to the broad bump observed in SAXS measurements.

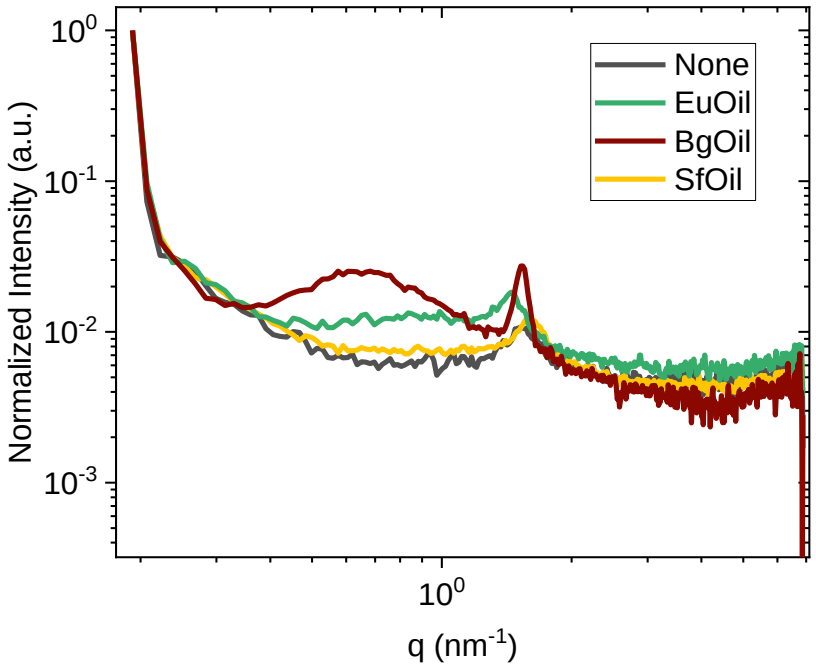

Figure 6. 8 SAXS curves of 1.6 wt% of CTAB-PAA-$EO_{90}PO_{60}EO_{90}$ nanoparticles with 0.48 wt% of different oils. Measurements were performed one week after sample preparation.

6.4. Conclusion

The present study shows the possibility of obtaining stable nanoparticles capable of loading hydrophobic ingredients by a straightforward method. It uses triblock copolymers ($EO_xPO_yEO_x$) to disperse the liquid-crystalline phase formed by oppositely charged surfactants and polymers. The procedure is simple, involves widely available materials, and does not require high energy input. The suspensions have water-like viscosity, which is adequate for spray formulations or to be adapted using rheology modifiers when necessary.

Cryo-TEM images provided a clear depiction of the morphology of the nanoparticles, evidencing their spherical shape and sizes of tens to hundreds of

nanometers depending on the $EO_xPO_yEO_x$ used. Despite expectations of a core-shell structure with a "hairy" shell extending towards the aqueous media, the cryo-TEM images did not show evidence of the expected shell, possibly due to resolution limitations, lack of electron contrast, or solvation effects. However, dynamic light scattering (DLS) measurements confirmed the presence of nanoparticles with hydrodynamic diameters consistent with the formation of a shell, as evidenced by the difference between DLS and TEM measurements. Moreover, longer EO blocks contributed to enhanced stability, with nanoparticles containing $EO_{90}PO_{60}EO_{90}$ stable for at least 6 months. Zeta potential measurements further supported the role of EO blocks in stabilizing the nanoparticles because all samples presented similar positive zeta potential values.

Although electron microscopy could not reveal the hypothetical structure, small-angle X-ray scattering (SAXS) provided additional insights. The core is formed by concentrated CTAB micelles neutralized by PAA chains but is not liquid crystalline. The nanoparticles have a mass fractal surface structure, indicating their surface is not smooth, which agrees with a hairy shell. Hence, we propose that the hydrophobic PO blocks are probably inside the micelles, whereas the hydrophilic EO blocks probably extend towards the aqueous medium, providing stability. The differences are small when varying the copolymer structure or the oil type, showing the nanoparticles' versatility as vehicles of oily ingredients in the aqueous medium. For samples containing 1.6 wt% of CTAB-PAA-EO90PO60EO90 nanoparticles, at least 0.48 wt% of different oils can be loaded, resulting in 30% oil relative to the particle mass with stability of at least 6 months.

In conclusion, our study advances the understanding of colloidal and surface science by providing detailed insights into the formation, structure, and stability of nanoparticles composed of CTAB-PAA-$EO_xPO_yEO_x$ copolymers. Our findings suggest an interplay between copolymer composition, nanoparticle structure, and stability, with implications for various applications in pharmaceuticals, cosmetics, and beyond. The proposed core-shell structure, inspired by previous studies with charged-neutral diblock copolymers [2,59,144], highlights the ease of preparation and versatility of these nanoparticles for loading hydrophobic ingredients and potentially delivering them to target sites. Moreover,

considering the pH-sensitivity of PAA, future studies can investigate the system at different pH levels to explore the possibility of pH-controlled release

6.5. Funding

This study was financed in part by the Brazilian agencies: Conselho Nacional de Desenvolvimento Científico e Tecnológico (CNPq), Fundação Carlos Chagas Filho de Amparo à Pesquisa do Estado do Rio de Janeiro (FAPERJ, Programa Jovem Pesquisador Fluminense E-26/201.674/2021) and Coodenação de Aperfeiçoamento de Pessoal de Nível Superior - Brasil (CAPES, Finance Code 001). KOL received a scholarship from FAPERJ (E-26/203.210/2022). MOF, SCSC, and LOP received scholarships from CNPq (140638/2021-0, 131657/2021-6, and 180745/2022-0, respectively). AMP received a grant from CNPq (304212/2022-9).

6.6. Acknowledgments

We acknowledge the Brazilian Nanotechnology National Laboratory (LNNano) for the shift allocation and support with Cryo-TEM measurements (Proposal 20230640), with a special thanks to Gisele Dalmonico for her assistance during the shift. We thank Oxiteno for generously providing the triblock copolymers. We are grateful to Cristiano Luis Pinto de Oliveira and his team from the Institute of Physics of the University of São Paulo (USP) for the SUPERSAXS package and supporting SAXS measurements.

6.7. Declaration of competing interest

The authors declare that they have no known competing financial interests or personal relationships that could have appeared to influence the work reported in this paper.

6.8. Supplementary Materials

6.8.1.Optimization of the Experimental Procedure

All concentrations used in the experiments are described in **Table 6.3**. For clarity, chemicals concentrations will be denoted as $[CTAB]_a$, $[PAA]_b$ and $[EO_xPO_yEO_x]_c$, where a, b and c represent the respective concentrations employed in $mmol.L^{-1}$. The chemical structure of the compounds employed in this study are illustrated in **Scheme 6.2,** for oils we used the major component.

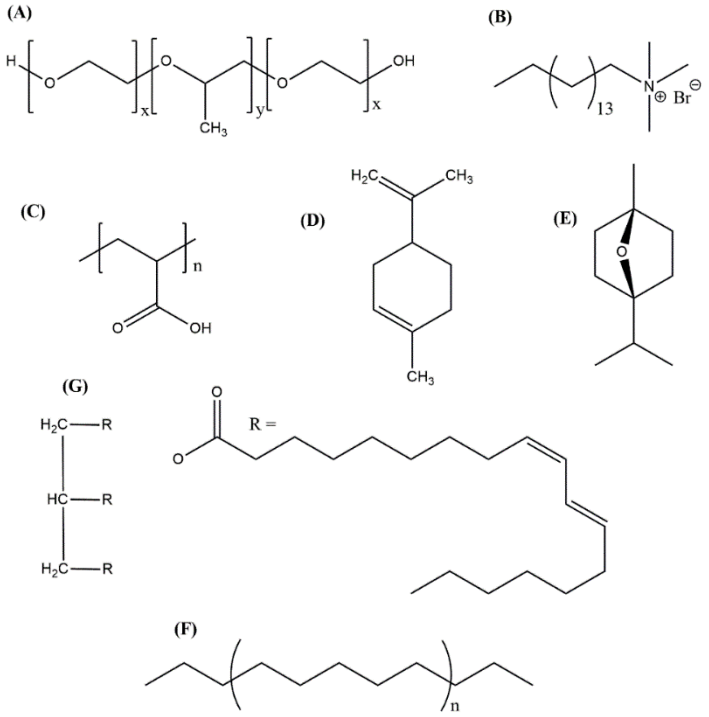

Scheme 6. 2 Chemical structures of (A) $EO_xPO_yEO_x$ triblock copolymer, (B) CTAB, (C) PAA, (D) limonene (the major component of BOil), (E) eucalyptol, (the major component of EOil) (F) paraffin (the major component of MOil) (G) linoleic acid (the major component of SFOil).

Table 6.3: Concentrations of Hexadecyltrimethyl ammonium bromide(CTAB), polyacrylic acid, PAA and different triblock copolymers (EO90PO60EO90) used in this work.

[CTAB] $mmol.L^{-1}$	**[PAA] $mmol.L^{-1}$**	**[$EO_{90}PO_{60}EO_{90}$] $mmol.L^{-1}$**
2.7	2.7	0.15
8.2	8.2	0.46
13.7	13.7	0.77

27.4	27.4	1.54
54.8	54.8	3.08
13.7	13.7	0
13.7	13.7	0.03
13.7	13.7	0.13
13.7	13.7	0.26
13.7	13.7	1.54
		$EO_{10}PO_{30}EO_{10}$ mmol.L^{-1}
13.7	13.7	3.3
		$EO_{04}PO_{30}EO_{04}$ mmol.L^{-1}
13.7	13.7	4.4
		$EO_{20}PO_{60}EO_{20}$ mmol.L^{-1}
13.7	13.7	1.8

6.8.2 Methods of preparation

The investigation started by employing $EO_{90}PO_{60}EO_{90}$, chosen for its heightened hydrophilicity. Throughout the text, polymer's concentration is expressed in terms of repeating units. Previous studies highlighted the impact of different methodologies on the dispersibility of a concentrated phase [31,161], hence, to determine the optimal sample preparation method, a concentration of 13.7 mmol.L^{-1} was fixed for CTAB and PAA monomers.

Three distinct methodologies were explored. Initially, a CTAB-PAA mixture was prepared, followed by the gradual addition of $EO_{90}PO_{60}EO_{90}$. However, $EO_{90}PO_{60}EO_{90}$ demonstrated an inability to dissolve the formed CTAB-PAA complex due to strong electrostatic interactions, rendering the complex insoluble. An alternative approach involving gradual CTAB drops addition to a PAA-$EO_{90}PO_{60}EO_{90}$ mixture, but this resulted in turbidity and some phase separation, which was attributed to the tendency of PAA-$EO_{90}PO_{60}EO_{90}$ to form larger micellar aggregates, as observed by Wang at al. in their study [180]. The final method utilized a mixture of CTAB-$EO_{90}PO_{60}EO_{90}$ with PAA added drop by drop, yielding a milk-like sample characterized by high stability.

6.8.3 Effect of $EO_{90}PO_{60}EO_{90}$ on the dispersion of CTAB-PAA complex and formation of nanoparticles:

To assess the optimal $EO_{90}PO_{60}EO_{90}$ proportion to obtain the nanoparticles, samples were prepared with the same CTAB and PAA concentration, varying the copolymer concentration. Images in **Figure 6.9** depict distinct system changes as $EO_{90}PO_{60}EO_{90}$ concentration increased. Particle size analysis confirmed macroscopic observations, indicating a crucial role of $EO_{90}PO_{60}EO_{90}$ concentration in phase behaviour. Initially, a solid formed at concentrations up to 0.13 mmol. L^{-1} of $EO_{90}PO_{60}EO_{90}$, **Figure 6.9A-6.9C**. This solid, characterized by thin filaments visible only to the naked eye, in imagens 1B and 1C, was not captured in images. Subsequently, a mixture of solid and a highly turbid sample emerged, indicating the beginning of nanoparticles' formation up to 0.26 mmol. L^{-1} of $EO_{90}PO_{60}EO_{90}$, **Figure 6.9D**. Following this stage, the sample transitioned into a white and turbid dispersion without any solid formation above 0.77 mmol. L^{-1} of $EO_{90}PO_{60}EO_{90}$ and the same behaviour was observed up to 1.54 mmol. L^{-1} of $EO_{90}PO_{60}EO_{90}$.

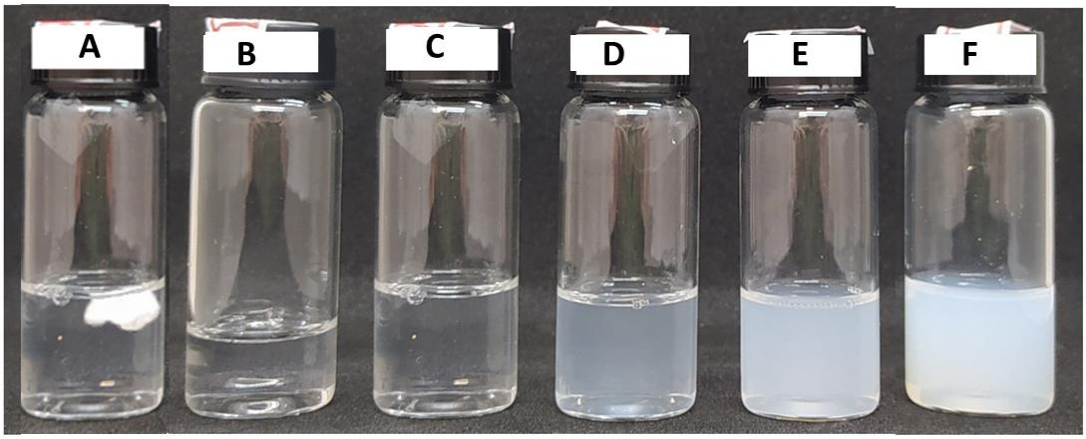

Figure 6.9: Photographs of samples containing 13.7 mmol.L^{-1} CTAB 13.7 mmol.L^{-1} PAA monomers and $EO_{90}PO_{60}EO_{90}$ in the following concentrations: **A)** none; **B)** 0.03 mmol.L^{-1}; **C)** 0.13 mmol.L^{-1}; **D)** 0.26 mmol.L^{-1}; **E)** 0.77 mmol.L^{-1}; **F)** 1.54 mmol.L^{-1}.

Particle size was determined using DLS, yielding results consistent with macroscopic observations, **Figure 6.10**. Particle size analysis of $[EO_{90}PO_{60}EO_{90}]_{0.13}$ and $[EO_{90}PO_{60}EO_{90}]_{0.26}$ was conducted after separating the

solid and liquid components, revealing diameters above 1 μm for $[EO_{90}PO_{60}EO_{90}]_{0.13}$, outside the measured range of the technique, and 350 nm for $[EO_{90}PO_{60}EO_{90}]_{0.26,}$ confirming the formation of nanoparticles. An increase in $EO_{90}PO_{60}EO_{90}$ concentration resulted in a reduction in particle diameter, with $[EO_{90}PO_{60}EO_{90}]_{0.77}$ measuring 161 nm and $[EO_{90}PO_{60}EO_{90}]_{1.54}$ 110 nm. This suggests a crucial role of the copolymer in phase behaviour, consistent with previous findings in similar systems where increased nonionic surfactant concentration led to enhanced miscibility in water of different P-S complexes [162].

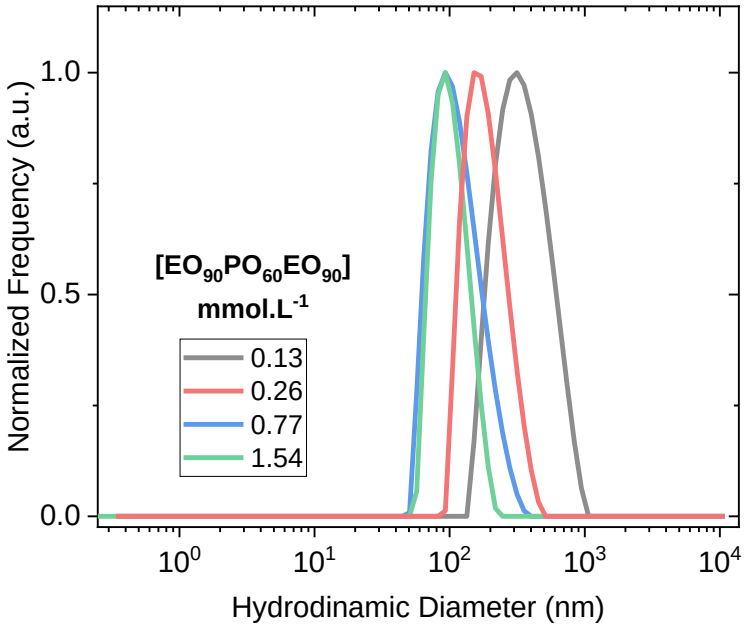

***Figure 6.10**: Hydrodynamic diameter distribution of samples containing CTAB-PAA-$EO_{90}PO_{60}EO_{90}$ by DLS at different triblock copolymer, $EO_{90}PO_{60}EO_{90}$, concentrations.*

Both $[EO_{90}PO_{60}EO_{90}]_{0.77}$ and $[EO_{90}PO_{60}EO_{90}]_{1.54}$ exhibited similar particle sizes with stability maintained for at least 45 days at 25 °C, therefore considering the eventual application of these systems on bigger scales we decided to fix 0.77 $mmol.L^{-1}$ as the copolymer concentration.

Following adjustment of copolymer concentration, we investigated the impact of varying CTAB-PAA concentrations on the size distribution of the systems (ranging from $CTAB_{2.7}$-$PAA_{2.7}$-$[EO_{90}PO_{60}EO_{90}]_{0.15}$ to $CTAB_{27.4}$-$PAA_{27,4}$-$[EO_{90}PO_{60}EO_{90}]_{1.54}$. **Figure 6.11**) to determine the optimal concentration of the surfactant and polyion for utilizing this system as nanocarriers. Gradually increasing CTAB-PAA concentration from samples such as $CTAB_{2.7}$-$PAA_{2.7}$-$[EO_{90}PO_{60}EO_{90}]_{0.15}$ to $CTAB_{13.7}$-$PAA_{13.7}$-$[EO_{90}PO_{60}EO_{90}]_{0.77}$, **Figure 6.11A-6.11C**, resulted in a slight increase of the size, as observed in DLS measurements at **Figure 6.11**. However, $CTAB_{27.4}$-$PAA_{27,4}$-$[EO_{90}PO_{60}EO_{90}]_{1.54}$, **Figure 6.11D**, exhibited a notable change. This behaviour suggests that the system may be approaching a phase transition, as evidenced by the drastic transformation of $CTAB_{54,8}$-$PAA_{54,8}$-$[EO_{90}PO_{60}EO_{90}]_{3,08}$ into a gel-like sample with high viscosity, **Figure 6.11E**, making the measurement of its size through DLS unfeasible.

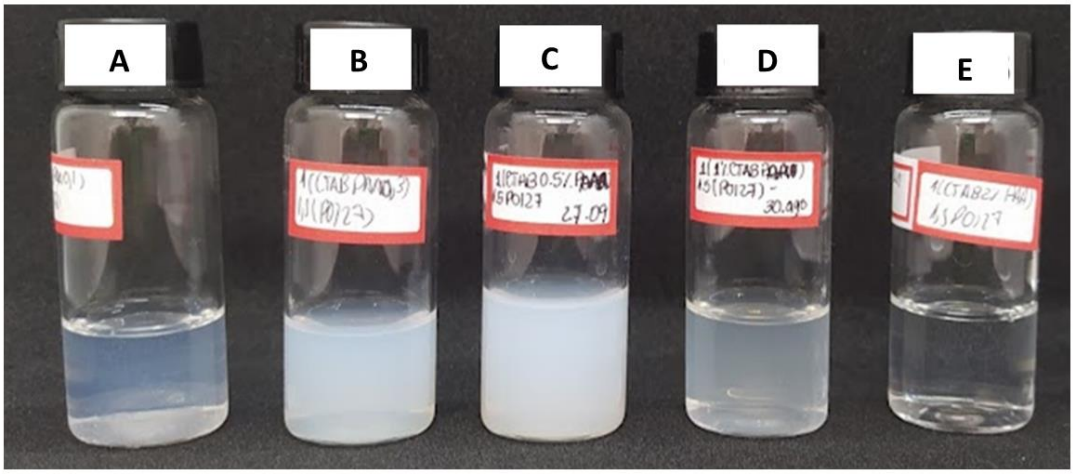

Figure 6.11: Photographs of samples containing CTAB-PAA-$EO_{90}PO_{60}EO_{90}$ in the following concentrations: **A)** CTAB 2.7 $mmol.L^{-1}$, PAA 2.7 $mmol.L^{-1}$ and $EO_{90}PO_{60}EO_{90}$ 0.15 $mmol.L^{-1}$; **B)** CTAB 8.2 $mmol.L^{-1}$, PAA 8.2 $mmol.L^{-1}$ and $EO_{90}PO_{60}EO_{90}$ 0.46 $mmol.L^{-1}$; **C)** CTAB 13.7 $mmol.L^{-1}$, PAA 13.7 $mmol.L^{-1}$ and $EO_{90}PO_{60}EO_{90}$ 0.77 $mmol.L^{-1}$; **D)** CTAB 27.4 $mmol.L^{-1}$, PAA 27.4 $mmol.L^{-1}$ and $EO_{90}PO_{60}EO_{90}$ 1.54 $mmol.L^{-1}$; **E)** CTAB 54.8 $mmol.L^{-1}$, PAA 54.8 $mmol.L^{-1}$ and $EO_{90}PO_{60}EO_{90}$ 3.08 $mmol.L^{-1}$.

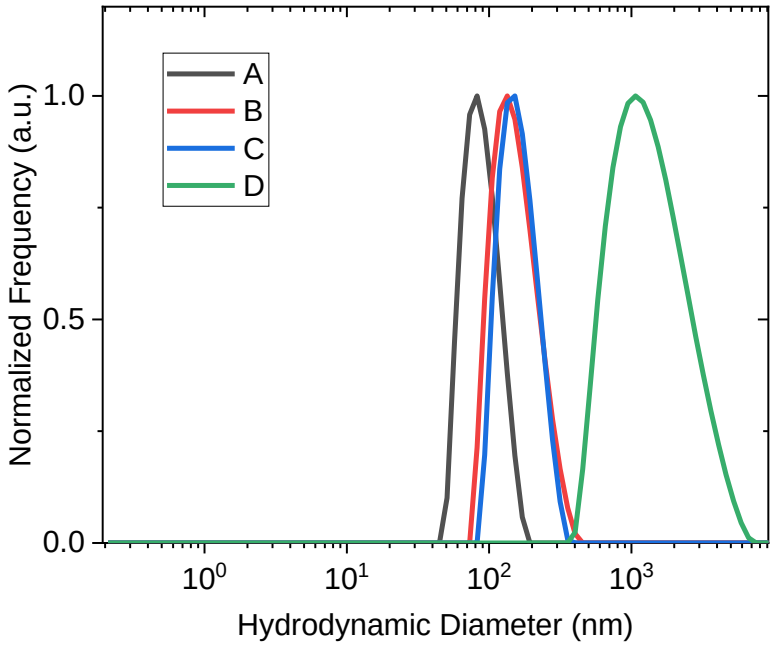

Figure 6.12: Hydrodynamic diameter distribution of samples containing CTAB-PAA-$EO_{90}PO_{60}EO_{90}$ by DLS in the following concentration: **A)** CTAB 2.7 mmol.L^{-1}, PAA 2.7 mmol.L^{-1} and $EO_{90}PO_{60}EO_{90}$ 0.15 mmol.L^{-1}; **B)** CTAB 8.2 mmol.L^{-1}, PAA 8.2 mmol.L^{-1} and $EO_{90}PO_{60}EO_{90}$ 0.46 mmol.L^{-1}; **C)** CTAB 13.7 mmol.L^{-1}, PAA 13.7 mmol.L^{-1} and $EO_{90}PO_{60}EO_{90}$ 0.77 mmol.L^{-1}; **D)** CTAB 27.4 mmol.L^{-1}, PAA 27.4 mmol.L^{-1} and $EO_{90}PO_{60}EO_{90}$ 1.54 mmol.L^{-1}.

Mineral oil loading was assessed in all samples with $EO_{90}PO_{60}EO_{90}$ concentrations up to 0.77mM, higher concentrated samples was not tested considering the phase transition proposed. Mineral oil was encapsulated in both $CTAB_{8,2}$-$PAA_{8,2}$-$[EO_{90}PO_{60}EO_{90}]_{0,46}$ and $CTAB_{13.7}$-$PAA_{13.7}$-$[EO_{90}PO_{60}EO_{90}]_{0.77}$, however, the last one showed high stability and oil entrapment while the first one had oil separation after two hours, therefore, we selected this sample as the optimal concentration for further study.

In order to determine the maximum oil loading capacity of $CTAB_{13.7}$-$PAA_{13.7}$-$[EO_{90}PO_{60}EO_{90}]_{0.77}$ sample, we tested with various proportions of Moil, up to 0.64 wt%. However, at this concentration, we observed oil separation and 0.48 wt%

were selected as the highest amount of oil to be loaded into the nanoparticles. (**Figure 6.13**)

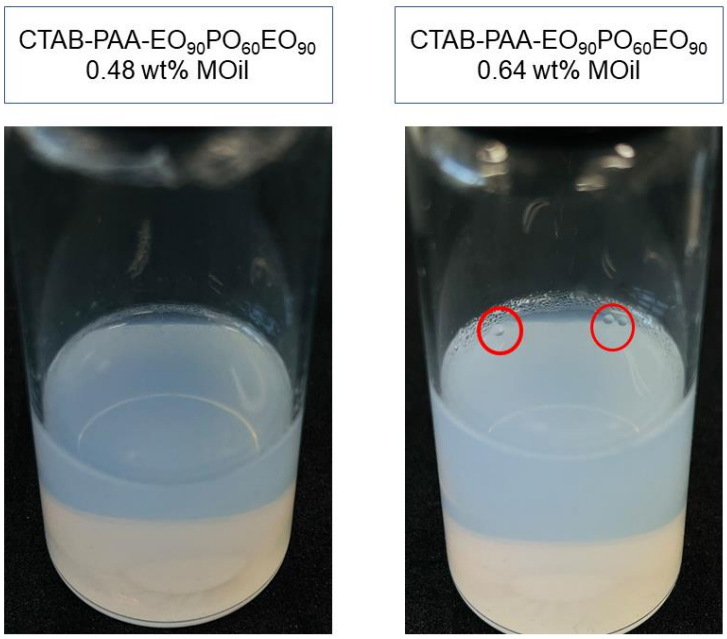

Figure 6.13: Pictures of CTAB-PAA-$EO_xPO_yEO_x$ nanoparticles at 1.6 wt % with 0.48 wt% and 0.64 wt% of Mineral Oil, respectively.

6.8.4 Structural evaluation by Small Angle X-Ray Scattering

To evaluate the structure of the particles, SAXS measurements were performed for samples containing CTAB-$EO_{90}PO_{60}EO_{90}$/$EO_{04}PO_{30}EO_{04}$ and pure CTAB, **Figure 6.14** contains all scattering patterns for samples.

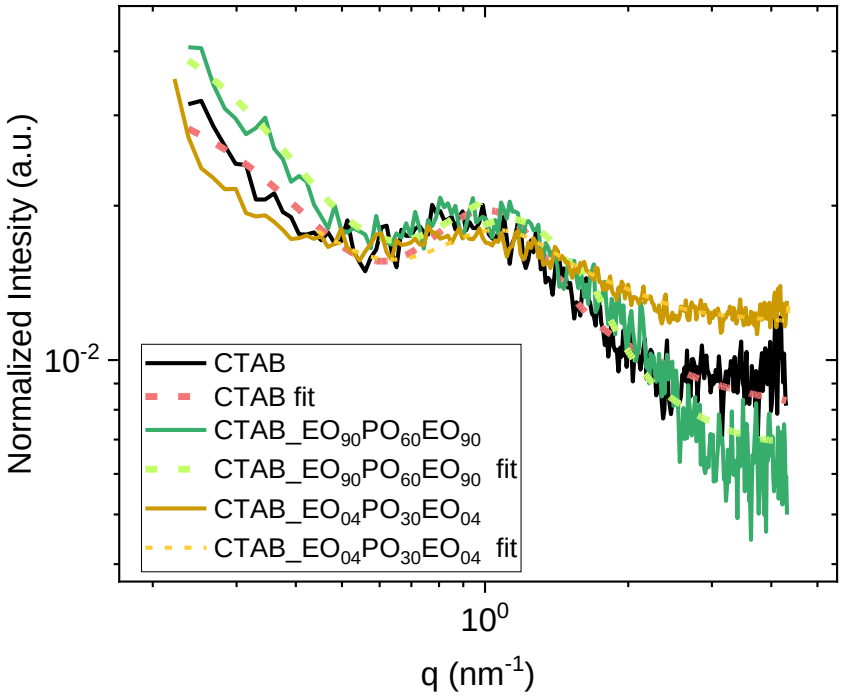

Figure 6.14: SAXS Curves, with normalized intensity in arbitrary units (with background subtraction as a function of the scattering vector q CTAB and CTAB-$EO_{90}PO_{60}EO_{90}$/$EO_{04}PO_{30}EO_{04}$.

Fitting parameters and model were the same as described by Wu et al[181]. CTAB and CTAB-$EO_{90}PO_{60}EO_{90}$/$EO_{04}PO_{30}EO_{04}$ were fitted using core-shell ellipsoidal model.

SAXS measurements of CTAB 0.5 wt%, CTAB-$EO_{90}PO_{60}EO_{90}$, and CTAB-$EO_{04}PO_{30}EO_{04}$ in aqueous solutions at 0.97% were used to characterize the micelles that composed the particles' core. A core-shell ellipsoidal model was used, where the core is composed by surfactant alkyl chains and PO blocks, and the shell is composed by surfactant hydrophilic groups (alkyltrimethylammonium bromide and EO blocks).

For $EO_{90}PO_{60}EO_{90}$, a core shell sphere model was used for fitting the parameters. The obtained parameters by the best fitting are presented in **Table 6.4**, and these values agree with previous structural parameters measured for CTAB in SAXS described in literature [182].

Table 6. 4: Structural parameters obtained by fitting SAXS data to the core-shell ellipsoidal (CTAB and CTAB-$EO_{90}PO_{60}EO_{90}$/$EO_{04}PO_{30}EO_{04}$) and sphere model ($EO_{90}PO_{60}EO_{90}$).

Sample	Model				
	Core-Shell Ellipsoidal			Core-Shell Sphere	
	a (nm)	b (nm)	t_e (nm)	r (nm)	t_r(nm)
CTAB	2.9	2.4	0.6	-	-
CTAB-$EO_{90}PO_{60}EO_{90}$	3.2	1.5	2.0	-	-
CTAB-$EO_{04}PO_{30}EO_{04}$	4.2	1.4	1.7	-	-
$EO_{90}PO_{60}EO_{90}$	-	-	-	4.7	2.5

Upon $EO_{90}PO_{60}EO_{90}$ addition, mixed micelles of CTAB-$EO_xPO_yEO_x$ still presented a core-shell prolate ellipsoidal shape but the semimajor radius increased, while the semi minor axis reduced to b = 1.5 nm, indicating the unidirectional growth of the micelle related with polymer addition, when compared to pure CTAB micelles. Alexandridis, et al.[183,184] also described similar dimensions in SDS and $EO_{90}PO_{60}EO_{90}$ micelles, using 3 wt% (fixed) $EO_{90}PO_{60}EO_{90}$. The authors showed four different regions of association between SDS and copolymer, based on their concentration range. These regions could be summarized as: no association between SDS and copolymer micelles, the formation of $EO_{90}PO_{60}EO_{90}$-rich SDS/$EO_{90}PO_{60}EO_{90}$ assemblies, SDS-rich SDS-$EO_{90}PO_{60}EO_{90}$ assemblies or free SDS micelles and SDS-$EO_{90}PO_{60}EO_{90}$, respectively, with increasing SDS concentration. Unidirectional growth of the micelle was also observed upon polymer addition. Although this range of concentrations was studied for SDS, we can predict that in our system we are in the same region that led to the formation of CTAB-rich CTAB-$EO_{90}PO_{60}EO_{90}$ assemblies, which can be observed in SAXS scattering curves, since the shape of the data obtained are more comparable to pure CTAB micelles. Shell thickness for mixed micelles of CTAB with $EO_xPO_yEO_x$ micelles also increased when compared to pure CTAB micelles, 3.3 times higher, which we associate with EO groups presented at the shell structure. The structural parameters presented the same tendency for CTAB-$EO_{04}PO_{30}EO_{04}$. Fitting values showed micelles with a semimajor axis a = 4.2 nm, and a semi minor axis b = 1.4 nm, with shell thickness of 1.7 nm. Mixed micelles of CTAB-$EO_{04}PO_{30}EO_{04}$ are slightly bigger than the

ones of CTAB-$EO_{90}PO_{60}EO_{90}$, although the latter is a longer polymer. Hence, this difference could be due to the higher molar concentration of $EO_{04}PO_{30}EO_{04}$ (4.39 mmol.L^{-1}) compared to $EO_{90}PO_{60}EO_{90}$ (0.77 mmol.L^{-1}).

6.8.5 Structural evaluation by Cryo-TEM and DLS

CTAB-PAA-$EO_xPO_yEO_x$ systems were also characterized using DLS and Cryo-TEM. Additional Cryo-TEM images are provided in **Figures 6.15 to 18**, and the correlation functions obtained from DLS are presented in **Figure 6.19.**

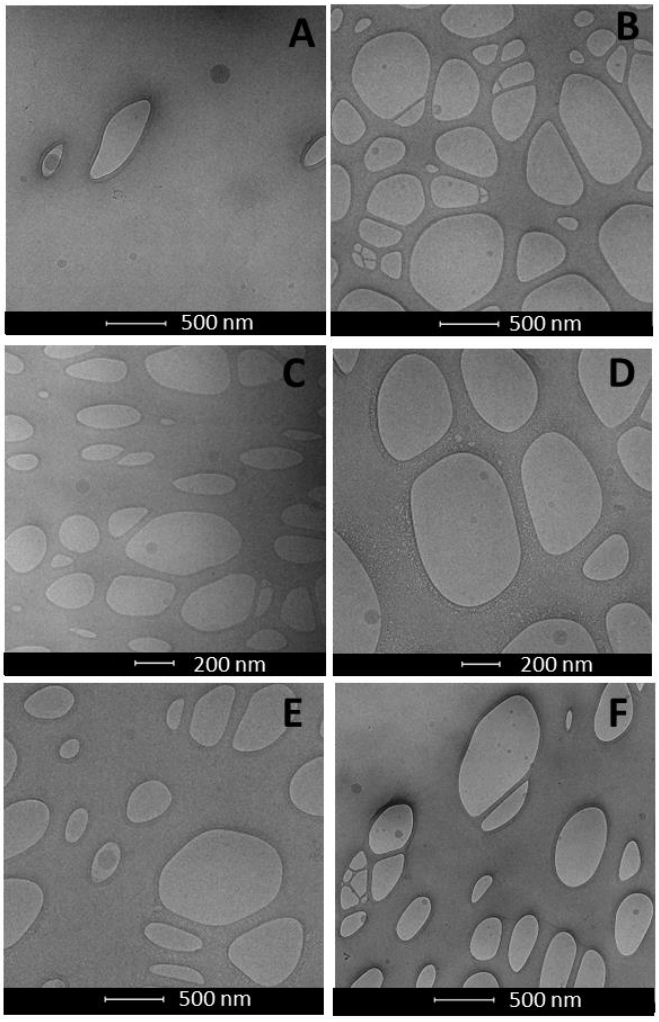

Figure 6. 15: Cryo-TEM images of different CTAB-PAA- $EO_{04}PO_{30}EO_{04}$

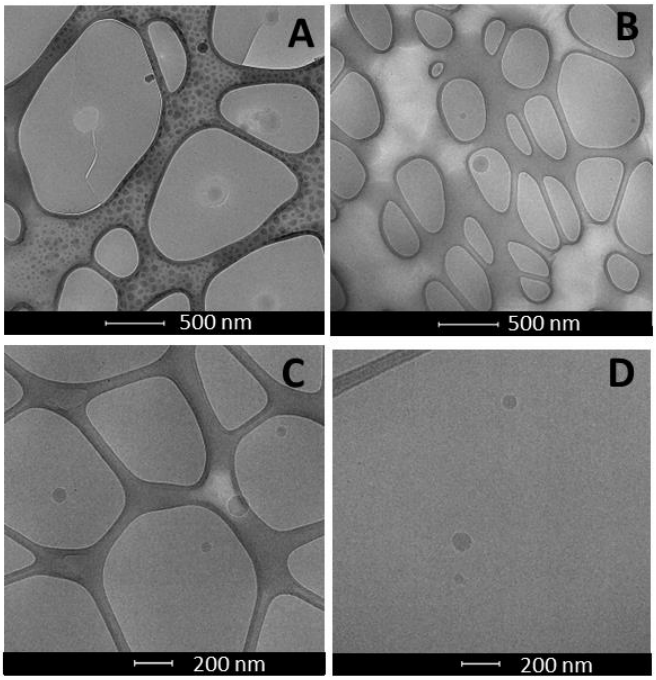

Figure 6.16: Cryo-TEM images of different CTAB-PAA- $EO_{04}PO_{30}EO_{04}$ and Moil

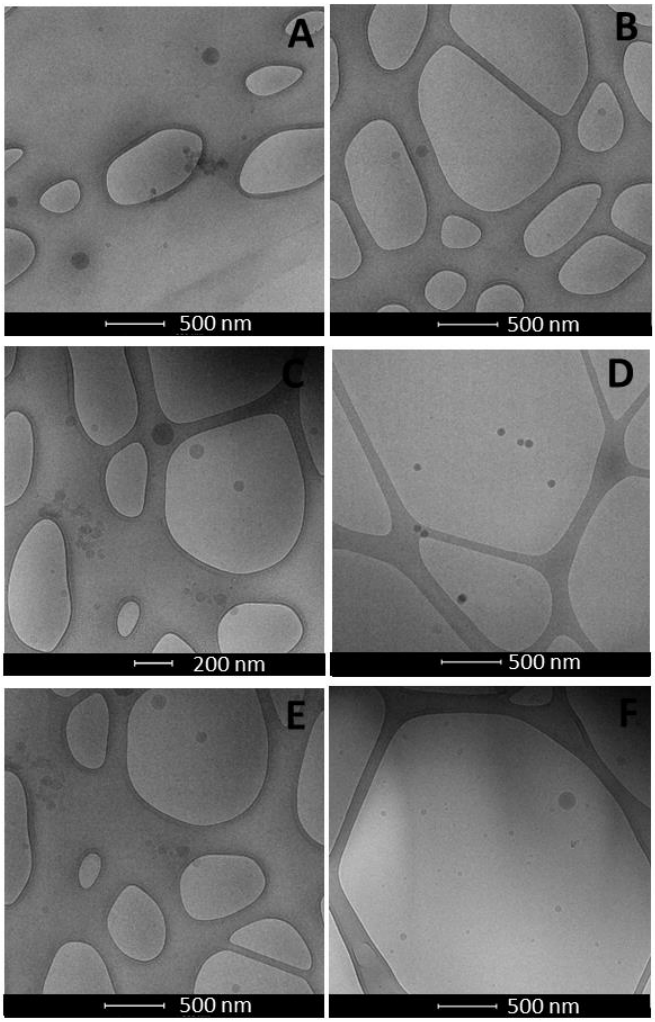

Figure 6. 17: Cryo-TEM images of different CTAB-PAA- $EO_{90}PO_{60}EO_{90}$

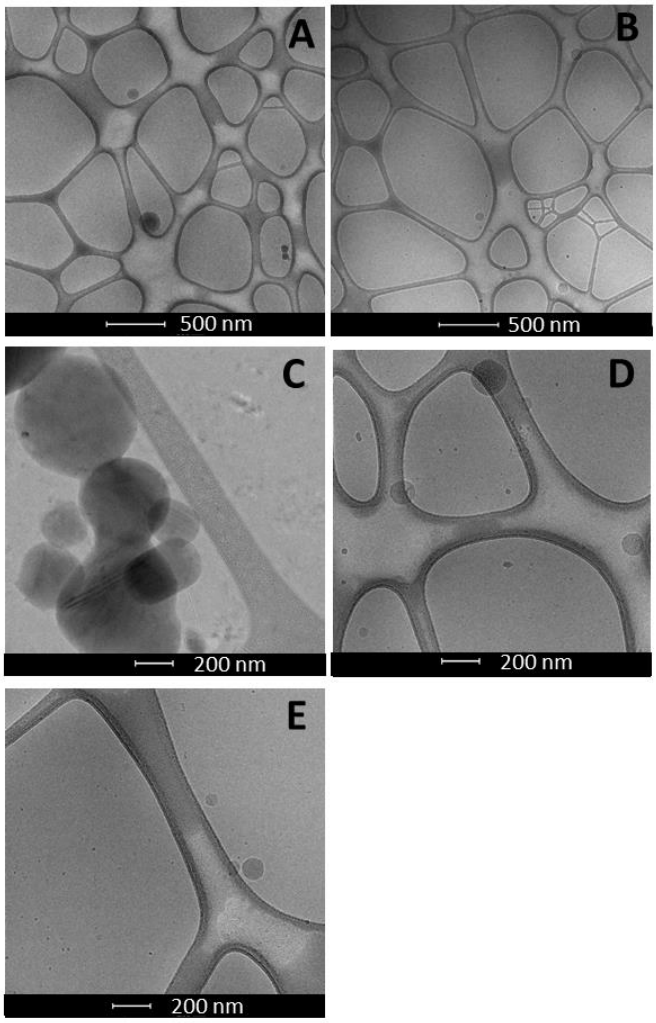

Figure 6. 18: Cryo-TEM images of different CTAB-PAA- $EO_{90}PO_{60}EO_{90}$ and MOil

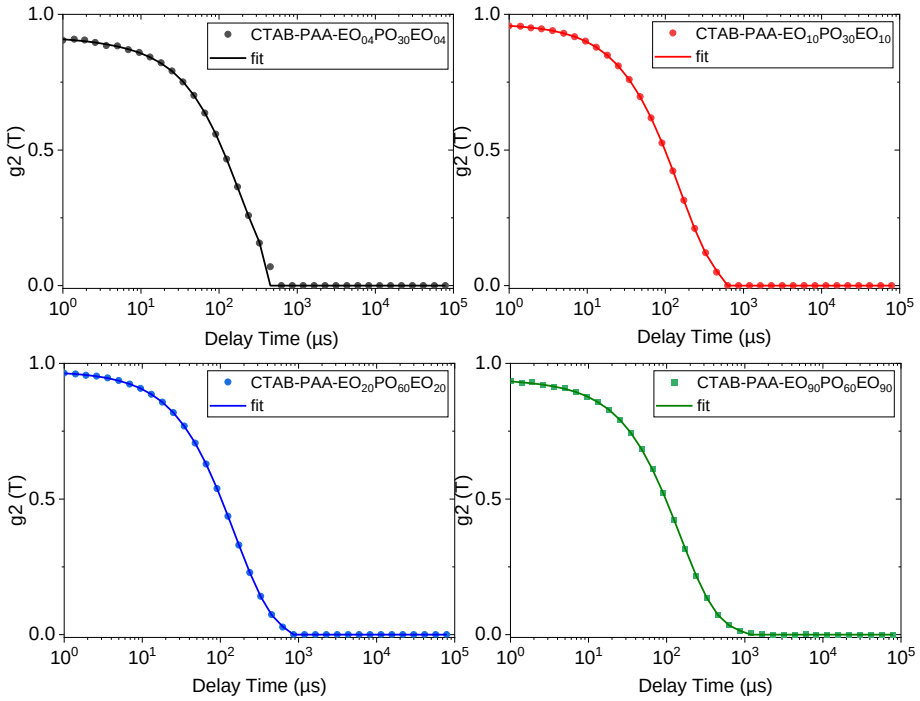

Figure 6. 19: Correlation Functions of samples containing CTAB-PAA-$EO_xPO_yEO_x$ nanoparticles at 1.6 wt % measured by DLS.

CHAPTER 7

Cocamidopropyl betaine can behave as a cationic surfactant and electrostatically associate with polyacids of high molecular weight

Matheus Ouverney Ferreira [a], Huliana Francisca Câmara de Assis [a], Ana Maria Percebom

*[a]Department of Chemistry, Pontifical Catholic University of Rio de Janeiro (PUC-Rio), 22451-900, Rio de Janeiro/RJ.

**** apercebom@puc-rio.br (corresponding author)***

Abstract:

Many practical applications, especially cosmetics, use mixtures of zwitterionic surfactants with polymers, but the scarcity of studies limits the control of their mixture properties. In the specific case of cocamidopropyl betaine (CAPB) and polyanions, the occurrence of phase separation with no previous characterization and the lack of knowledge of the involved parameters motivated the present study. Comparison of mixtures of CAPB with polyacrylic acid (PAA) of different chain lengths indicated phase separation only occurs if the chain is long enough to promote bridging. Surface tension measurements confirmed the aggregation between CAPB and PAA, but not at neutral pH. Scattering techniques allowed to elucidate the structures formed by CAPB with the polymers at different conditions. The results demonstrate that the association between PAA and CAPB occurs even when the polymeric chain is short because PAA reduces the pH and the protonated form of CAPB behaves as a cationic surfactant. However, there is no bridging when the micelles are associated with short chains, being still water-soluble. In conclusion, low pH is important for the association between CAPB and PAA, but high degree of polymerization is a requirement for the phase separation, whereas ionic strength is not essential for these phenomena.

Keywords: Polyelectrolyte, SAXS, DLS, amphoteric surfactant, cocoamidopropyl betaine, poly(sodium 4-styrenesulfonate).

Graphical Abstract:

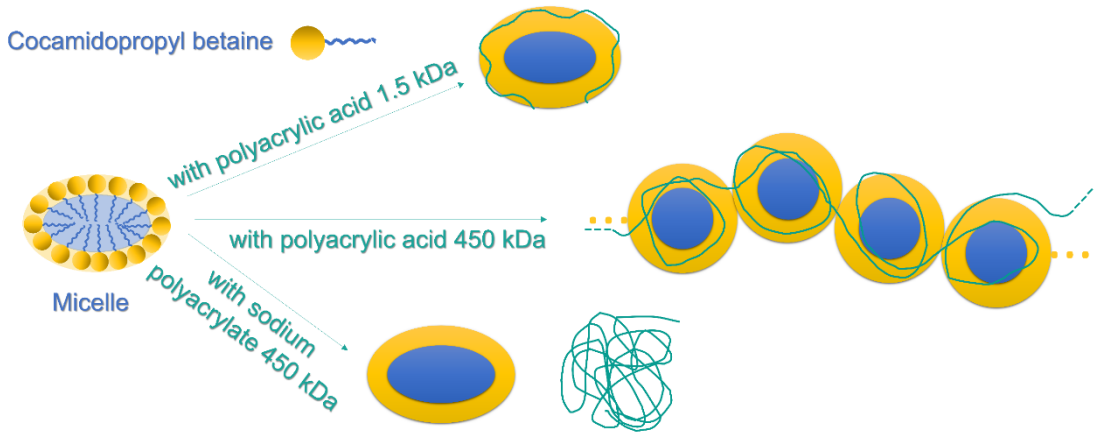

7.1. Introduction

Many applications such as cosmetics, household products, and enhanced oil recovery use polymers and surfactants due to their individual properties. However, their combination gives rise to new properties that can be inconvenient when not known. This problem can happen especially with zwitterionic surfactants and polyelectrolytes due to the frequent use but lack of studies on this pair. The interactions between surfactants and polymers can lead to new structures, depending on their chemical nature, concentration, and other conditions, such as pH and ionic force. Many studies have shown the structures formed by different pairs of polymers and surfactants in the past decades, bringing some practical conclusions. At surfactant concentrations below the critical micellar concentration (CMC), the molecules can adsorb on polymer chains forming aggregates at the concentration called critical aggregation concentration (CAC). Once the polymer is saturated, surfactant molecules start forming free micelles at a concentration higher than the original CMC. It can be explained by the strong interactions between polymers and surfactants and the reduced contact between the alkyl chain and water [141,185]. There are different types of segregative and associative phase separation phenomena above the

CMC [140]. For systems of polyelectrolytes with oppositely charged surfactants, electrostatic complexation can lead to separation into one phase concentrated in polymer and surfactant and one dilute solution [141,186]. The addition of electrolytes can hinder the phase separation [187]. The ionic strength and species' chemical nature directly affect the formed structures and the phase behavior [188] but zwitterionic surfactants combined with polymers are still scarcely studied.

Zwitterionic surfactants contain positive and negative charges in the headgroup. Betaine-based surfactants are the main representatives of zwitterionics, which in their structure have a quaternary ammonium and a carboxylic acid group. Due to the possibility of protonation of the carboxylic group, they are also considered amphoteric. They can be completely biodegradable and based on natural, renewable sources such as stripped coconut fatty acid. They present good cleaning performance [189] and act as foam boosters [190,191] with low skin irritation [192], and even reduce the irritating effect of anionic detergents on the skin [193] and human oral mucosa [194]. The presence of two opposite charges on the headgroups makes them neutral and with lower CMC values than the ionic surfactants, guaranteeing mildness to the skin and eyes, resistance to hard water, and high compatibility with other surfactants [195]. Due to that, cocamidopropyl betaine (CAPB) is broadly used in shampoos and body washes for children and is the most used secondary surfactant in cosmetics, personal care, hygiene, and dishwashing products [196,197]. With the recent boom of "sulfate-free" shampoos (also popularly known as low-poo), CAPB is becoming the primary surfactant in many formulations. They are also widely applied as additives for enhanced oil recovery, analytical separation, bioremediation, nanoscience, electrochemistry, and wastewater treatment.[198]

There are many studies about mixtures of CAPB with other surfactants, mainly anionic, because they are commonly combined in the applications mentioned above. Mixing CAPB with anionic surfactants can form wormlike micelles with useful rheological properties [199–203]. However, at pH < 4.2, the mixture becomes less viscous and more turbid because CAPB behaves like a cationic surfactant, forming bilayers instead of wormlike micelles [204]. CAPB suppliers usually suggest the use at pH > 4 to avoid unexpected results due to

the changes in phase behavior. Hence, using CAPB in the presence of polyacids can cause significant changes. However, there are many examples of polyacids in cosmetics, such as Carbopol – a copolymer of polyacrylic acid – and hyaluronic acid – a polysaccharide functionalized with carboxylic acids. For applications in enhanced oil recovery, different studies have already used a mixture of betaine-based surfactant combined with anionic sulfonated polymers [205–208]

Still, there are only a few studies in the literature about mixtures of zwitterionic surfactants and polymers in general, and even less when considering carboxylic betaines and polyacids or polyanions. Studies with sultaine and betaine surfactants indicated that nonionic polymers do not interact or associate with zwitterionic surfactants nor significantly affect their CMC [195,209–211]. Whereas the cationic polymers, poly(diallyldimethylammonium chloride) and Eudragit E100, presented no signals of interactions with zwitterionic surfactants [212,213], poly[3-(methacrylamido)propyl trimethylammonium chloride] formed complexes with lauramidopropyl hydrosysultaine in a particular range of concentration [214]. Among polyelectrolytes, poly(sodium 4-styrenesulfonate), NaPSS, is the most studied with zwitterionic surfactants. Surface tension measurements [209] and isothermal titration calorimetry [211] showed NaPSS induces the formation of aggregates with zwitterionic surfactants in concentrations lower than the CMC due to the predominance of hydrophobic contributions. However, DLS measurements indicated electrostatic interactions could also be relevant in certain conditions [214]. When weak polyanions without significant hydrophobic groups are in the salt form, there is no evidence of interactions with zwitterionic surfactant [209,213,215,216]. However, in the polyacid form, they can make complexes with zwitterionic surfactants due to hydrogen bonds, as suggested by isothermal titration calorimetry and simulation [211,217,218]. These are the only reported studies on this theme to the best of our knowledge.

Although the information about the complexes formed by the combination of polyelectrolytes and zwitterionic surfactants is still scarce, both substances are broadly used in different applications. The combination of CAPB with polyacids – both so frequent in cosmetics – can bring unexpected properties when it is not well understood to be controlled, and even undesired phenomena, such as phase

separation and precipitation, destabilizing the product. Hence, it is crucial to understand the parameters governing the self-assembly structures formed when mixing these compounds, to allow the control of their properties.

We investigated mixtures of CAPB with polyacrylic acid, PAA, of different molecular weights at different pHs. We also compared some results replacing PAA with poly(sodium 4-styrenesulfonate), NaPSS, a stronger polyelectrolyte in the salt form, which has an aromatic ring guaranteeing a hydrophobic part.

Surface tension measurements brought insights into the interactions between commercial CAPB and PAA, whereas scattering techniques – Small Angle X-Ray Scattering (SAXS) and Dynamic Light Scattering (DLS), allowed the elucidation of the structures formed at the nanoscale. This information allowed us to understand the observed macroscopic behavior, such as the propensity to phase separation, and determine the main parameters to control them.

7.2. Materials and Methods

7.2.1. Materials

Polyacrylic acids with two different molecular weights and degrees of polymerization, Mw = 1.8 kDa, DP ~ 18, 99.9% purity and Mv = 450 kDa, DP ~ 4400, 99.9% purity, and poly(sodium 4-styrenesulfonate) (NaPSS), Mw = 70 kDa, DP ~ 340, 99.9% purity were purchased from Sigma Aldrich and used as received. Oxiteno gently provided CAPB in the form of Oxitaine CP 30 CM (28 wt % in aqueous solution, with 5 wt % of NaCl). According to the company, this surfactant is derived from stripped coconut fatty acids, providing a chain distribution of 12 to 18 carbon atoms (mainly 12), with approximately 63% of carbons from renewable sources and complete biodegradability. ^{1}H Nuclear Magnetic Resonance (NMR) spectroscopy confirmed the molecular structure of CAPB (Supplementary Material). For all experiments, deionized water obtained from a Milli-Q® system (0.2 mm filter, resistivity above 18.2 MΩ·cm^{-1}) was used.

7.2.2.Potentiometric titrations

A CAPB solution at 0.058 mol L^{-1} was titrated with PAA 450 kDa solution at 0.058 mol L^{-1}, monitoring pH, turbidity, precipitation, and any visual change after each addition, to identify the pH for phase separation in the presence of PAA.

Potentiometric titrations also allowed to study the behavior of the mixture of CAPB and PAA in different pHs and determine its pKa. For that, two different aqueous solutions were titrated with HCl 0.1 mol L^{-1}: NaOH 0.1 mol L^{-1} (reference curve); and CAPB 0.058 mol L^{-1} mixed with PAA 0.058 mol L^{-1} in NaOH 0.1 mol L^{-1} (sample). The value of pH was measured after each addition of acid. The intersection of the neutralization curve of the sample with the reference curve gives the isoelectric point (IP) [200,219].

7.2.3.Surface tensiometry

The surface tension (γ) values of aqueous solutions of CAPB at different concentrations were determined by Du Noüy ring method in the absence and presence of PAA 450 kDa at two different pHs. Measurements were performed in triplicate with an SEO Surface Tension Analyzer DST 60 equipped with a Platinum wire ring of 6.022 cm of circumference and calibrated with Milli-Q® water at 25 ºC, with a correction factor R/r = 48.95.

The experimental data points were used to determine the values of breakpoints related to a bulk cooperative association. When a plateau followed a sharp decrease of γ after a defined breakpoint, the region of rapid decrease of γ and the plateau region were fitted to straight lines. The breakpoint was determined as the intersection of the two lines, indicating the critical micellar concentration (CMC) or the critical association concentration (CAC).

7.2.4.Sample preparation

Aqueous mixtures of polymers and surfactants were prepared at specific concentrations by adding the calculated weight of the polymer and volume of the surfactant solution to water. The chosen proportion guaranteed a stoichiometric ratio between the polymeric repeating units and surfactant molecules (for example, acrylic acid:CAPB = 1:1). The range of concentration was selected to be higher than the CMC and to guarantee the diffusive regime for dynamic light scattering and not too much interference for small-angle X-ray scattering (SAXS) measurements, but still with sufficient scattering intensity.

PAA 450 kDa was titrated with sodium hydroxide solution until pH = 7.0 to verify the effect of pH on the physicochemical properties. The obtained solution was called NaPA 450 kDa, which was also used to obtain stoichiometric mixtures with CAPB in water.

7.2.5.Sample characterization

First, visual observation allowed to determine in which samples the phase separation occurred or not, to identify the parameters related to it. Dynamic light scattering (DLS) and small-angle X-ray scattering (SAXS) measurements were performed to characterize the colloidal structure resulting from the mixture of CAPB and the different polymers.

For DLS experiments, 2.0 mL of each sample was added to a polystyrene cuvette with four optically clear sides and a path length of 10 mm. The cuvettes were previously rinsed several times with freshly filtered water obtained from Milli-Q® system and immediately covered after the sample addition to avoiding dust contamination. The DLS equipment was a SZ-100 Nanopartica, from Horiba, equipped with a 10 mW laser with a wavelength of 532 nm. All measurements were performed in triplicate, with time exposure of 120 s, at a temperature of 25.0 °C and angles of 90 and 173 °. The obtained autocorrelation functions were treated using the software HORIBA NextGen Project SZ-100, with Inverse LaPlace Transforme (ILT) to provide intensity distributions and mean values of hydrodynamic radii.

SAXS experiments were performed at the SAXS1 beamline of the Brazilian Synchrotron Light Laboratory (LNLS, Campinas-SP, Brazil). The beam wavelength was 1.488 Å. Samples were set in a mica window as the sample holder with a thermal bath to regulate the temperature (25.0 ºC) for 120 s. The distance between the sample holder and the detector was 0.9 m. Detector Pilatus 330 K was used to collect 2D images, which were subtracted from pure water and integrated using the software Fit2D. The integrated curves of intensity, I(q), as a function of scattering vector, q, were treated using SasView 4.2.2 [220].

7.3. Results and Discussion

7.3.1. CAPB aqueous solutions

In the concentration range of study (up to 2 wt %), CAPB does not cause significant changes in water viscosity and clarity. Surface tension (γ) measurements of CAPB aqueous solutions at different concentrations, **Figure 7.1**, indicated its capacity to lower the surface tension of water to 33 mN m^{-1}, which remains nearly constant due to a cooperative association from 2.0 x 10^{-4} mol L^{-1} , assumed to be the CMC. It is worth mentioning that the CAPB solution also contains NaCl which may affect the CMC value. The molar concentration of NaCl is very close to the surfactant concentration and varies from 5 x 10^{-7} to 0.01 mol L^{-1} in **Figure 7.1**. Many studies reported different values of CMC for CAPB ranging from 7 x 10^{-5} to 3 x 10^{-3} mol L^{-1}, which is probably due to differences in composition, ionic strength, and method of measurement [198,201,221–224]. CAPB is formed mainly by dodecyl chains but can have other alkyl chains present, and the composition can vary for different suppliers. The presence of salt is common in commercial CAPB, and there is a lack of systematic control in the different reports. Besides, the measurement method can also affect the CMC value. Hence, the result from the CAPB used in the present study is essential for comparison with systems containing polymers.

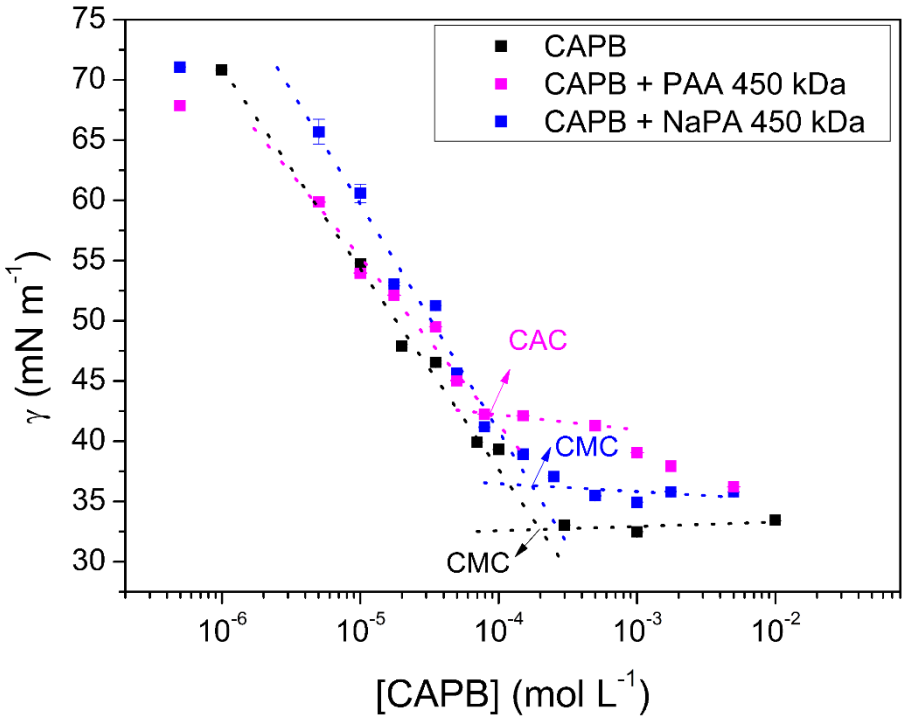

Figure 7. 1 Surface tension values of CAPB aqueous solutions at different concentrations in the absence or presence of PAA or NaPA of 450 kDa (0.01 mol L^{-1}). The error bars are the standard deviations from triplicates. The arrows indicate the intersection of the dotted lines obtained by linear least-squares fits as described in detail in the text (for interpretation of the colors in this figure, the reader is referred to the web version of this article).

7.3.2.Mixtures of CAPB and polymers in water

7.3.2.1. Conditions for phase separation

Images of stoichiometric mixtures of CAPB and three different polymers (0.029 mol L^{-1} of each), **Figure 7.2**, show that phase separation occurs only with PAA 450 kDa. Polymer molar concentration is expressed in terms of repeating units throughout the text. The combination with PAA 1.8 kDa forms a clear solution under the same conditions. The pH of both mixtures is 4.5. The results indicate that the degree of polymerization has an essential role in phase behavior.

Probably, there is a threshold on the polymer length to promote bridging between the different micelles and lead to phase separation. Mixtures of oppositely charged polymers and surfactants exhibit similar behavior. Svensson *et al.* have shown that the attraction between PAA and cationic surfactants decreases with decreasing the polymeric chain length, leading to increased miscibility with water [225]. Results from scattering techniques will also indicate the occurrence of the same phenomenon in the present study.

Although NaPSS of 70 kDa is not as long as PAA 450 kDa, it is a stronger polyelectrolyte and has hydrophobic aromatic groups that could favor phase separation. However, the mixture of NaPSS of 70 kDa and CAPB remains soluble. This behavior assigns that phase separation is also related to acidity because the polymer is in its salt form, and the mixture is spontaneously close to neutrality (pH 6.8). It can be confirmed when observing the mixture of CAPB with PAA converted to the salt form: NaPA 450 kDa, which also forms a clear solution (pH 7.0). We also prepared a sample of CAPB and PAA 450 kDa with NaCl (at the same concentration of NaOH used to titrate NaPA) to verify whether the ionic strength from the sodium counter ions is not the cause. This mixture has a pH of 4.2 and still phase separates, confirming the two most important parameters for this phenomenon are acidity and degree of polymerization.

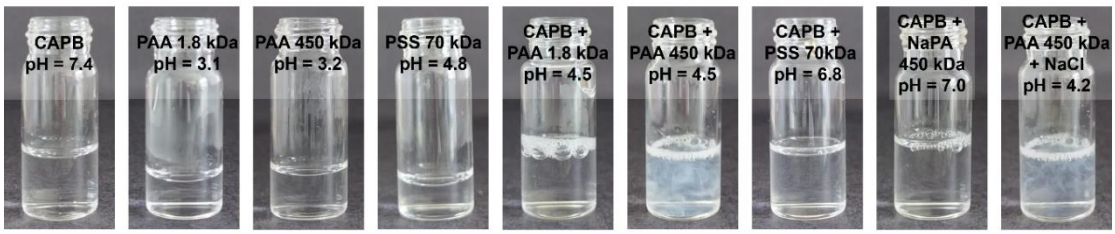

Figure 7. 2: Photographs of aqueous samples of CAPB (0.029 mol L-1 or 1.0 wt %) and different polymers (0.029 mol L-1 or 0.2 wt % to PAA and 0.6 wt % to NaPSS) immediately after mixture to verify the conditions to phase separation through turbidity, and the achieved pH. The concentration of NaCl from the CAPB reactant is estimated as 0.03 mol L-1 or 0.18 wt %.

Previous studies on the interaction of betaine surfactants with ionic surfactants show they interact much more strongly with anionic than with cationic

surfactants [226]. However, electron-neutral mixtures of anionic and betaine surfactants do not phase separate, and they are commonly used due to their high compatibility [219]. It confirms that the phase separation requires the high molecular weight of the anionic polymers to occur.

7.3.2.2. Potentiometric titrations

Before the titration, CAPB and PAA 450 kDa 0.058 mol L^{-1} aqueous solutions had pH values of 5.82 and 2.72, respectively. After each polymer addition to the surfactant solution, the mixture remained clear before reaching a pH of 4.79 (**Figure 7.7 SM**). After that, the solution became increasingly turbid with pH reduction, indicating phase separation. According to potentiometric titrations, the IP of the mixture, pH = 3.8 (**Figure 7.8 SM**), is lower than the threshold pH of phase separation. Since PAA has a pKa of 4.2-4.5 [168,169] and CAPB has an IP of 4.0 [220], they must already have protonated carboxylic units at pH = 3.8. However, they probably also have some remaining negatively charged units, which can electrostatically complex to the positively charged quaternary ammonium groups of CAPB. Therefore, associative complexation occurs when the solution pH gets closer to the IP of the mixture. The lower the pH, the more carboxylate groups become protonated, and the cationic character of CAPB increases. Besides, hydrogen bonds between carboxylic acid/carboxylate units could also favor the association between PAA and CAPB at low pH, as already described for polyacids with other zwitterionic surfactants [211,217] and predicted by simulations [218].

7.3.2.3. Tensiometry and CMC

Surface tension measurements (**Figure 7.1**) can provide information about the association process between CAPB and PAA 450 kDa. The CAPB concentration dependence of γ shows an onset of association to PAA 450 kDa at 8.8×10^{-5} mol L^{-1}. This is the critical association concentration (CAC), lower than the CMC of the pure surfactant, confirming the attraction between CAPB and

PAA. At concentrations higher than 1 x 10^{-3} mol L^{-1} (after the plateau), PAA is saturated with CAPB and the free CAPB concentration increase again, lowering γ.

In the presence of NaPA 450 kDa (when pH = 7.0), the breakpoint (1.8 x 10^{-4} mol L^{-1}) is very close to the CMC measured for pure CAPB (2.0 x 10^{-4} mol L^{-1}). Indeed, zwitterionic surfactants are expected to have no distinct interaction with homopolymers [185]. Hence, the difference in CAPB concentration dependence of γ in the presence of PAA or NaPA confirms that only protonated species of CAPB act like cationic surfactants.

7.3.2.4. Structural characterization

DLS and SAXS measurements provided results to elucidate the structures formed by CAPB in the presence of polymer. CAPB aqueous solution at 0.029 mol L^{-1} (or 1.0 wt %) has one population of micelles with a mean hydrodynamic radius (R_H) of 3.2 ± 0.2 nm measured by DLS (**Figure 7.3**). According to Tanford's equation [110], the length of a straight alkyl chain is 1.668 nm for 12 C and 2.427 nm for 18 C, so the radius of a spherical CAPB micelle should be in this range. The greater value can be due to the large polar head of CAPB, the hydration shell or an indication that CAPB micelles are slightly anisometric. SAXS results will confirm the anisometry.

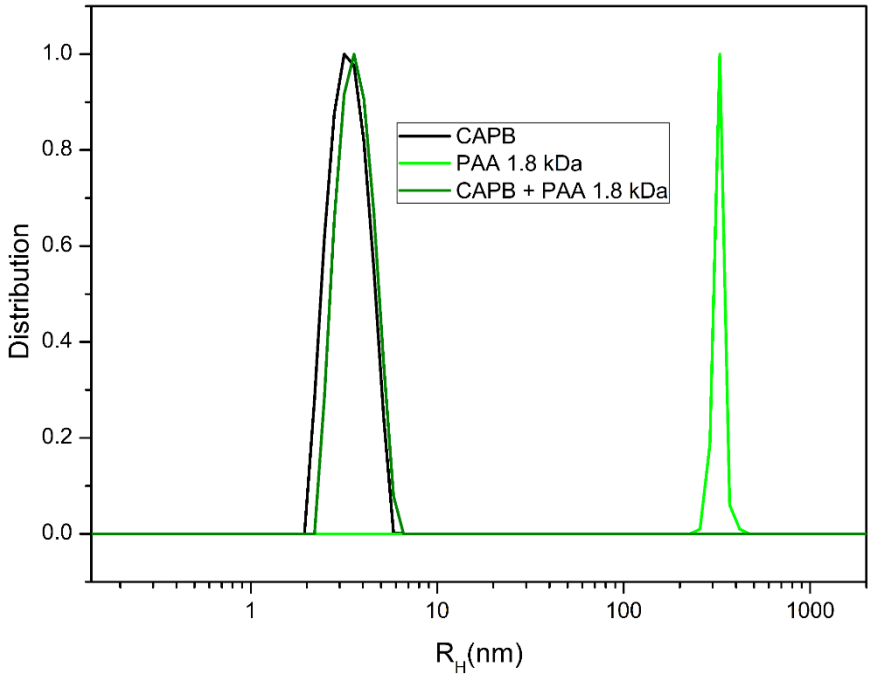

Figure 7. 3: Intensity distribution of hydrodynamic radii obtained by DLS for aqueous samples of CAPB (0.029 mol L-1), PAA 1.8 kDa (0.029 mol L-1), and the mixture of CAPB and PAA 1.8 kDa (0.029 mol L-1) (for interpretation of the colors in this figure, the reader is referred to the web version of this article). The concentration of NaCl from the CAPB reactant is estimated as 0.03 mol L-1 or 0.18 wt %.

DLS results of PAA samples could not be interpreted as actual hydrodynamic radii. For PAA 450 kDa, the autocorrelation function could not be fitted to provide a relaxation time **(Figure 7.9 SM**). For 1.8 kDa, although the distribution shows a population with R_H = 279 ± 27 nm, this size does not correspond to a single chain, indicating a slow relaxation process or interchain interactions, which are typical for polyelectrolytes [227]. However, this result is important to verify a change in conformation with the addition of CAPB.

When mixing CAPB with PAA 1.8 kDa, there is only one population of 3.6 ± 0.3 nm, which is very close to the micellar size. The dramatic conformation change of the polymer is probably because the chains are only neutralizing and

wrapping the surfactant micelles. Phase separation did not allow measuring the mixture of CAPB with PAA 450 kDa by DLS.

SAXS curve of CAPB sample exhibits a profile typical of micelles with different scattering length densities for the non-polar and polar regions (**Figure 7.4**). Due to that, we tested several models based on core-shell morphology to fit the experimental curve, where the core corresponds to the region formed by hydrocarbon chains, and the shell corresponds to the region of polar heads (with and without polydispersity). The best fitting was obtained with the model for the form factor of an ellipsoid core-shell (see Supplementary Material) and the parameters: semi-major axis of core = 3.08 nm, semi-minor axis of core = 1.65 nm, and shell thickness = 1.15 nm. The values of electron densities were kept constant at 275 e/nm^3 for the core and 334 e/nm^3 for the solvent [228] but allowed to vary for the shell, obtaining the value of 356 e/nm^3 (hence these values were fixed to the next fittings). The value of the semi-minor axis of the core is close to the expected length of a straight dodecyl chain (1.668 nm, according to Tanford's equation [110]). The other parameters corroborate with the hydrodynamic radius obtained by DLS, confirming CAPB micelles are ellipsoidal. For clarity, all the fitting curves are exhibited in **Figure 7.10.**

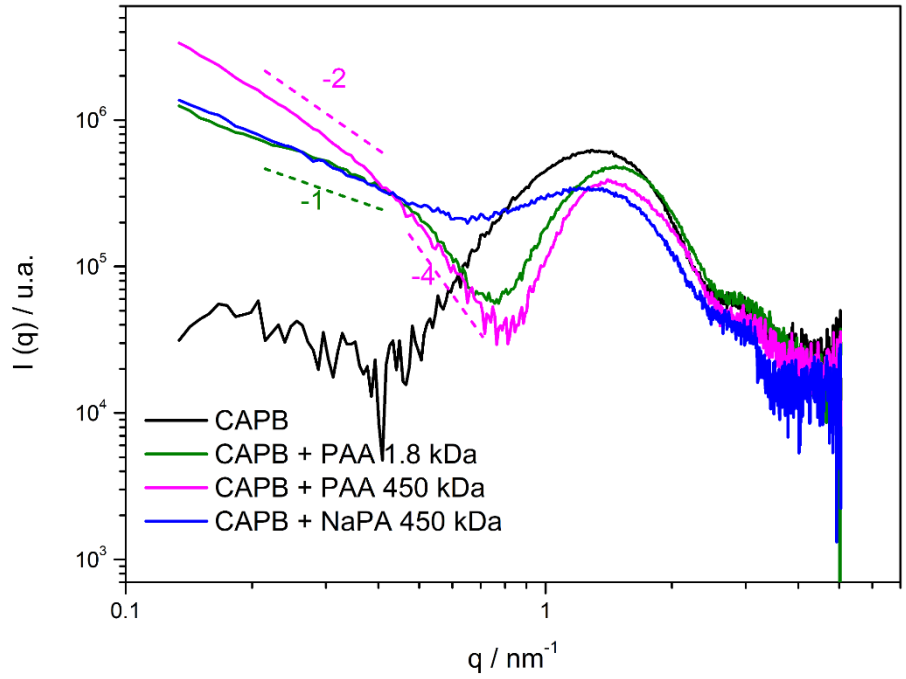

Figure 7. 4 SAXS curves of aqueous solutions of CAPB (0.029 mol L^{-1}) with different polymers (0.029 mol L^{-1}) (for interpretation of the colors in this figure, the reader is referred to the web version of this article). The concentration of NaCl from the CAPB reactant is estimated as 0.03 mol L^{-1} or 0.18 wt %.

The addition of polymers to the CAPB aqueous solution significatively changes the SAXS profile (**Figure 7.4**). The signal corresponding to the micelle form factor, P(q), is shifted to the right, indicating the micellar cross-section decreases. However, the slope of the curve at low values of q is increased, indicating either a higher aspect ratio or interparticle interference. For the sample of CAPB and PAA 1.8 kDa, curve fitting using the model for the form factor of an ellipsoid core-shell provided the parameters: semi-major axis of core = 2.62 nm, semi-minor axis of core = 1.48 nm, and shell thickness = 1.42 nm. The dimensions are close to the ones obtained for pure CAPB micelles but indicate a slight compaction of the hydrophobic core and a thicker shell in the presence of PAA 1.8 kDa.

The curve of the sample containing CAPB and PAA 450 kDa could not be fitted using the ellipsoid core-shell model, so other models were tried. The fractal core-shell model provided the best fitting and describes the scattering from core-shell spheres as building blocks of a fractal structure. For that, the structure factor, S(q), from the well-known Teixeira model [229,230], is combined with the form factor, P(q), of core-shell spheres. This model has been successfully applied to describe structures formed by protein-surfactant [229] or polymer-surfactant [156] interactions as a "pearl-necklace" (of core-shell “pearls”).

For the lower q-range, the curves can be described by $I(q) \sim q^{-\alpha}$, where the exponent, α, is related to the fractality of the scattering objects. Some typical values of the exponent can be found in references [173,175]. For example, when α = 1, the structure can be attributed to low-dimensional objects as randomly distributed rods [173], and when α = 2, the structure can be an ideal linear polymer or swollen branched polymer (mass fractal) [175]. For the sample of CAPB with PAA 450 kDa, α = 2.1, indicating a mass fractal, with a shell thickness of 1.4 nm, a core radius of 1.7 nm, and a correlation length longer than 15 nm (lower q-range would be necessary to determine this value precisely).

The fractal core-shell model was then applied to the CAPB and PAA 1.8 kDa sample, providing α = 1.1, which agrees with the formation of isolated anisometric micelles. The other parameters obtained were a shell thickness of 1.3 nm, a core radius of 1.7 nm, and a correlation length of 5.2 nm. Although the curve can be fitted to the “pearl-necklace” model, results show that the structure would be formed by only one “pearl”, indicating that the simpler core-shell ellipsoid model is the best way to describe the system.

The SAXS profiles are not changed upon addition of NaCl, indicating that ionic strength does not affect the formed structure (**Figure 7.11**). However, the addition of NaOH leads to a pattern completely different from the previous ones, and the curve could not be fitted using either the model for core-shell ellipsoids or core-shell cylinders. It could only be fitted by using identical parameters to CAPB micelles combined with a power-law of -1.3, which could be related to the scattering from the free polymeric chains. It suggests that the polymer chains of NaPA 450 kDa do not complex with CAPB surfactant, so the polymers and the micelles coexist as separated species in the same solution.

To summarize the results obtained with the scattering techniques, **Table 7.1** presents the parameters from all the different models, and **Figure 7.5** depicts schemes of the proposed structures. In summary, CAPB forms ellipsoid micelles, which can be neutralized and wrapped by PAA. The short chains of PAA 1.8 kDa do not promote bridging, but PAA 450 kDa can form connect several CAPB micelles as a necklace. However, polymer chains in the salt form do not wrap CAPB micelles.

Table 7. 1: Parameters obtained from fitting of SAXS curves using different models.

Sample	DLS	SAXS	Core-Shell Ellipsoid			Fractal Core-Shell				Power-Law
	R_h (nm)	Model	R_2 (nm)	R_1 (nm)	t (nm)	R (nm)	Ø	D_f	l (nm)	α
CAPB	3.2 ± 0.2	ECS	3.1	1.7	1.1					
CAPB + PAA 1.8 kDa	279 ± 27	ECS	2.6	1.5	1.4					
	3.6 ± 0.3	FCS			1.3	1.7	0.06	1.1	5.2	
CAPB + PAA 450 kDa		FCS			1.4	1.7	0.06	2.0	> 15	
CAPB + NaPA 450 kDa		ECS + PL	3.1	1.7	1.1					1.3

ECS: ellipsoid core-shell; FCS: fractal core-shell; PL: power-law.

R_1: semi-minor axis of core

R_2: semi-major axis of core

t: thickness of hydrophilic shell

Ø: volume fraction

D_f: fractal dimension

l: length correlation

α: power law

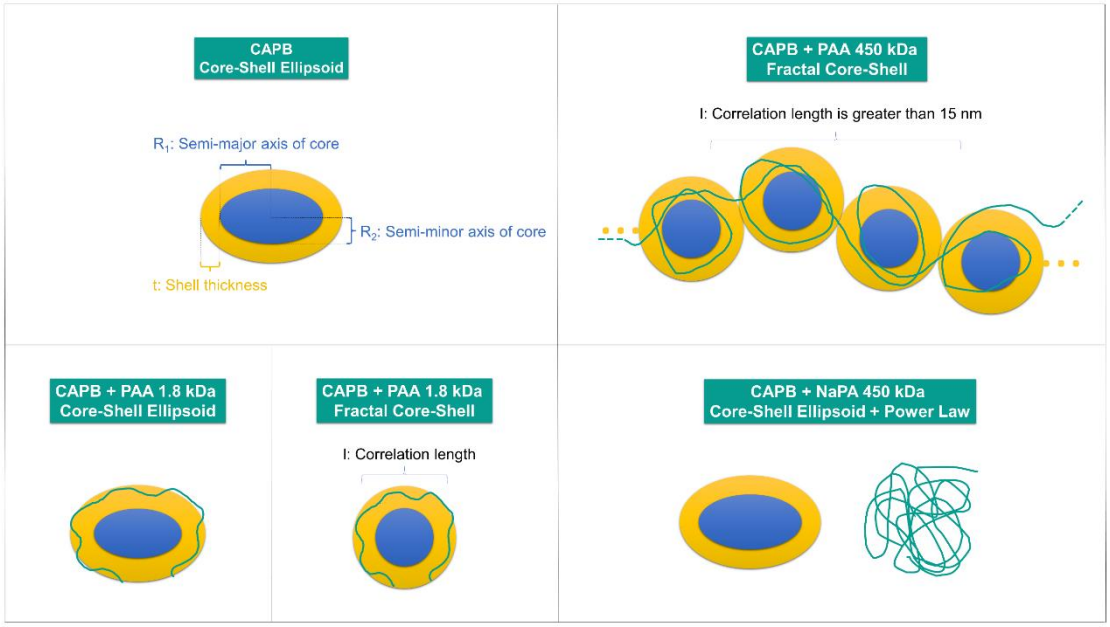

Figure 7.5: Schematic representation of structures according to SAXS results proportionally to the obtained dimensions.

The association of CAPB with PAA 1.8 and 450 kDa can be explained by electrostatic attraction and hydrogen bonds formed at low pH, which does not occur with NaPA 450 kDa. Results indicated CAPB behaves as a cationic surfactant due to the protonation of the carboxylate group. In aqueous mixtures of oppositely charged surfactants and polyelectrolytes, the macromolecules encircle the micelles to neutralize them, forming an electrostatic complex [225]. The longer the polymers are, the more micelles they can tie to each other. It can explain the difference between using PAA 1.8 and 400 kDa. Probably, the same complexation occurs, but there is no bridging between micelles by PAA 1.8 kDa to lead to phase separation, maintaining the complex soluble in water. maintaining the complex soluble in water. According to their degree of polymerization, PAA 1.8 and 450 kDa have 25 and 6250 carboxylic units, respectively. The aggregation number of CAPB micelles has been reported as 84 [233]. Considering a stoichiometric ratio between the polymeric units and the surfactant ions, we can estimate around 3 chains of PAA 1.8 kDa per CAPB micelle, and around 74 CAPB micelles per PAA 450 kDa chain. Besides, the fully extended lengths of PAA 1.8 and 450 kDa were estimated as 6 and 1572 nm, respectively, and the perimeter of a CAPB micelle is around 22 nm (see

Supplementary Material for calculations). These dimensions confirm that a single chain of PAA 1.8 kDa does not surround more than one CAPB micelle, whereas PAA 450 kDa could wrap and bridge many of them. This bridging explains the phase separation of CAPB with PAA 450 kDa, which is very similar to the behavior described for cationic surfactants with the same polymer. The attraction between oppositely charged surfactants and polymers increases with longer polymer chains, decreasing water miscibility [225].

7.4. Conclusions

When the polyanions are long enough to promote bridging between CAPB micelles, phase separation occurs, as previously observed with cationic surfactants [225]. However, for CAPB, this behavior is only observed with the acid form of the polymer and is not significantly affected by ionic strength. The threshold pH to observe the phase separation is 4.79, confirming that CAPB behaves as a cationic surfactant due to the protonation of the carboxylate group at low pHs.

Indeed, NaPA 450 kDa did not cause significant changes in the CMC of CAPB (2.5×10^{-4} mol L^{-1}). However, PAA 450 kDa, induced the appearance of a CAC (7.9×10^{-5} mol L^{-1}) lower than the CMC. For the first time, structural characterization by scattering techniques confirmed the formation of CAPB micelles surrounded by the polyacid. PAA 1.8 kDa can only individually wrap the micelles, whereas PAA 450 kDa can connect the micelles by bridging. Nevertheless, there is no association between CAPB and the salt form of the polymer, NaPA 450 kDa. The bridging is the cause of phase separation of CAPB at low pH, which could be even more pronounced at high concentrations of surfactants and polyions, as the typical range of most applications.

The study allowed us to understand the macroscopic behavior of the mixture, such as the propensity to phase separation due to the cationic character of CAPB in an acidic medium. It shows that polymerization degree and pH are the key parameters to tuning the miscibility and structures formed by betaine-

based surfactants and anionic polymers, which is essential for controlling the properties of their mixtures in real applications.

7.5 Notes:

The authors declare no competing financial interest.

7.6. Acknowledgements:

We acknowledge the Brazilian Synchrotron Light Laboratory (LNLS) for allocating SAXS beamtime (Proposal 20190031) and the support from the staff; LASURF for allowing the use of the tensiometer; and Oxiteno for gently providing CAPB.

7.7. Funding sources:

This work was supported in part by the Coordenação de Aperfeiçoamento de Pessoal de Nível Superior – Brasil (CAPES) – Finance Code 001. HFCA thanks CNPq for PIBIC scholarship.

7.8. Supplementary Materials

^{1}H NMR characterization of CAPB

The spectrum of cocamidopropyl betaine in deuterated water (D_2O) was measured at 25 °C in a Bruker Advance III HD 400 MHZ spectrometer. The signal of water was supressed from spectra before data treatment. The data processing was carried out using MestrReNova software and the results are presented in **Figure 7.6** and **Table 7.2.** Integration of signals confirms CAPB is formed by molecules with different alkyl chain lengths (from C12 to C18).

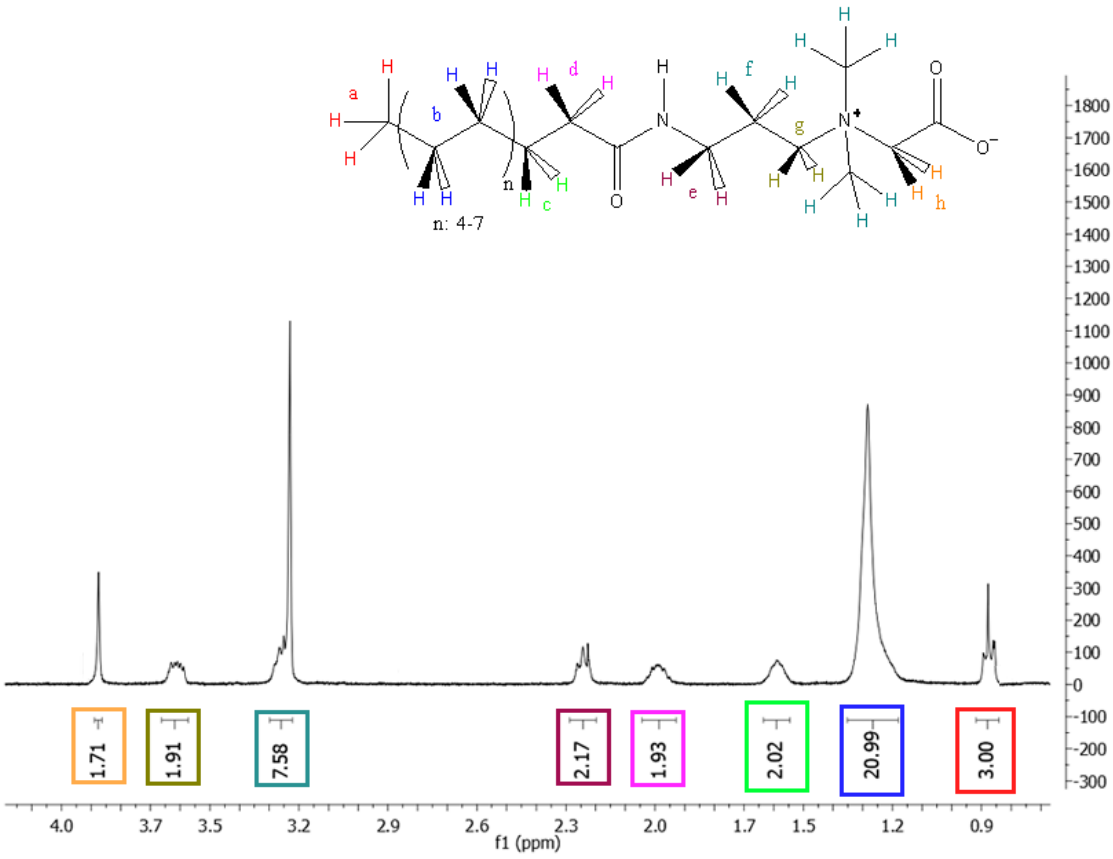

Figure 7.6: ^{1}H NMR spectrum of CAPB.

Table 7. 2: Parameters obtained by integration of signals of 1H NMR spectrum of CAPB.

	a	b	c	d	e	f	g	h
CAPB	0.83-0.86 (3H;dd)	1.25 (21 H,s)	1.56 (2H, s)	1.96 (2H,s)	2.21-2.20 (2H,d)	3.20-3.24 (8H,m)	3.58-3.6(2H,d)	3.85(2H,s)

Supplementary figures of results:

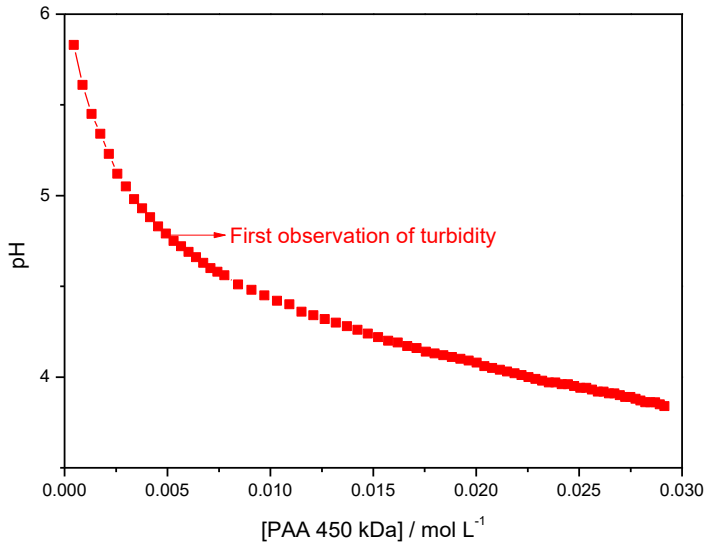

Figure 7.7: Potentiometric titration of CAPB aqueous solution at 0.058 mol L^{-1} with PAA 450 kDa aqueous solution at 0.058 mol L^{-1}.

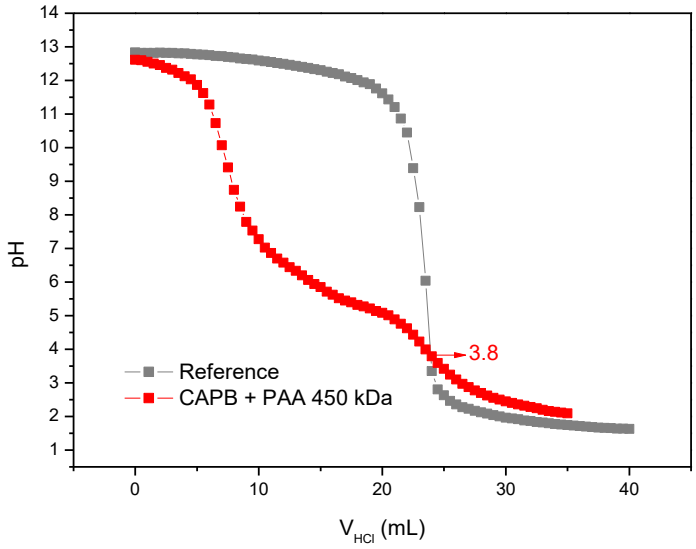

Figure 7. 8 : Potentiometric titration of solutions in the presence of NaOH 0.1 mol L^{-1} to determine the isoelectric point according to the method of reference: J.-Q. Guan, C.-H. Tung, G.-Z. Li, Modification of Alkylbetaine by Incorporation of Hydroxypropyl Group: Preparation, Surface Activity, and Biodegradability of N-

Alkoxy-Hydroxypropyl-N, N-Dimethyl-Glycine Betaine Surfactants, J. Dispers. Sci. Technol. 19 (1998) 63–76.

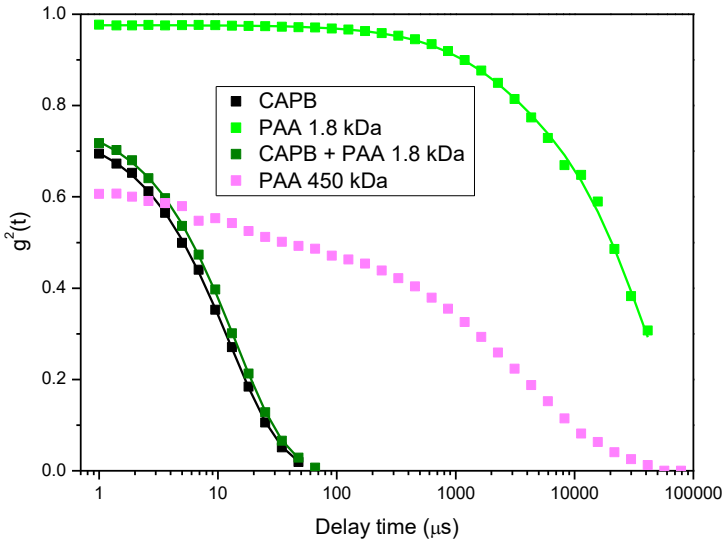

Figure 7. 9: Autocorrelation functions obtained by DLS from aqueous solutions of CAPB (0.0292 mol L^{-1}) with different polymers and their respective fittings.

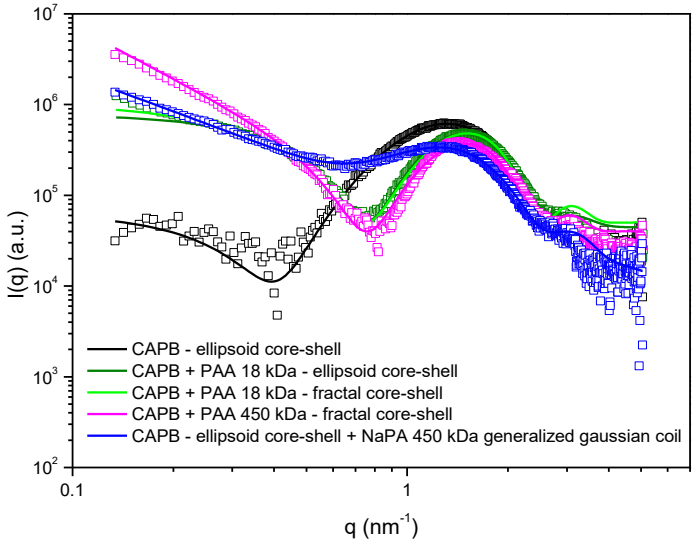

Figure 7. 10: SAXS curves of aqueous solutions of CAPB (0.0292 mol L^{-1}) with different polymers and their respective fittings.

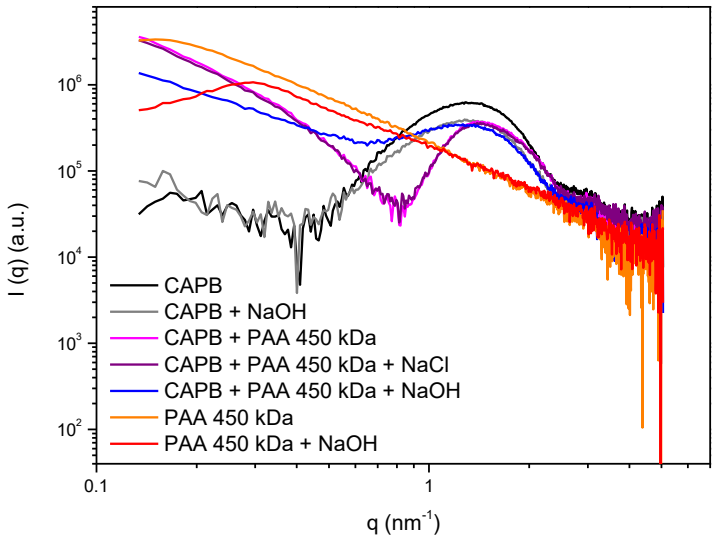

Figure 7.11: SAXS results of aqueous solutions of CAPB and polymers with and without the addition of NaOH (up to pH = 7) or NaCl (0.1 mol L^{-1}).

Model Function of Ellipsoid core-shell from SASView software [231,232]**:**

Intensity is calculated as that for solid ellipsoids, but with separate terms of the core-shell and shell-solvent boundaries:

$$I(q) = \frac{scale}{V}\langle P^2(q)\rangle + Background \qquad \text{Equation 7.1}$$

where scale is related to the absolute intensity factor and V is the ellipsoid volume.

$$\langle P^2(q)\rangle = \int d\mu \, |P(q,\mu)|^2 \qquad \text{Equation 7.2}$$

$$P(q,\mu) = (\rho_c - \rho_{sh})V_c[3j_i(u_c)/u_c] + (\rho_{sh} - \rho_s)V_t[3j_i(u_t)/u_t] \quad \text{Equation 7.3}$$

$$u_i = q[A_i^2\mu^2 + B_i^2(1-\mu)]^{1/2} \qquad \text{Equation 7.4}$$

where *ρ* is the scattering length density, *A* is the minor axis, *B* is the major axis, and *c*, *sh*, *s* and *t* denote the core, shell, solvent, and overall, respectively.

Estimation of the length of fully extended PAA

The length (l) of a fully extended polymeric chain can be estimated as:

$$l = N \cdot d \cdot sen\left(\frac{\theta}{2}\right) \quad \text{Equation 7.5}$$

where N is the number of covalent bonds, d is the bond length, and θ is the bond angle.

Since the molecular mass of an acrylic acid unit is 72 g/mol, which has 2 C–C bond, the number of covalent bonds for PAA can be obtained by:

$$N = \frac{2 \cdot M_w}{72\ g/mol} - 1 \qquad \text{Equation 7.6}$$

For a C–C bond, d = 0,154 nm and θ = 109,5 °.

Estimation of the perimeter of CAPB

Different approximation formulas can estimate the perimeter (p) of an ellipse, but we used the Equation S7, which is adequate when the values of polar and equatorial radii are not close to each other:

$$p = 2\pi\sqrt{\frac{a^2+b^2}{2}} \qquad \text{Equation 7.7}$$

where a and b are the ellipse's radii, which were calculated as, $a = (R_2 + t)$ and $b = (R_1 + t)$, from the values of Table 1.

CHAPTER 8

8.1. General conclusions of the thesis and suggestions for future works

This study successfully designed, synthesized, and characterized various soft materials using triblock copolymers to load hydrophobic ingredients into aqueous formulations. Employing straightforward preparation methods and biocompatible chemicals, the research demonstrated the relevant roles of triblock copolymers on the stability and properties of each strategy:

- Core-shell hydrogel particles were developed using poly(diallyldimethylammonium chloride) (PDADMAC) and OCNF, we showed that upon incorporating triblock copolymer we were capable of incorporating mineral oil, and with microfluidics the reduction of the size of these particles.

- Micro- and nanoparticles were successfully produced from lamellar phases by mixing sodium lauryl sulfate (SDS) with various fatty alcohols or acids, achieving effective oil encapsulation.

- Nanoparticles were obtained through the electrostatic complexation of hexadecyltrimethylammonium bromide (CTAB) with polyacrylic acid (PAA), resulting in low-viscosity suspensions with enhanced stability.

Triblock copolymers created hydrophobic compartments to ensure oil loading and improved the dispersibility and stability of the colloidal systems in water.

Moreover, we were able to understand how the pH and molecular weight of polyanions affect the phase behavior of a CAPB and PAA mixture, successfully connecting nanostructures with macroscopic behavior, which is essential for controlling properties in real applications.

For future work further exploration of the triblock copolymers with different ratios of hydrophilic and hydrophobic blocks could enhance oil loading capabilities. This optimization could target specific applications, such as tailored delivery rates or improved stability in varying pH environments. We could also extend the study's findings to different fields, such as pharmaceuticals or food science, where controlled release of hydrophobic ingredients is beneficial. Besides that, investigating other factors like temperature and ionic strength in

more depth, particularly for their effects on stability and encapsulation efficiency in varying environmental conditions could increase particles' applications.

8.2. Declaration of generative AI in scientific writing

During the preparation of this text, the author utilized ChatGPT to assist with reviewing and editing the content to enhance readability and language. Generative AI was employed as a tool to support the manuscript's improvement under human oversight and careful review. After using this service, the author thoroughly reviewed and edited the content.

CHAPTER 9

Bibliography

[1] J. Van Der Gucht, Grand Challenges in Soft Matter Physics, Front. Phys. 6 (2018) 87. https://doi.org/10.3389/fphy.2018.00087.

[2] A. de Azevedo Stavale, G. Oliva Fonseca, P. Severo Duarte, L. Costa Macedo, A.M. Percebom, Nanoparticles of surfactant and block copolymers with high uptake of oily ingredients for cosmetic formulations, Colloids Surf. Physicochem. Eng. Asp. 581 (2019) 123779. https://doi.org/10.1016/j.colsurfa.2019.123779.

[3] U. Adhikari, A. Goliaei, L. Tsereteli, M.L. Berkowitz, Properties of poloxamer molecules and poloxamer micelles dissolved in water and next to lipid bilayers: Results from computer simulations, J. Phys. Chem. B 120 (2016) 5823–5830. https://doi.org/10.1021/acs.jpcb.5b11448.

[4] D. Ćirin, V. Krstonošić, M. Poša, Properties of poloxamer 407 and polysorbate mixed micelles: Influence of polysorbate hydrophobic chain, J. Ind. Eng. Chem. 47 (2017) 194–201. https://doi.org/10.1016/j.jiec.2016.11.032.

[5] A. Garg, D.S. Tomar, K. Bhalala, M. Wahajuddin, Development and investigation of Artemether loaded binary solid lipid nanoparticles: Physicochemical characterization and in-situ single-pass intestinal permeability, J. Drug Deliv. Sci. Technol. 60 (2020) 102072. https://doi.org/10.1016/j.jddst.2020.102072.

[6] E.B. Souto, A. Zielinska, S.B. Souto, A. Durazzo, M. Lucarini, A. Santini, A.M. Silva, A.G. Atanasov, C. Marques, L.N. Andrade, P. Severino, (+)-limonene 1,2-epoxide-loaded slns: Evaluation of drug release, antioxidant activity, and cytotoxicity in an HaCaT cell line, Int. J. Mol. Sci. 21 (2020) 1–11. https://doi.org/10.3390/ijms21041449.

[7] I. Baldim, L. Tonani, M.R. von Zeska Kress, W. Pereira Oliveira, Lippia sidoides essential oil encapsulated in lipid nanosystem as an anti-Candida agent, Ind. Crops Prod. 127 (2019) 73–81. https://doi.org/10.1016/j.indcrop.2018.10.064.

[8] A.C. Santos, F. Morais, A. Simões, I. Pereira, J.A.D. Sequeira, M. Pereira-Silva, F. Veiga, A. Ribeiro, Nanotechnology for the development of new cosmetic formulations, Expert Opin. Drug Deliv. 16 (2019) 313–330. https://doi.org/10.1080/17425247.2019.1585426.

[9] X. Li, J. Li, Y. Kuang, S. Guo, L. Mo, Y. Ni, Stabilization of Pickering emulsions with cellulose nanofibers derived from oil palm fruit bunch, Cellulose 27 (2020) 839–851. https://doi.org/10.1007/s10570-019-02803-4.

[10] K.M.Z. Hossain, L. Deeming, K.J. Edler, Recent progress in Pickering emulsions stabilised by bioderived particles, RSC Adv. 11 (2021) 39027–39044. https://doi.org/10.1039/D1RA08086E.

[11] K.P. Sai Sateesh Sagiri, Arfat Anis, Review on Encapsulation of Vegetable Oils Strategies, Preparation Methods, and Applications.pdf, Polym.-Plast. Technol. Eng. 55 (2015) 291–311. https://doi.org/10.1080/03602559.2015.1050521.

[12] W. Dong, R. Bodmeier, Encapsulation of lipophilic drugs within enteric microparticles by a novel coacervation method, Int. J. Pharm. 326 (2006) 128–138. https://doi.org/10.1016/j.ijpharm.2006.07.013.

[13] F. Casanova, L. Santos, Encapsulation of cosmetic active ingredients for topical application-a review, J. Microencapsul. 33 (2016) 1–17. https://doi.org/10.3109/02652048.2015.1115900.

[14] I. Jarak, C.L. Varela, E. Tavares da Silva, F.F.M. Roleira, F. Veiga, A. Figueiras, Pluronic-based nanovehicles: Recent advances in anticancer therapeutic applications, Eur. J. Med. Chem. 206 (2020). https://doi.org/10.1016/j.ejmech.2020.112526.

[15] P. Zarrintaj, J.D. Ramsey, A. Samadi, Z. Atoufi, M.K. Yazdi, M.R. Ganjali, L.M. Amirabad, E. Zangene, M. Farokhi, K. Formela, M.R. Saeb, M. Mozafari, S. Thomas, Poloxamer: A versatile tri-block copolymer for biomedical applications, Acta Biomater. 110 (2020) 37–67. https://doi.org/10.1016/j.actbio.2020.04.028.

[16] E.S. Lee, Y.T. Oh, Y.S. Youn, M. Nam, B. Park, J. Yun, J.H. Kim, H.T. Song, K.T. Oh, Binary mixing of micelles using Pluronics for a nano-sized drug delivery system, Colloids Surf. B Biointerfaces 82 (2011) 190–195. https://doi.org/10.1016/j.colsurfb.2010.08.033.

[17] S.R. Croy, G.S. Kwon, The effects of Pluronic block copolymers on the aggregation state of nystatin, J. Controlled Release 95 (2004) 161–171. https://doi.org/10.1016/j.jconrel.2003.11.003.

[18] K.T. Oh, T.K. Bronich, A.V. Kabanov, Micellar formulations for drug delivery based on mixtures of hydrophobic and hydrophilic Pluronic® block copolymers, J. Controlled Release 94 (2004) 411–422. https://doi.org/10.1016/j.jconrel.2003.10.018.

[19] J.M. Taylor, K. Scale, S. Arrowsmith, A. Sharp, S. Flynn, S. Rannard, T.O. McDonald, Using pyrene to probe the effects of poloxamer stabilisers on internal lipid microenvironments in solid lipid nanoparticles, Nanoscale Adv. 2 (2020) 5572–5577. https://doi.org/10.1039/d0na00582g.

[20] A.V. Kabanov, P. Lemieux, S. Vinogradov, V. Alakhov, Pluronic® block copolymers: Novel functional molecules for gene therapy, Adv. Drug Deliv. Rev. 54 (2002) 223–233. https://doi.org/10.1016/S0169-409X(02)00018-2.

[21] M. Senthilkumar, B. Sheelarani, R.G. Joshi, S. Dash, Solubilization and interaction of ciprofloxacin with pluronics and their mixed micelles, New J. Chem. 43 (2019) 16530–16537. https://doi.org/10.1039/c9nj03383a.

[22] D. Patel, D. Ray, S. Tiwari, K. Kuperkar, V.K. Aswal, P. Bahadur, SDS triggered transformation of highly hydrophobic Pluronics® nanoaggregate into polymer-rich and surfactant-rich mixed micelles, J. Mol. Liq. 345 (2022) 117812. https://doi.org/10.1016/j.molliq.2021.117812.

[23] D. Patel, N. Tripathi, D. Ray, V.K. Aswal, K. Kuperkar, P. Bahadur, CTAB induced growth and shrinkage of Pluronics® P103 micelles: Experimental and theoretical rationale, J. Mol. Liq. 391 (2023) 123315. https://doi.org/10.1016/j.molliq.2023.123315.

[24] A.M. Bodratti, P. Alexandridis, Formulation of poloxamers for drug delivery, J. Funct. Biomater. 9 (2018). https://doi.org/10.3390/jfb9010011.

[25] M.Yu. Kozlov, N.S. Melik-Nubarov, E.V. Batrakova, A.V. Kabanov, Relationship between Pluronic Block Copolymer Structure, Critical Micellization Concentration and Partitioning Coefficients of Low Molecular Mass Solutes, Macromolecules 33 (2000) 3305–3313. https://doi.org/10.1021/ma991634x.

[26] David A. RICHARD, Micelle-based delivery of dermal therapeutic materials, 2009. https://doi.org/US 2016/0279162 Al.

[27] Adam M. Rotunda, Topical skin formulations and wound care products with integrated cbd delivery mechanisms for skin rejuvenation, wound care and healing, pain and itch relief, and scar prevention and treatment, 2020. https://doi.org/US 2020/0352849 Al.

[28] C. Brent R. Constantz, Portola Valley, CA (US); Jacob Schneider, San Jose, CA (US); Christopher L. Camire, Moigan Hill, CA (US); Seung-Hee Kang, San Jose, CA (US); Ken Hines, Palo Alto, (19) United States Patent Application Publication, 1 (2017) 3–5.

[29] O. (US) Dongcui Li, North Royalton, OH (US); Shui-Jen Raymond Hsu, Foothill Ranch, CA (US); Krishnan Chari, Hudson, Surfactant Responsive Emulsion Polymerized Micro-Gels, 2019. https://doi.org/US 2019/0345282 Al.

[30] M. Wulff-Pérez, A. Torcello-Gómez, M.J. Gálvez-Ruíz, A. Martín-Rodríguez, Stability of emulsions for parenteral feeding: Preparation and characterization of o/w nanoemulsions with natural oils and Pluronic f68 as surfactant, Food Hydrocoll. 23 (2009) 1096–1102. https://doi.org/10.1016/j.foodhyd.2008.09.017.

[31] K. Pojják, R. Mészáros, Preparation of Stable Electroneutral Nanoparticles of Sodium Dodecyl Sulfate and Branched Poly(ethylenimine) in the Presence of Pluronic F108 Copolymer, Langmuir 27 (2011) 14797–14806. https://doi.org/10.1021/la203759r.

[32] M. Nakano, T. Teshigawara, A. Sugita, W. Leesajakul, A. Taniguchi, T. Kamo, H. Matsuoka, T. Handa, Dispersions of Liquid Crystalline Phases of the Monoolein/Oleic Acid/Pluronic F127 System, Langmuir 18 (2002) 9283–9288. https://doi.org/10.1021/la026297r.

[33] M. Mitov, Liquid-Crystal Science from 1888 to 1922: Building a Revolution, ChemPhysChem 15 (2014) 1245–1250. https://doi.org/10.1002/cphc.201301064.

[34] T.F. Tadros, S. Léonard, C. Verboom, V. Wortel, M. Taelman, F. Roschzttardtz, Cosmetic Emulsions Based on Surfactant Liquid Crystalline Phases: Structure, Rheology and Sensory Evaluation, in: T.F. Tadros (Ed.), Colloids Cosmet. Pers. Care, 1st ed., Wiley, 2008: pp. 93–105. https://doi.org/10.1002/9783527631131.ch6.

[35] I.W. Hamley, Diffuse scattering from lamellar structures, Soft Matter 18 (2022) 711–721. https://doi.org/10.1039/D1SM01758F.

[36] T.F. Tadros, Applied surfactants: principles and applications, 2. repr, Wiley-VCH, Weinheim, 2008.

[37] K. Steck, S. Dieterich, C. Stubenrauch, F. Giesselmann, Surfactant-based lyotropic liquid crystal gels – the interplay between anisotropic order and gel formation, J. Mater. Chem. C 8 (2020) 5335–5348. https://doi.org/10.1039/D0TC00561D.

[38] A. Maria Percebom Sette Da Silva, Autoassociação de sais complexos de surfatantes e copolímeros aleatórios e enxertados, Doutora em Ciências, Universidade Estadual de Campinas, 2012. https://doi.org/10.47749/T/UNICAMP.2012.880196.

[39] H. Iwai, J. Fukasawa, T. Suzuki, A liquid crystal application in skin care cosmetics, Int. J. Cosmet. Sci. 20 (1998) 87–102. https://doi.org/10.1046/j.1467-2494.1998.171741.x.

[40] A. Isogai, Emerging Nanocellulose Technologies: Recent Developments, Adv. Mater. 33 (2021) 2000630. https://doi.org/10.1002/adma.202000630.

[41] M.J. Hope, M.B. Bally, L.D. Mayer, A.S. Janoff, P.R. Cullis, Generation of multilamellar and unilamellar phospholipid vesicles, Chem. Phys. Lipids 40 (1986) 89–107. https://doi.org/10.1016/0009-3084(86)90065-4.

[42] N.K. Gupta, V.K. Dixit, Development and evaluation of vesicular system for curcumin delivery, Arch. Dermatol. Res. 303 (2011) 89–101. https://doi.org/10.1007/s00403-010-1096-6.

[43] T. Toniazzo, M.S. Peres, A.P. Ramos, S.C. Pinho, Encapsulation of quercetin in liposomes by ethanol injection and physicochemical characterization of dispersions and lyophilized vesicles, Food Biosci. 19 (2017) 17–25. https://doi.org/10.1016/j.fbio.2017.05.003.

[44] M.L. Manca, F. Marongiu, I. Castangia, A. Catalán-Latorre, C. Caddeo, G. Bacchetta, G. Ennas, M. Zaru, A.M. Fadda, M. Manconi, Protective effect of grape extract phospholipid vesicles against oxidative stress skin damages, Ind. Crops Prod. 83 (2016) 561–567. https://doi.org/10.1016/j.indcrop.2015.12.069.

[45] L. Hanley, S.M. Ghazani, A.G. Marangoni, Giant multilamellar and large unilamellar lecithin vesicles for the encapsulation and oral delivery of

cannabinoids, Food Chem. 433 (2024) 137291. https://doi.org/10.1016/j.foodchem.2023.137291.

[46] A. Lohani, A. Verma, Vesicles: Potential nano carriers for the delivery of skin cosmetics, J. Cosmet. Laser Ther. 19 (2017) 485–493. https://doi.org/10.1080/14764172.2017.1358451.

[47] G.M. Eccleston, M.K. Behan-Martin, G.R. Jones, E. Towns-Andrews, Synchrotron X-ray investigations into the lamellar gel phase formed in pharmaceutical creams prepared with cetrimide and fatty alcohols, Int. J. Pharm. 203 (2000) 127–139. https://doi.org/10.1016/S0378-5173(00)00447-6.

[48] A. Svensson, L. Piculell, B. Cabane, P. Ilekti, A New Approach to the Phase Behavior of Oppositely Charged Polymers and Surfactants, J. Phys. Chem. B 106 (2002) 1013–1018. https://doi.org/10.1021/jp0120458.

[49] G.M. Eccleston, Phase transitions in ternary systems and oil-in-water emulsions containing cetrimide and fatty alcohols, Int. J. Pharm. 27 (1985) 311–323. https://doi.org/10.1016/0378-5173(85)90079-1.

[50] A.M. Percebom, G.A. Ferreira, D.R. Catini, J.S. Bernardes, W. Loh, Phase Behavior Controlled by the Addition of Long-Chain *n* -Alcohols in Systems of Cationic Surfactant/Anionic Polyion Complex Salts and Water, J. Phys. Chem. B 122 (2018) 4861–4869. https://doi.org/10.1021/acs.jpcb.8b01788.

[51] R. Zana, Aqueous surfactant-alcohol systems: A review, Adv. Colloid Interface Sci. 57 (1995) 1–64. https://doi.org/10.1016/0001-8686(95)00235-I.

[52] A.M. Percebom, W. Loh, Controlling the phase structures of polymer/surfactant complexes by changing macromolecular architecture and adding n-alcohols, J. Colloid Interface Sci. 466 (2016) 377–387. https://doi.org/10.1016/j.jcis.2015.12.050.

[53] K. Fontell, A. Khan, B. Lindström, D. Maciejewska, S. Puang-Ngern, Phase equilibria and structures in ternary systems of a cationic surfactant (C16 TABr or (C16 TA)2SO4), alcohol, and water, Colloid Polym. Sci. 269 (1991) 727–742. https://doi.org/10.1007/BF00657411.

[54] X. Mulet, B.J. Boyd, C.J. Drummond, Advances in drug delivery and medical imaging using colloidal lyotropic liquid crystalline dispersions, J.

Colloid Interface Sci. 393 (2013) 1–20. https://doi.org/10.1016/j.jcis.2012.10.014.

[55] A.P. Lukas Costa Macedo, Partículas líquido-cristalinas estabilizadas por surfactantes etoxilados em dispersões aquosas, PUCRio, 2020.

[56] A. Azevedo Stavale, A.M. Percebom, Nanopartículas núcleo-casca de polímeros e surfactantes para formulação de um protetor solar para cabelos, (2018).

[57] L. Piculell, Understanding and Exploiting the Phase Behavior of Mixtures of Oppositely Charged Polymers and Surfactants in Water, Langmuir 29 (2013) 10313–10329. https://doi.org/10.1021/la401026j.

[58] M. Annaka, K. Morishita, S. Okabe, Electrostatic self-assembly of neutral and polyelectrolyte block copolymers and oppositely charged surfactant, J. Phys. Chem. B 111 (2007) 11700–11707. https://doi.org/10.1021/jp074404q.

[59] G.A. Ferreira, W. Loh, Liquid crystalline nanoparticles formed by oppositely charged surfactant-polyelectrolyte complexes, Curr. Opin. Colloid Interface Sci. 32 (2017) 11–22. https://doi.org/10.1016/j.cocis.2017.08.003.

[60] Y. Shen, P. Somasundaran, Introduction of a nonionic sugar-based surfactant to an oppositely charged hydrophobically modified polyelectrolyte and surfactant binary system, Colloids Surf. Physicochem. Eng. Asp. 570 (2019) 274–281. https://doi.org/10.1016/j.colsurfa.2019.03.040.

[61] P. Hervé, M. Destarac, J.-F. Berret, J. Lal, J. Oberdisse, I. Grillo, Novel core-shell structure for colloids made of neutral/polyelectrolyte diblock copolymers and oppositely charged surfactants, Europhys. Lett. EPL 58 (2002) 912–918. https://doi.org/10.1209/epl/i2002-00104-y.

[62] J.-F. Berret, G. Cristobal, P. Hervé, J. Oberdisse, I. Grillo, Structure of colloidal complexes obtained from neutral/poly- electrolyte copolymers and oppositely charged surfactants, Eur. Phys. J. E 9 (2002) 301–311. https://doi.org/10.1140/epje/i2002-10063-7.

[63] N. Muhd Julkapli, S. Bagheri, Nanocellulose as a green and sustainable emerging material in energy applications: a review, Polym. Adv. Technol. 28 (2017) 1583–1594. https://doi.org/10.1002/pat.4074.

[64] S.S. Nair, J. Zhu, Y. Deng, A.J. Ragauskas, High performance green barriers based on nanocellulose, Sustain. Chem. Process. 2 (2014) 23. https://doi.org/10.1186/s40508-014-0023-0.

[65] T. Rusconi, L. Riva, C. Punta, M. Solé, I. Corsi, Environmental safety of nanocellulose: an acute *in vivo* study with marine mussels *Mytilus galloprovincialis*, Environ. Sci. Nano 11 (2024) 61–77. https://doi.org/10.1039/D3EN00135K.

[66] D.J. Gardner, G.S. Oporto, R. Mills, M.A.S.A. Samir, Adhesion and Surface Issues in Cellulose and Nanocellulose, J. Adhes. Sci. Technol. 22 (2008) 545–567. https://doi.org/10.1163/156856108X295509.

[67] A.K. Tamo, Nanocellulose-based hydrogels as versatile materials with interesting functional properties for tissue engineering applications, J. Mater. Chem. B 12 (2024) 7692–7759. https://doi.org/10.1039/D4TB00397G.

[68] J. Peng, V. Calabrese, S.J. Veen, P. Versluis, K.P. Velikov, P. Venema, E. Van Der Linden, Rheology and microstructure of dispersions of protein fibrils and cellulose microfibrils, Food Hydrocoll. 82 (2018) 196–208. https://doi.org/10.1016/j.foodhyd.2018.03.033.

[69] A. Isogai, T. Saito, H. Fukuzumi, TEMPO-oxidized cellulose nanofibers, Nanoscale 3 (2011) 71–85. https://doi.org/10.1039/C0NR00583E.

[70] S. Afewerki, R. Alimohammadzadeh, S.H. Osong, C. Tai, P. Engstrand, A. Córdova, Sustainable Design for the Direct Fabrication and Highly Versatile Functionalization of Nanocelluloses, Glob. Chall. 1 (2017) 1700045. https://doi.org/10.1002/gch2.201700045.

[71] R. Song, E. Zhu, R. Hou, F. Niu, J. Bao, D. Chen, Z. Shi, Q. Yang, C. Xiong, Nanocellulose-based composite beads as the amphoteric adsorbent for effective adsorption of cationic and anionic dyes, Cellulose 31 (2024) 5077–5095. https://doi.org/10.1007/s10570-024-05835-7.

[72] X. Yue, M. Miao, X. Feng, Incorporating of Oxidized Cellulose Nanofibers@ D -Limonene Pickering Emulsion into Chitosan for Fully Biobased Coatings toward Fruits Protection, ACS Sustain. Chem. Eng. 11 (2023) 15102–15113. https://doi.org/10.1021/acssuschemeng.3c04396.

[73] S.L. Kadam, P. Yadav, S. Bhutkar, V.D. Patil, P.G. Shukla, K. Shanmuganathan, Sustained release insect repellent microcapsules using

modified cellulose nanofibers (mCNF) as pickering emulsifier, Colloids Surf. Physicochem. Eng. Asp. 582 (2019) 123883. https://doi.org/10.1016/j.colsurfa.2019.123883.

[74] H. Shi, K.M.Z. Hossain, D. Califano, C. Callaghan, E.E. Ekanem, J.L. Scott, D. Mattia, K.J. Edler, Stable Cellulose Nanofibril Microcapsules from Pickering Emulsion Templates, Langmuir 38 (2022) 3370–3379. https://doi.org/10.1021/acs.langmuir.1c03025.

[75] V. Calabrese, D. Califano, M.A. Da Silva, J. Schmitt, S.J. Bryant, K.M.Z. Hossain, A.M. Percebom, A. Pérez Gramatges, J.L. Scott, K.J. Edler, Core–Shell Spheroidal Hydrogels Produced via Charge-Driven Interfacial Complexation, ACS Appl. Polym. Mater. 2 (2020) 1213–1221. https://doi.org/10.1021/acsapm.9b01086.

[76] M. Ouverney Ferreira, H.F. Câmara De Assis, A.M. Percebom, Cocamidopropyl betaine can behave as a cationic surfactant and electrostatically associate with polyacids of high molecular weight, Colloids Surf. Physicochem. Eng. Asp. 654 (2022) 130123. https://doi.org/10.1016/j.colsurfa.2022.130123.

[77] J.C. Courtenay, M.A. Johns, F. Galembeck, C. Deneke, E.M. Lanzoni, C.A. Costa, J.L. Scott, R.I. Sharma, Surface modified cellulose scaffolds for tissue engineering, Cellulose 24 (2017) 253–267. https://doi.org/10.1007/s10570-016-1111-y.

[78] A.P. Hammersley, FIT2D: A multi-purpose data reduction, analysis and visualization program, J. Appl. Crystallogr. 49 (2016). https://doi.org/10.1107/S1600576716000455.

[79] P.J. Oliveira C, SUPERSAXS program package for data treatment, analysis, and modeling, (2009). https://portal.if.usp.br/gfcx/pt-br/node/354.

[80] E. Spruijt, A.H. Westphal, J.W. Borst, M.A. Cohen Stuart, J. Van Der Gucht, Binodal Compositions of Polyelectrolyte Complexes, Macromolecules 43 (2010) 6476–6484. https://doi.org/10.1021/ma101031t.

[81] E. Kizilay, A.B. Kayitmazer, P.L. Dubin, Complexation and coacervation of polyelectrolytes with oppositely charged colloids, Adv. Colloid Interface Sci. 167 (2011) 24–37. https://doi.org/10.1016/j.cis.2011.06.006.

[82] R. Chollakup, W. Smitthipong, C.D. Eisenbach, M. Tirrell, Phase Behavior and Coacervation of Aqueous Poly(acrylic acid)−Poly(allylamine)

Solutions, Macromolecules 43 (2010) 2518–2528. https://doi.org/10.1021/ma902144k.

[83] C. Preetz, A. Rübe, I. Reiche, G. Hause, K. Mäder, Preparation and characterization of biocompatible oil-loaded polyelectrolyte nanocapsules, Nanomedicine Nanotechnol. Biol. Med. 4 (2008) 106–114. https://doi.org/10.1016/j.nano.2008.03.003.

[84] M. Kim, S.J. Yeo, C.B. Highley, J.A. Burdick, P.J. Yoo, J. Doh, D. Lee, One-Step Generation of Multifunctional Polyelectrolyte Microcapsules *via* Nanoscale Interfacial Complexation in Emulsion (NICE), ACS Nano 9 (2015) 8269–8278. https://doi.org/10.1021/acsnano.5b02702.

[85] Y. Zou, J. Song, X. You, J. Yao, S. Xie, M. Jin, X. Wang, Z. Yan, G. Zhou, L. Shui, Interfacial Complexation Induced Controllable Fabrication of Stable Polyelectrolyte Microcapsules Using All-Aqueous Droplet Microfluidics for Enzyme Release, ACS Appl. Mater. Interfaces 11 (2019) 21227–21238. https://doi.org/10.1021/acsami.9b02788.

[86] R. Atkin, P. Davies, J. Hardy, B. Vincent, Preparation of Aqueous Core/Polymer Shell Microcapsules by Internal Phase Separation, Macromolecules 37 (2004) 7979–7985. https://doi.org/10.1021/ma048902y.

[87] M.A. Trojer, H. Andersson, Y. Li, J. Borg, K. Holmberg, M. Nydén, L. Nordstierna, Charged microcapsules for controlled release of hydrophobic actives. Part III: the effect of polyelectrolyte brush- and multilayers on sustained release, Phys. Chem. Chem. Phys. 15 (2013) 6456. https://doi.org/10.1039/c3cp50417d.

[88] B.N. Estevinho, F. Rocha, Application of Biopolymers in Microencapsulation Processes, in: Biopolym. Food Des., Elsevier, 2018: pp. 191–222. https://doi.org/10.1016/B978-0-12-811449-0.00007-4.

[89] J. Song, F. Babayekhorasani, P.T. Spicer, Soft Bacterial Cellulose Microcapsules with Adaptable Shapes, Biomacromolecules 20 (2019) 4437–4446. https://doi.org/10.1021/acs.biomac.9b01143.

[90] C.E. Sing, S.L. Perry, Recent progress in the science of complex coacervation, Soft Matter 16 (2020) 2885–2914. https://doi.org/10.1039/D0SM00001A.

[91] D.J.C. Araújo, A.V. Machado, M.C.L.G. Vilarinho, Availability and Suitability of Agroindustrial Residues as Feedstock for Cellulose-Based Materials: Brazil Case Study, Waste Biomass Valorization 10 (2019) 2863–2878. https://doi.org/10.1007/s12649-018-0291-0.

[92] S.R. Kline, Reduction and analysis of SANS and USANS data using IGOR Pro, J. Appl. Crystallogr. 39 (2006) 895–900. https://doi.org/10.1107/S0021889806035059.

[93] J. Schmitt, V. Calabrese, M.A. Da Silva, S. Lindhoud, V. Alfredsson, J.L. Scott, K.J. Edler, TEMPO-oxidised cellulose nanofibrils; probing the mechanisms of gelation *via* small angle X-ray scattering, Phys. Chem. Chem. Phys. 20 (2018) 16012–16020. https://doi.org/10.1039/C8CP00355F.

[94] A.A. Golosova, J. Adelsberger, A. Sepe, M.A. Niedermeier, P. Lindner, S.S. Funari, R. Jordan, C.M. Papadakis, Dispersions of Polymer-Modified Carbon Nanotubes: A Small-Angle Scattering Investigation, J. Phys. Chem. C 116 (2012) 15765–15774. https://doi.org/10.1021/jp303582t.

[95] C.-Y. Chen, S.-H. Chan, J.-Y. Li, K.-H. Wu, H.-L. Chen, J.-H. Chen, W.-Y. Huang, S.-A. Chen, Formation and Thermally-Induced Disruption of Nanowhiskers in Poly(3-hexylthiophene)/Xylene Gel Studied by Small-Angle X-ray Scattering, Macromolecules 43 (2010) 7305–7311. https://doi.org/10.1021/ma1008034.

[96] V. Calabrese, J.C. Muñoz-García, J. Schmitt, M.A. Da Silva, J.L. Scott, J. Angulo, Y.Z. Khimyak, K.J. Edler, Understanding heat driven gelation of anionic cellulose nanofibrils: Combining saturation transfer difference (STD) NMR, small angle X-ray scattering (SAXS) and rheology, J. Colloid Interface Sci. 535 (2019) 205–213. https://doi.org/10.1016/j.jcis.2018.09.085.

[97] S. Manet, A. Lecchi, M. Impéror-Clerc, V. Zholobenko, D. Durand, C.L.P. Oliveira, J.S. Pedersen, I. Grillo, F. Meneau, C. Rochas, Structure of Micelles of a Nonionic Block Copolymer Determined by SANS and SAXS, J. Phys. Chem. B 115 (2011) 11318–11329. https://doi.org/10.1021/jp200212g.

[98] H.E. Bakker, T.H. Besseling, J.E.G.J. Wijnhoven, P.H. Helfferich, A. Van Blaaderen, A. Imhof, Microelectrophoresis of Silica Rods Using Confocal

Microscopy, Langmuir 33 (2017) 881–890. https://doi.org/10.1021/acs.langmuir.6b03863.

[99] F.A. Morrison, Electrophoresis of a particle of arbitrary shape, J. Colloid Interface Sci. 34 (1970) 210–214. https://doi.org/10.1016/0021-9797(70)90171-2.

[100] R. Bourne, ImageJ, in: Fundam. Digit. Imaging Med., Springer London, London, 2010: pp. 185–188. https://doi.org/10.1007/978-1-84882-087-6_9.

[101] C.A. Dreiss, Wormlike micelles: where do we stand? Recent developments, linear rheology and scattering techniques, Soft Matter 3 (2007) 956. https://doi.org/10.1039/b705775j.

[102] V. Calabrese, M.A. Da Silva, L. Porcar, S.J. Bryant, K.M.Z. Hossain, J.L. Scott, K.J. Edler, Filler size effect in an attractive fibrillated network: a structural and rheological perspective, Soft Matter 16 (2020) 3303–3310. https://doi.org/10.1039/C9SM02175B.

[103] K.M.Z. Hossain, V. Calabrese, M.A. Da Silva, S.J. Bryant, J. Schmitt, J.H. Ahn-Jarvis, F.J. Warren, Y.Z. Khimyak, J.L. Scott, K.J. Edler, Monovalent Salt and pH-Induced Gelation of Oxidised Cellulose Nanofibrils and Starch Networks: Combining Rheology and Small-Angle X-ray Scattering, Polymers 13 (2021) 951. https://doi.org/10.3390/polym13060951.

[104] I. Grillo, I. Morfin, S. Prévost, Structural Characterization of Pluronic Micelles Swollen with Perfume Molecules, Langmuir 34 (2018) 13395–13408. https://doi.org/10.1021/acs.langmuir.8b03050.

[105] V.A. Feitosa, V.C.D. Almeida, B. Malheiros, R.D.D. Castro, L.R.S. Barbosa, N.N.P. Cerize, C.D.O. Rangel-Yagui, Polymeric micelles of pluronic F127 reduce hemolytic potential of amphiphilic drugs, Colloids Surf. B Biointerfaces 180 (2019) 177–185. https://doi.org/10.1016/j.colsurfb.2019.04.045.

[106] H. Fukuzumi, R. Tanaka, T. Saito, A. Isogai, Dispersion stability and aggregation behavior of TEMPO-oxidized cellulose nanofibrils in water as a function of salt addition, Cellulose 21 (2014) 1553–1559. https://doi.org/10.1007/s10570-014-0180-z.

[107] R. Curvello, V.S. Raghuwanshi, G. Garnier, Engineering nanocellulose hydrogels for biomedical applications, Adv. Colloid Interface Sci. 267 (2019) 47–61. https://doi.org/10.1016/j.cis.2019.03.002.

[108] K. Aramaki, M.K. Hossain, C. Rodriguez, M.H. Uddin, H. Kunieda, Miscibility of block copolymers and surfactants in lamellar liquid crystals, Macromolecules 36 (2003) 9443–9450. https://doi.org/10.1021/ma0350664.

[109] G. Popescu, J. Barauskas, T. Nylander, F. Tiberg, Liquid crystalline phases and their dispersions in aqueous mixtures of glycerol monooleate and glyceryl monooleyl ether, Langmuir 23 (2007) 496–503. https://doi.org/10.1021/la062344u.

[110] D.F. Evans, H. Wennerstrom, The Colloidal Domain - Where Physics, Chemistry, Biology, and Technology meet., Wiley-VCH, 1999.

[111] G.A. Ferreira, L. Piculell, W. Loh, Addition of *n* -Alcohols Induces a Variety of Liquid-Crystalline Structures in Surfactant-Rich Cores of Dispersed Block Copolymer/Surfactant Nanoparticles, ACS Omega 1 (2016) 1104–1113. https://doi.org/10.1021/acsomega.6b00267.

[112] P. Kudla, T. Sokolowski, B. Blümich, K.-P. Wittern, Phase behavior of liquid–crystalline emulsion systems, J. Colloid Interface Sci. 349 (2010) 554–559. https://doi.org/10.1016/j.jcis.2010.05.085.

[113] G. Tiddy, Surfactant-water liquid crystal phases, Phys. Rep. 57 (1980) 1–46. https://doi.org/10.1016/0370-1573(80)90041-1.

[114] V.D. Hoang, C.P. Cong, H.H. Tran, H.M.T. Nguyen, T.T. Nguyen, Influence of fatty alcohol mixing ratios on physicochemical properties of stearyl–cetyl–polysorbate 60–water ternary system: Insights from experiments and computer simulations, Colloid Polym. Sci. 299 (2021) 1885–1900. https://doi.org/10.1007/s00396-021-04874-x.

[115] G.A. Ferreira, W. Loh, Structural Parameters of Lamellar Phases Formed by the Self-Assembly of Dialkyldimethylammonium Bromides in Aqueous Solution, J. Braz. Chem. Soc. (2015). https://doi.org/10.5935/0103-5053.20150297.

[116] R.Y. Lochhead, Basic Physical Sciences for the Formulation of Cosmetic Products, in: Cosmet. Sci. Technol., Elsevier, 2017: pp. 39–76. https://doi.org/10.1016/B978-0-12-802005-0.00003-3.

[117] C.S.B. Ruiz, Produção e propriedades de álcoois graxos etoxilados com distribuição estreita de oligômeros, Mestrado em Físico-Química,

Universidade de São Paulo, 1997. https://doi.org/10.11606/D.46.1997.tde-19062009-095123.

[118] R. Ganguly, A. Kunwar, S. Kota, S. Kumar, V.K. Aswal, Micellar structural transitions and therapeutic properties in tea tree oil solubilized pluronic P123 solution, Colloids Surf. Physicochem. Eng. Asp. 537 (2018) 478–484. https://doi.org/10.1016/j.colsurfa.2017.10.045.

[119] A. Oshiro, D.C. Da Silva, J.C. De Mello, V.W.R. De Moraes, L.P. Cavalcanti, M.K.K.D. Franco, M.I. Alkschbirs, L.F. Fraceto, F. Yokaichiya, T. Rodrigues, D.R. De Araujo, Pluronics F-127/l-81 binary hydrogels as drug-delivery systems: Influence of physicochemical aspects on release kinetics and cytotoxicity, Langmuir 30 (2014) 13689–13698. https://doi.org/10.1021/la503021c.

[120] G. Tae, D. Won, Composition for forming pluronic-based hydrogel with improved stability, 1 (2015).

[121] A.J. Tilley, C.J. Drummond, B.J. Boyd, Disposition and association of the steric stabilizer Pluronic® F127 in lyotropic liquid crystalline nanostructured particle dispersions, J. Colloid Interface Sci. 392 (2013) 288–296. https://doi.org/10.1016/j.jcis.2012.09.051.

[122] J.S. Vankayala, S.N. Battula, R. Kandasamy, G.A. Mariya, M.E.E. Franklin, H.A. Pushpadass, L.N. Naik, Surfactants and fatty alcohol based novel nanovesicles for resveratrol: Process optimization, characterization and evaluation of functional properties in RAW 264.7 macrophage cells, J. Mol. Liq. 261 (2018) 387–396. https://doi.org/10.1016/j.molliq.2018.04.058.

[123] L. Shi, Z. Li, L. Yu, H. Jia, L. Zheng, Effects of Surfactants and Lipids on the Preparation of Solid Lipid Nanoparticles Using Double Emulsion Method, J. Dispers. Sci. Technol. 32 (2011) 254–259. https://doi.org/10.1080/01932691003659130.

[124] N. Philip, C. Veerakumar, A. Sreekumar, Lauryl alcohol and stearyl alcohol eutectic for cold thermal energy storage in buildings: Preparation, thermophysical studies and performance analysis, J. Energy Storage 31 (2020) 101600. https://doi.org/10.1016/j.est.2020.101600.

[125] S. Martins, I. Tho, D.C. Ferreira, E.B. Souto, M. Brandl, Physicochemical properties of lipid nanoparticles: Effect of lipid and surfactant composition,

Drug Dev. Ind. Pharm. 37 (2011) 815–824. https://doi.org/10.3109/03639045.2010.545414.

[126] E. Summerton, G. Zimbitas, M. Britton, S. Bakalis, Crystallisation of sodium dodecyl sulfate and the corresponding effect of 1-dodecanol addition, J. Cryst. Growth 455 (2016) 111–116. https://doi.org/10.1016/j.jcrysgro.2016.10.005.

[127] Z. Li, S. Peng, X. Chen, Y. Zhu, L. Zou, W. Zhou, W. Liu, C. Liu, Effect of dynamic high pressure microfluidization on structure and stability of pluronic F127 modified liposomes, J. Dispers. Sci. Technol. 40 (2019) 982–989. https://doi.org/10.1080/01932691.2018.1489281.

[128] C.L. Usma, I.E. Pacios, C.S. Renamayor, Lyotropic Lamellar Structures of a Long-Chain Imidazolium and Their Application as Nanoreactors for X-ray-Initiated Polymerization, J. Phys. Chem. B 121 (2017) 2502–2510. https://doi.org/10.1021/acs.jpcb.6b12101.

[129] W. Karl, R. Perla, C. Gérard, C. Franck, N.-M. Luc, B. Hayat, F. Denis, Effect of surfactant on structure thermal behavior of cetyl stearyl alcohols: DSC and X-ray scattering studies, J. Therm. Anal. Calorim. 123 (2016) 1411–1417. https://doi.org/10.1007/s10973-015-5074-2.

[130] M.P. Sheetz, S.I. Chan, Effect of sonication on the structure of lecithin bilayers, Biochemistry 11 (1972) 4573–4581. https://doi.org/10.1021/bi00774a024.

[131] A.L.R. De Souza, T. Andreani, F.M. Nunes, D.L. Cassimiro, A.E. De Almeida, C.A. Ribeiro, V.H.V. Sarmento, M.P.D. Gremião, A.M. Silva, E.B. Souto, Loading of praziquantel in the crystal lattice of solid lipid nanoparticles: Studies by DSC and SAXS, J. Therm. Anal. Calorim. 108 (2012) 353–360. https://doi.org/10.1007/s10973-011-1871-4.

[132] Kesharwani, Vipin et al. “A review on therapeutics application of eucalyptus oil.” *International Journal of Herbal Medicine* 6 (2018): 110-115.

[133] M. Navarra, C. Mannucci, M. Delbò, G. Calapai, Citrus bergamia essential oil: from basic research to clinical application, Front. Pharmacol. 6 (2015). https://doi.org/10.3389/fphar.2015.00036.

[134] A.A. Ansari, M. Kamil, Kabir-ud-Din, Polymer-Surfactant Interactions and the Effect of Tail Size Variation on Micellization Process of Cationic ATAB

Surfactants in Aqueous Medium, J. Dispers. Sci. Technol. 34 (2013) 722–730. https://doi.org/10.1080/01932691.2012.685850.

[135] L. Brannon-Peppas, Interactions of surfactants with polymers and proteins, 1993. https://doi.org/10.1016/0168-3659(93)90115-l.

[136] M. Lukic, I. Pantelic, S. Savic, An overview of novel surfactants for formulation of cosmetics with certain emphasis on acidic active substances, Tenside Surfactants Deterg. 53 (2016) 7–19. https://doi.org/10.3139/113.110405.

[137] C.D. Bain, P.M. Claesson, D. Langevin, R. Meszaros, T. Nylander, C. Stubenrauch, S. Titmuss, R. von Klitzing, Complexes of surfactants with oppositely charged polymers at surfaces and in bulk, Adv. Colloid Interface Sci. 155 (2010) 32–49. https://doi.org/10.1016/j.cis.2010.01.007.

[138] A.L. Kwiatkowski, V.S. Molchanov, A.I. Kuklin, Y.M. Chesnokov, O.E. Philippova, Salt-Induced Transformations of Hybrid Micelles Formed by Anionic Surfactant and Poly(4-vinylpyridine), Polymers 14 (2022) 5086. https://doi.org/10.3390/polym14235086.

[139] P. Raffa, Interactions between an associative amphiphilic block polyelectrolyte and surfactants in water: Effect of charge type on solution properties and aggregation, Polymers 13 (2021). https://doi.org/10.3390/polym13111729.

[140] M.V.A. Queirós, W. Loh, From Associative to Segregative Phase Separation: The Phase Behavior of Poly(acrylate)/Dodecyltrimethylammonium Complex Salts in the Presence of NaBr and NaCl, J. Phys. Chem. B 125 (2021) 2968–2975. https://doi.org/10.1021/acs.jpcb.0c11245.

[141] B. Lindman, F. Antunes, S. Aidarova, M. Miguel, T. Nylander, Polyelectrolyte-surfactant association—from fundamentals to applications, Colloid J. 76 (2014) 585–594. https://doi.org/10.1134/S1061933X14050111.

[142] K. Pojják, E. Bertalanits, R. Mészáros, Effect of Salt on the Equilibrium and Nonequilibrium Features of Polyelectrolyte/Surfactant Association, Langmuir 27 (2011) 9139–9147. https://doi.org/10.1021/la2021353.

[143] J. Janiak, S. Bayati, L. Galantini, N.V. Pavel, K. Schillén, Nanoparticles with a Bicontinuous Cubic Internal Structure Formed by Cationic and Non-ionic

Surfactants and an Anionic Polyelectrolyte, Langmuir 28 (2012) 16536–16546. https://doi.org/10.1021/la303938k.

[144] J.S. Bernardes, W. Loh, Structure and phase equilibria of mixtures of the complex salt hexadecyltrimethylammonium polymethacrylate, water and different oils, J. Colloid Interface Sci. 318 (2008) 411–420. https://doi.org/10.1016/j.jcis.2007.10.030.

[145] A.M. Percebom, L. Piculell, W. Loh, Polyion–Surfactant Ion Complex Salts Formed by a Random Anionic Copolyacid at Different Molar Ratios of Cationic Surfactant: Phase Behavior with Water and *n* -Alcohols, J. Phys. Chem. B 116 (2012) 2376–2384. https://doi.org/10.1021/jp2103403.

[146] R.J. Allen, P.B. Warren, Phase behaviour of oppositely charged polymer/surfactant mixtures, Europhys. Lett. EPL 64 (2003) 468–474. https://doi.org/10.1209/epl/i2003-00234-2.

[147] J. Mirtič, A. Paudel, P. Laggner, S. Hudoklin, M.E. Kreft, J. Kristl, Polyelectrolyte–surfactant–complex nanoparticles as a delivery platform for poorly soluble drugs: A case study of ibuprofen loaded cetylpyridinium-alginate system, Int. J. Pharm. 580 (2020) 119199. https://doi.org/10.1016/j.ijpharm.2020.119199.

[148] K. Pojják, E. Fegyver, R. Mészáros, Effect of Linear Nonionic Polymer Additives on the Kinetic Stability of Dispersions of Poly(diallyldimethylammonium chloride)/Sodium Dodecylsulfate Nanoparticles, Langmuir 29 (2013) 10077–10086. https://doi.org/10.1021/la4021542.

[149] K. Bali, Z. Varga, A. Kardos, R. Mészáros, Impact of local inhomogeneities on the complexation between poly(diallyldimethylammoniumchloride) and sodium dodecyl sulfate, Colloids Surf. Physicochem. Eng. Asp. 574 (2019) 21–28. https://doi.org/10.1016/j.colsurfa.2019.04.052.

[150] T.K. Bronich, A.V. Kabanov, V.A. Kabanov, K. Yu, A. Eisenberg, Soluble Complexes from Poly(ethylene oxide)- *block* -polymethacrylate Anions and *N* -Alkylpyridinium Cations, Macromolecules 30 (1997) 3519–3525. https://doi.org/10.1021/ma970197o.

[151] J.-F. Berret, P. Hervé, O. Aguerre-Chariol, J. Oberdisse, Colloidal Complexes Obtained from Charged Block Copolymers and Surfactants: A Comparison between Small-Angle Neutron Scattering, Cryo-TEM, and

Simulations, J. Phys. Chem. B 107 (2003) 8111–8118. https://doi.org/10.1021/jp027740+.

[152] J.-F. Berret, J. Oberdisse, Electrostatic self-assembly in polyelectrolyte-neutral block copolymers and oppositely charged surfactant solutions, Phys. B Condens. Matter 350 (2004) 204–206. https://doi.org/10.1016/j.physb.2004.04.027.

[153] J.-F. Berret, B. Vigolo, R. Eng, P. Hervé, I. Grillo, L. Yang, Electrostatic Self-Assembly of Oppositely Charged Copolymers and Surfactants: A Light, Neutron, and X-ray Scattering Study, Macromolecules 37 (2004) 4922–4930. https://doi.org/10.1021/ma0498722.

[154] J.-F. Berret, Controlling electrostatic co-assembly using ion-containing copolymers: From surfactants to nanoparticles, Adv. Colloid Interface Sci. 167 (2011) 38–48. https://doi.org/10.1016/j.cis.2011.01.008.

[155] A.M. Percebom, J. Janiak, K. Schillén, L. Piculell, W. Loh, Micellization of water-soluble complex salts of an ionic surfactant with hairy polymeric counterions, Soft Matter 9 (2013) 515–526. https://doi.org/10.1039/C2SM26683K.

[156] A.M. Percebom, L.R.S. Barbosa, R. Itri, W. Loh, How does the ethoxylated grafting of polyelectrolytes affect the self-assembly of polyanion-cationic surfactant complex salts?, Langmuir 30 (2014) 11493–11503. https://doi.org/10.1021/la5019604.

[157] Y. Guo, J. Shen, M. Li, Y. Shang, H. Liu, Effects of nonionic surfactant and salts on the interactions between oppositely charged star-shaped copolymer and ionic surfactant in aqueous solutions, J. Mol. Liq. 266 (2018) 789–796. https://doi.org/10.1016/j.molliq.2018.02.048.

[158] J. Janiak, L. Piculell, G. Olofsson, K. Schillén, The aqueous phase behavior of polyion–surfactant ion complex salts mixed with nonionic surfactants, Phys Chem Chem Phys 13 (2011) 3126–3138. https://doi.org/10.1039/C0CP01031F.

[159] Y. Shen, P. Somasundaran, Introduction of a nonionic sugar-based surfactant to an oppositely charged hydrophobically modified polyelectrolyte and surfactant binary system, Colloids Surf. Physicochem. Eng. Asp. 570 (2019) 274–281. https://doi.org/10.1016/j.colsurfa.2019.03.040.

[160] E. Fegyver, R. Mészáros, The impact of nonionic surfactant additives on the nonequilibrium association between oppositely charged polyelectrolytes and ionic surfactants, Soft Matter 10 (2014) 1953–1962. https://doi.org/10.1039/c3sm52889h.

[161] E. Fegyver, R. Mészáros, Fine-Tuning the Nonequilibrium Behavior of Oppositely Charged Macromolecule/Surfactant Mixtures via the Addition of Nonionic Amphiphiles, Langmuir 30 (2014) 15114–15126. https://doi.org/10.1021/la503928x.

[162] J. Janiak, M. Tomšič, D. Lundberg, G. Olofsson, L. Piculell, K. Schillén, Soluble Aggregates in Aqueous Solutions of Polyion–Surfactant Ion Complex Salts and a Nonionic Surfactant, J. Phys. Chem. B 118 (2014) 9745–9756. https://doi.org/10.1021/jp411701g.

[163] E. Fegyver, R. Mészáros, Complexation between Sodium Poly(styrenesulfonate) and Alkyltrimethylammonium Bromides in the Presence of Dodecyl Maltoside, J. Phys. Chem. B 119 (2015) 5336–5346. https://doi.org/10.1021/acs.jpcb.5b01206.

[164] K. Pojják, R. Mészáros, Association between branched poly(ethyleneimine) and sodium dodecyl sulfate in the presence of neutral polymers, J. Colloid Interface Sci. 355 (2011) 410–416. https://doi.org/10.1016/j.jcis.2010.12.051.

[165] K. Pojják, R. Mészáros, Novel Self-Assemblies of Oppositely Charged Polyelectrolytes and Surfactants in the Presence of Neutral Polymer, Langmuir 25 (2009) 13336–13339. https://doi.org/10.1021/la903761r.

[166] R. Ganguly, A. Kunwar, B. Dutta, S. Kumar, K.C. Barick, A. Ballal, V.K. Aswal, P.A. Hassan, Heat-induced solubilization of curcumin in kinetically stable pluronic P123 micelles and vesicles: An exploit of slow dynamics of the micellar restructuring processes in the aqueous pluronic system, Colloids Surf. B Biointerfaces 152 (2017) 176–182. https://doi.org/10.1016/j.colsurfb.2017.01.023.

[167] B. Naskar, S. Ghosh, S.P. Moulik, Solution behavior of normal and reverse triblock copolymers (pluronic L44 and 10R5) individually and in binary mixture, Langmuir 28 (2012) 7134–7146. https://doi.org/10.1021/la3000729.

[168] T. Swift, L. Swanson, M. Geoghegan, S. Rimmer, The pH-responsive behaviour of poly(acrylic acid) in aqueous solution is dependent on molar mass, Soft Matter 12 (2016) 2542–2549. https://doi.org/10.1039/C5SM02693H.

[169] R. Arnold, The titration of polymeric acids, J. Colloid Sci. 12 (1957) 549–556. https://doi.org/10.1016/0095-8522(57)90060-0.

[170] M. Zhao, S.A. Eghtesadi, M.B. Dawadi, C. Wang, S. Huang, A.E. Seymore, B.D. Vogt, D.A. Modarelli, T. Liu, N.S. Zacharia, Partitioning of Small Molecules in Hydrogen-Bonding Complex Coacervates of Poly(acrylic acid) and Poly(ethylene glycol) or Pluronic Block Copolymer, Macromolecules 50 (2017) 3818–3830. https://doi.org/10.1021/acs.macromol.6b02815.

[171] S. Nawaz, P. Carbone, Coarse-Graining Poly(ethylene oxide)–Poly(propylene oxide)–Poly(ethylene oxide) (PEO–PPO–PEO) Block Copolymers Using the MARTINI Force Field, J. Phys. Chem. B 118 (2014) 1648–1659. https://doi.org/10.1021/jp4092249.

[172] D.W. Schaefer, J.E. Martin, A.J. Hurd, K.D. Keefer, Structure of Random Materials, in: N. Boccara, M. Daoud (Eds.), Phys. Finely Divid. Matter, Springer Berlin Heidelberg, Berlin, Heidelberg, 1985: pp. 31–37. https://doi.org/10.1007/978-3-642-93301-1_5.

[173] G. Beaucage, Small-Angle Scattering from Polymeric Mass Fractals of Arbitrary Mass-Fractal Dimension, J. Appl. Crystallogr. 29 (1996) 134–146. https://doi.org/10.1107/S0021889895011605.

[174] G. Porod, Die Röntgenkleinwinkelstreuung von dichtgepackten kolloiden Systemen: I. Teil, Kolloid-Z. 124 (1951) 83–114. https://doi.org/10.1007/BF01512792.

[175] D.W. Schaefer, J.E. Martin, K.D. Keefer, Structure of fractal aggregates from small angle X-Ray Scattering, J. Phys. Colloq. 46 (1985) C3-127-C3-135. https://doi.org/10.1051/jphyscol:1985311.

[176] L. Vitorazi, J.-F. Berret, W. Loh, Self-Assembly of Complex Salts of Cationic Surfactants and Anionic–Neutral Block Copolymers. Dispersions with Liquid-Crystalline Internal Structure, Langmuir 29 (2013) 14024–14033. https://doi.org/10.1021/la402624u.

[177] S. Krimm, The hydrophobic effect: Formation of micelles and biological membranes, Charles Tanford, Wiley-Interscience, New York, 1980, 233 pp.

price: $18.50., J. Polym. Sci. Polym. Lett. Ed. 18 (1980) 687–687. https://doi.org/10.1002/pol.1980.130181008.

[178] R. Garcés, E. Martínez-Force, J.J. Salas, M. Venegas-Calerón, Current advances in sunflower oil and its applications, Lipid Technol. 21 (2009) 79–82. https://doi.org/10.1002/lite.200900016.

[179] M. Akamatsu, K. Saito, H. Iwase, T. Ogura, K. Sakai, H. Sakai, Contrast Variation Small-Angle Neutron Scattering Study of Solubilization of Perfumes in Cationic Surfactant Micelles, Langmuir 37 (2021) 10770–10775. https://doi.org/10.1021/acs.langmuir.1c01489.

[180] Y. Wang, S.A. Sukhishvili, Hydrogen-bonded polymer complexes and nanocages of weak polyacids templated by a Pluronic® block copolymer, Soft Matter 12 (2016) 8744–8754. https://doi.org/10.1039/C6SM01869F.

[181] C.F. Wu, S.H. Chen, L.B. Shih, J.S. Lin, Direct Measurement of Counterion Distribution around Cylindrical Micelles by Small-Angle X-Ray Scattering, Phys. Rev. Lett. 61 (1988) 645–648. https://doi.org/10.1103/PhysRevLett.61.645.

[182] T. Schmutzler, T. Schindler, M. Schmiele, M.-S. Appavou, S. Lages, A. Kriele, R. Gilles, T. Unruh, The influence of n- hexanol on the morphology and composition of CTAB micelles, Colloids Surf. Physicochem. Eng. Asp. 543 (2018) 56–63. https://doi.org/10.1016/j.colsurfa.2017.12.039.

[183] S. Kancharla, D. Bedrov, M. Tsianou, P. Alexandridis, Structure and composition of mixed micelles formed by nonionic block copolymers and ionic surfactants in water determined by small-angle neutron scattering with contrast variation, J. Colloid Interface Sci. 609 (2022) 456–468. https://doi.org/10.1016/j.jcis.2021.10.176.

[184] S. Kancharla, N.A. Zoyhofski, L. Bufalini, B.F. Chatelais, P. Alexandridis, Association between nonionic amphiphilic polymer and ionic surfactant in aqueous solutions: Effect of polymer hydrophobicity and micellization, Polymers 12 (2020) 1–23. https://doi.org/10.3390/POLYM12081831.

[185] K. Holmberg, B. Jönsson, B. Kronberg, B. Lindman, Surfactants and Polymers in Aqueous Solution, 1st ed., Wiley, 2002. https://doi.org/10.1002/0470856424.

[186] P.L. Dubin, R. Oteri, Association of polyelectrolytes with oppositely charged mixed micelles, J. Colloid Interface Sci. 95 (1983) 453–461. https://doi.org/10.1016/0021-9797(83)90205-9.

[187] B. Lindman, A. Khan, E. Marques, M.G. Da Miguel, L. Piculell, K. Thalberg, Phase behavior of polymer-surfactant systems in relation to polymer-polymer and surfactant-surfactant mixtures, Pure Appl. Chem. 65 (1993) 953–958. https://doi.org/10.1351/pac199365050953.

[188] L. Piculell, B. Lindman, Association and segregation in aqueous polymer/polymer, polymer/surfactant, and surfactant/surfactant mixtures: similarities and differences, Adv. Colloid Interface Sci. 41 (1992) 149–178. https://doi.org/10.1016/0001-8686(92)80011-L.

[189] T. Tamura, T. Iihara, S. Nishida, S. Ohta, Clearning performance and foaming properties of lauroylamidopropylbetaine/nonionics mixed systems, J. Surfactants Deterg. 2 (1999) 207–211. https://doi.org/10.1007/s11743-999-0075-6.

[190] R.R. Prajapati, S.S. Bhagwat, Effect of Foam Boosters on the Micellization and Adsorption of Sodium Dodecyl Sulfate, J. Chem. Eng. Data 57 (2012) 3644–3650. https://doi.org/10.1021/je3008155.

[191] E.S. Basheva, D. Ganchev, N.D. Denkov, K. Kasuga, N. Satoh, K. Tsujii, Role of Betaine as Foam Booster in the Presence of Silicone Oil Drops, Langmuir 16 (2000) 1000–1013. https://doi.org/10.1021/la990777+.

[192] A. Schnuch, H. Lessmann, J. Geier, W. Uter, Is cocamidopropyl betaine a contact allergen? Analysis of network data and short review of the literature, Contact Dermatitis 64 (2011) 203–211. https://doi.org/10.1111/j.1600-0536.2010.01863.x.

[193] I. Nicander, I. Rantanen, B.L. Rozell, E. Söderling, S. Ollmar, The ability of betaine to reduce the irritating effects of detergents assessed visually, histologically and by bioengineering methods, Skin Res. Technol. 9 (2003) 50–58. https://doi.org/10.1034/j.1600-0846.2003.00367.x.

[194] I. Rantanen, I. Nicander, K. Jutila, S. Ollmar, J. Tenovuo, E. Söderling, Betaine reduces the irritating effect of sodium lauryl sulfate on human oral mucosa in vivo, Acta Odontol. Scand. 60 (2002) 306–310. https://doi.org/10.1080/00016350260248292.

[195] M.K. Mullally, D.G. Marangoni, Micellar properties of zwitterionic surfactant - alkoxyethanol mixed micelles, Can. J. Chem. 82 (2004) 1223–1229. https://doi.org/10.1139/v04-022.

[196] S. Herrwerth, H. Leidreiter, H.H. Wenk, M. Farwick, I. Ulrich-Brehm, B. Grüning, Highly Concentrated Cocamidopropyl Betaine – The Latest Developments for Improved Sustainability and Enhanced Skin Care, Tenside Surfactants Deterg. 45 (2008) 304–308. https://doi.org/10.3139/113.100387.

[197] S.N. Blagojević, S.M. Blagojević, N.D. Pejić, Performance and Efficiency of Anionic Dishwashing Liquids with Amphoteric and Nonionic Surfactants, J. Surfactants Deterg. 19 (2016) 363–372. https://doi.org/10.1007/s11743-015-1784-5.

[198] R. Sarkar, A. Pal, A. Rakshit, B. Saha, Properties and applications of amphoteric surfactant: A concise review, J. Surfactants Deterg. 24 (2021) 709–730. https://doi.org/10.1002/jsde.12542.

[199] T. Iwasaki, M. Ogawa, K. Esumi, K. Meguro, Interactions between betaine-type zwitterionic and anionic surfactants in mixed micelles, Langmuir 7 (1991) 30–35. https://doi.org/10.1021/la00049a008.

[200] H. Lu, M. Yuan, B. Fang, J. Wang, Y. Guo, Wormlike Micelles in Mixed Amino Acid-Based Anionic Surfactant and Zwitterionic Surfactant Systems, J. Surfactants Deterg. 18 (2015) 589–596. https://doi.org/10.1007/s11743-015-1683-9.

[201] V.I. Yavrukova, G.M. Radulova, K.D. Danov, P.A. Kralchevsky, H. Xu, Y.W. Ung, J.T. Petkov, Rheology of mixed solutions of sulfonated methyl esters and betaine in relation to the growth of giant micelles and shampoo applications, Adv. Colloid Interface Sci. 275 (2020) 102062. https://doi.org/10.1016/j.cis.2019.102062.

[202] S. Różańska, J. Różański, Shear and extensional rheology of aqueous solutions of cocamidopropyl betaine and sodium dodecyl sulfate mixture, J. Dispers. Sci. Technol. 41 (2020) 733–741. https://doi.org/10.1080/01932691.2019.1611442.

[203] A.P. Williams, J.P. King, A.V. Sokolova, L. De Campo, R.F. Tabor, *In Situ* Nanostructural Analysis of Concentrated Wormlike Micellar Fluids Comprising Sodium Laureth Sulfate and Cocamidopropyl Betaine Using

Small-Angle Neutron Scattering, Langmuir 36 (2020) 14296–14305. https://doi.org/10.1021/acs.langmuir.0c02530.

[204] S. Różańska, Rheology of wormlike micelles in mixed solutions of cocoamidopropyl betaine and sodium dodecylbenzenesulfonate, Colloids Surf. Physicochem. Eng. Asp. 482 (2015) 394–402. https://doi.org/10.1016/j.colsurfa.2015.06.045.

[205] X. Zhou, M.S. Kamal, A.B. Fuseni, Comprehensive Investigation of Dynamic Characteristics of Amphoteric Surfactant–Sulfonated Polymer Solution on Carbonate Rocks in Reservoir Conditions, ACS Omega 5 (2020) 18123–18133. https://doi.org/10.1021/acsomega.0c01690.

[206] X. Li, B. Sarsenbekuly, H. Yang, Z. Huang, H. Jiang, X. Kang, M. Li, W. Kang, P. Luo, Rheological behavior of a wormlike micelle and an amphiphilic polymer combination for enhanced oil recovery, Phys. Fluids 32 (2020) 073105. https://doi.org/10.1063/5.0018211.

[207] S. Ayirala, A. Sofi, Z. Li, Z. Xu, Surfactant and surfactant-polymer effects on wettability and crude oil liberation in carbonates, J. Pet. Sci. Eng. 207 (2021) 109117. https://doi.org/10.1016/j.petrol.2021.109117.

[208] H. Zhao, W. Kang, H. Yang, Z. Huang, B. Zhou, B. Sarsenbekuly, Emulsification and stabilization mechanism of crude oil emulsion by surfactant synergistic amphiphilic polymer system, Colloids Surf. Physicochem. Eng. Asp. 609 (2021) 125726. https://doi.org/10.1016/j.colsurfa.2020.125726.

[209] R. Ribera, M.M. Velázquez, Effect of Water-Soluble Polymers on the Surface Properties of 3-(Dimethyldodecylammonio)Propanesulfonate in Aqueous Solutions, Langmuir 15 (1999) 6686–6691. https://doi.org/10.1021/la990115k.

[210] A.-M. Misselyn-Bauduin, A. Thibaut, J. Grandjean, G. Broze, R. Jérôme, Investigation of the Interactions of Polyvinylpyrrolidone with Mixtures of Anionic and Nonionic Surfactants or Anionic and Zwitterionic Surfactants by Pulsed Field Gradient NMR, J. Colloid Interface Sci. 238 (2001) 1–7. https://doi.org/10.1006/jcis.2001.7451.

[211] C. Brinatti, L.B. Mello, W. Loh, Thermodynamic study of the micellization of zwitterionic surfactants and their interaction with polymers in water by

isothermal titration calorimetry, Langmuir 30 (2014) 6002–6010. https://doi.org/10.1021/la5012346.

[212] E. Guzmán, S. Llamas, L. Fernández-Peña, F. Léonforte, N. Baghdadli, C. Cazeneuve, F. Ortega, R.G. Rubio, G.S. Luengo, Effect of a natural amphoteric surfactant in the bulk and adsorption behavior of polyelectrolyte-surfactant mixtures, Colloids Surf. Physicochem. Eng. Asp. 585 (2020) 124178. https://doi.org/10.1016/j.colsurfa.2019.124178.

[213] F. Ofridam, N. Lebaz, É. Gagnière, D. Mangin, A. Elaissari, Polymethylmethacrylate derivatives Eudragit E100 and L100 : Interactions and complexation with surfactants, Polym. Adv. Technol. 32 (2021) 379–390. https://doi.org/10.1002/pat.5093.

[214] D. Kim, H. Sakamoto, H. Matsuoka, Y. Saruwatari, Complex Formation of Sulfobetaine Surfactant and Ionic Polymers and Their Stimuli Responsivity, Langmuir 36 (2020) 12990–13000. https://doi.org/10.1021/acs.langmuir.0c02323.

[215] J. Yang, R. Pal, Investigation of Surfactant-Polymer Interactions Using Rheology and Surface Tension Measurements, Polymers 12 (2020) 2302. https://doi.org/10.3390/polym12102302.

[216] M. Mella, A. Tagliabue, L. Izzo, On the distribution of hydrophilic polyelectrolytes and their counterions around zwitterionic micelles: the possible impact on the charge density in solution, Soft Matter 17 (2021) 1267–1283. https://doi.org/10.1039/D0SM01541E.

[217] F.P. Cavasino, H. Hoffmann, C. Sbriziolo, M.L. Turco Liveri, Interactions of tetradecyldimethylaminoxide with polyacrylic and polymethacrylic acids in aqueous solution, Colloids Surf. Physicochem. Eng. Asp. 183–185 (2001) 689–697. https://doi.org/10.1016/S0927-7757(01)00495-2.

[218] M. Mella, A. Tagliabue, L. Mollica, S. Vaghi, L. Izzo, Inducing pH control over the critical micelle concentration of zwitterionic surfactants via polyacids adsorption: Effect of chain length and structure, J. Colloid Interface Sci. 606 (2022) 1636–1651. https://doi.org/10.1016/j.jcis.2021.07.076.

[219] J.-Q. Guan, C.-H. Tung, G.-Z. Li, Modification of Alkylbetaine by Incorporation of Hydroxypropyl Group: Preparation, Surface Activity, and Biodegradability of N-Alkoxy-Hydroxypropyl-N, N-Dimethyl-Glycine

Betaine Surfactants, J. Dispers. Sci. Technol. 19 (1998) 63–76. https://doi.org/10.1080/01932699808913161.

[220] M. Doucet, J.H. Cho, G. Alina, J. Bakker, W. Bouwman, P. Butler, K. Campbell, M. Gonzales, R. Heenan, A. Jackson, P. Juhas, S. King, P. Kienzle, J. Krzywon, A. Markvardsen, T. Nielsen, L. O'Driscoll, W. Potrzebowski, R. Ferraz Leal, T. Richter, P. Rozycko, T. Snow, A. Washington, SasView version 4.2.2, (2019). https://doi.org/10.5281/ZENODO.2652477.

[221] K.D. Danov, S.D. Kralchevska, P.A. Kralchevsky, K.P. Ananthapadmanabhan, A. Lips, Mixed Solutions of Anionic and Zwitterionic Surfactant (Betaine): Surface-Tension Isotherms, Adsorption, and Relaxation Kinetics, Langmuir 20 (2004) 5445–5453. https://doi.org/10.1021/la049576i.

[222] S.S. Tzocheva, K.D. Danov, P.A. Kralchevsky, G.S. Georgieva, A.J. Post, K.P. Ananthapadmanabhan, Solubility limits and phase diagrams for fatty alcohols in anionic (SLES) and zwitterionic (CAPB) micellar surfactant solutions, J. Colloid Interface Sci. 449 (2015) 46–61. https://doi.org/10.1016/j.jcis.2014.09.042.

[223] K. Staszak, D. Wieczorek, K. Michocka, Effect of Sodium Chloride on the Surface and Wetting Properties of Aqueous Solutions of Cocamidopropyl Betaine, J. Surfactants Deterg. 18 (2015) 321–328. https://doi.org/10.1007/s11743-014-1644-8.

[224] C. Dai, J. Zhao, L. Yan, M. Zhao, Adsorption behavior of cocamidopropyl betaine under conditions of high temperature and high salinity, J. Appl. Polym. Sci. 131 (2014) app.40424. https://doi.org/10.1002/app.40424.

[225] A. Svensson, J. Norrman, L. Piculell, Phase behavior of polyion-surfactant ion complex salts: Effects of surfactant chain length and polyion length, J. Phys. Chem. B 110 (2006) 10332–10340. https://doi.org/10.1021/jp057402j.

[226] M.J. Rosen, Synergism in mixtures containing zwitterionic surfactants, Langmuir 7 (1991) 885–888. https://doi.org/10.1021/la00053a012.

[227] J. Li, T. Ngai, C. Wu, The slow relaxation mode: from solutions to gel networks, Polym. J. 42 (2010) 609–625. https://doi.org/10.1038/pj.2010.59.

[228] P.S. Santiago, D.D.S. Neto, L.R.S. Barbosa, R. Itri, M. Tabak, Interaction of meso-tetrakis (4-sulfonatophenyl) porphyrin with cationic CTAC micelles investigated by small angle X-ray scattering (SAXS) and electron paramagnetic resonance (EPR), J. Colloid Interface Sci. 316 (2007) 730–740. https://doi.org/10.1016/j.jcis.2007.08.010.

[229] S.-H. Chen, J. Teixeira, Structure and Fractal Dimension of Protein-Detergent Complexes, Phys. Rev. Lett. 57 (1986) 2583–2586. https://doi.org/10.1103/PhysRevLett.57.2583.

[230] J. Teixeira, Small-angle scattering by fractal systems, J. Appl. Crystallogr. 21 (1988) 781–785. https://doi.org/10.1107/S0021889888000263.

[231] S.S. Berr, Solvent isotope effects on alkytrimethylammonium bromide micelles as a function of alkyl chain length, J. Phys. Chem. 91 (1987) 4760–4765. https://doi.org/10.1021/j100302a024.

[232] M. Doucet, J.H. Cho, G. Alina, J. Bakker, W. Bouwman, P. Butler, K. Campbell, M. Gonzales, R. Heenan, A. Jackson, P. Juhas, S. King, P. Kienzle, J. Krzywon, A. Markvardsen, T. Nielsen, L. O'Driscoll, W. Potrzebowski, R. Ferraz Leal, T. Richter, P. Rozycko, T. Snow, A. Washington, SasView version 4.2.2, (2019). https://doi.org/10.5281/zenodo.2652477.

[233] N.C. Christov, N.D. Denkov, P.A. Kralchevsky, K.P.Ananthapadmanabhan, A. Lips, Synergistic Sphere-to-Rod Micelle Transition in Mixed Solutions of Sodium Dodecyl Sulfate and Cocoamidopropyl Betaine, Langmuir. 20 (2004) 565–571. https://doi.org/10.1021/la035717p.

Permission of Use of Images

Preparation of Stable Electroneutral Nanoparticles of Sodium Dodecyl Sulfate and Branched Poly(ethylenimine) in the Presence of Pluronic F108 Copolymer

Author: Katalin Pojják, Róbert Mészáros
Publication: Langmuir
Publisher: American Chemical Society
Date: Dec 1, 2011

PERMISSION/LICENSE IS GRANTED FOR YOUR ORDER AT NO CHARGE

This type of permission/license, instead of the standard Terms and Conditions, is sent to you because no fee is being charged for your order. Please note the following:

- Permission is granted for your request in both print and electronic formats, and translations.
- If figures and/or tables were requested, they may be adapted or used in part.
- Please print this page for your records and send a copy of it to your publisher/graduate school.
- Appropriate credit for the requested material should be given as follows: "Reprinted (adapted) with permission from {COMPLETE REFERENCE CITATION}. Copyright {YEAR} American Chemical Society." Insert appropriate information in place of the capitalized words.
- One-time permission is granted only for the use specified in your RightsLink request. No additional uses are granted (such as derivative works or other editions). For any uses, please submit a new request.

If credit is given to another source for the material you requested from RightsLink, permission must be obtained from that source.

BACK CLOSE WINDOW

Nanoparticles of surfactant and block copolymers with high uptake of oily ingredients for cosmetic formulations

Author: Amanda de Azevedo Stavale,Gabriela Oliva Fonseca,Paola Severo Duarte,Lukas Costa Macedo,Ana Maria Percebom
Publication: Colloids and Surfaces A: Physicochemical and Engineering Aspects
Publisher: Elsevier
Date: 20 November 2019

Journal Author Rights

Please note that, as the author of this Elsevier article, you retain the right to include it in a thesis or dissertation, provided it is not published commercially. Permission is not required, but please ensure that you reference the journal as the original source. For more information on this and on your other retained rights, please visit: https://www.elsevier.com/about/our-business/policies/copyright#Author-rights

BACK CLOSE WINDOW